

Dissertation zur Erlangung des Doktorgrades
der Fakultät für Chemie und Pharmazie
der Ludwig-Maximilians-Universität München

The complex interplay of RNA-binding proteins and RISC in neurons

Janina Ehses

aus

Bonn, Deutschland

2021

ERKLÄRUNG

Diese Dissertation wurde im Sinne von §7 der Promotionsordnung vom 28. November 2011 von Herrn PROF. DR. MICHAEL A. KIEBLER betreut und von Herrn PROF. DR. KLAUS FÖRSTEMANN von der Fakultät für Chemie und Pharmazie vertreten.

EIDESSTATTLICHE VERSICHERUNG

Diese Dissertation wurde eigenständig und ohne unerlaubte Hilfe erarbeitet.

München, den 04. Februar 2021

JANINA EHSES

Dissertation eingereicht am: 08.02.2021

1. Gutachter: PROF. DR. KLAUS FÖRSTEMANN

2. Gutachter: PROF. DR. MICHAEL A. KIEBLER

Mündliche Prüfung am: 05.03.2021

Table of Content

Summary	I
List of publications	III
1 Introduction	1
1.1 <i>Neuronal RNA granules and the mRNP code</i>	1
1.2 <i>RNA interference</i>	3
1.2.1 The RNA induced silencing complex	4
1.2.2 Regulation of neuronal RISC	4
1.3 <i>The Staufen protein family</i>	6
1.3.1 Neuronal Staufen2	9
1.4 <i>HuR/ELAVL1</i>	11
2 Aims	13
3 Chapter A	14
4 Chapter B	31
5 Chapter C	69
5.1 <i>Introduction</i>	70
5.2 <i>Results and discussion</i>	73
5.3 <i>Materials and Methods</i>	75
6 Discussion and outlook	77
6.1 <i>How is RNAi regulated by the neuronal RBP network?</i>	77
6.1.1 miRNA biogenesis	77
6.1.2 RISC assembly and localization	78
6.1.3 Combinatorial binding of RBPs and RISC to mRNAs	80
6.2 <i>How does the RNA structure contribute to RNP assembly?</i>	82
6.3 <i>How does the RBP network contribute to neuronal physiology?</i>	83
References	86
Appendices	98

Summary

An extensive network of RNA-binding proteins (RBPs) is at the center of posttranscriptional gene regulation. Importantly, different RBPs – including microRNA-loaded Argonaute (Ago) – can bind to a single mRNA resulting in antagonistic or cooperative mode of actions, thereby determining the fate and function of an mRNA. Here, I investigated the impact of two different RBPs, HuR and Stau2 (Stau2), on microRNA/Ago-dependent gene expression homeostasis. The results of my thesis allow me to present a working model how these three RBPs might control neuronal function in a novel RNA-structure dependent manner.

HuR protein binds to AU-rich elements within mRNAs. In the case of *Regulator of G-protein signaling* (*Rgs4*) mRNA, I find that HuR binding occurs close to a miR-26/RISC binding site, resulting in *Rgs4* destabilization. As both binding sites are in close proximity within a predicted RNA hairpin structure, only synergistic action of HuR and miR-26 results in *Rgs4* repression. I propose a novel mechanism involving the trifold combination of HuR, miR-26-loaded Ago and RNA secondary structure in governing functional regulation of *Rgs4* mRNA in neurons.

Certain RBPs such as Stau2 protein bind to double-stranded RNAs (dsRNAs), thereby shaping local and global secondary structures of mRNAs. Based on preliminary data linking Stau2 and the miRNA pathway, I investigated Stau2-dependent expression, localization and function of the miRNA-induced silencing complex (RISC) in neurons. Proteome and small RNA transcriptome analysis in Stau2 deficient primary neurons revealed significant upregulation of several RISC associated proteins, including Ago1/2, while global miRNA levels were unaffected. This upregulation was accompanied by decreased global translation and translocation of Ago2 from Processing-bodies, sites of mRNA storage, to translating polysomes. Phenotypically, depletion of Ago1/2 reduced dendritic branching. This effect could be rescued by simultaneous knockdown of Stau2, suggesting that Ago1/2 and Stau2 functionally counterbalance each other in neurons. I hypothesize that Stau2's ability to bind to dsRNA stabilizes defined mRNA structures thereby governing association of RISC and mRNAs. Based on Stau2 hiCLIP experiments by our collaborator Jernej Ule, I was able to define a long-range RNA duplex in the 3'-untranslated region of *Rgs4* mRNA bound by Stau2 *in vivo*. This RNA duplex is necessary and sufficient to drive Stau2-dependent ribonucleoprotein particle (RNP) assembly as well as dendritic RNA localization in neurons.

Together, the data presented in my thesis support a model, in which balanced expression and interdependent action of RBPs, RISC and RNA structure shapes RNP assembly and gene expression homeostasis, important for neuronal function.

List of publications

This thesis is based on the following publications and manuscripts, reprinted in chapters A (1) and B (2).

- 1 **Janina Ehses**, Sandra M. Fernández-Moya, Luise Schröger, Michael A. Kiebler
Synergistic regulation of *Rgs4* mRNA by HuR and miR26/RISC in neurons.
RNA Biology 2020; <https://doi.org/10.1080/15476286.2020.1795409>.
- 2 **Janina Ehses**, Melina Schlegel, Luise Schröger, Rico Schieweck, Max Harner, Sophia Derdak, Martin Bilban, Michael A. Kiebler
The dsRBP Stauf2 governs RNP assembly of neuronal Argonaute proteins.
Manuscript to be submitted.

Additional publications and manuscripts with contributions by Janina Ehses during preparation of this thesis in chronological order:

- 3 **Janina Ehses**, Michael A. Kiebler, Sandra M. Fernández-Moya
RNA Transport: From Head to Toe in Radial Glial Cells.
Current Biology 2016, 26, R1285; <https://doi.org/10.1016/j.cub.2016.11.017>.
- 4 Stefan M. Berger, Iván Fernández-Lamo, Kai Schönig, Sandra M. Fernández-Moya, **Janina Ehses**, Rico Schieweck, Stefano Clementi, Thomas Enkel, Sascha Grothe, Oliver von Bohlen und Halbach, Inmaculada Segura, José María Delgado-García, Agnès Gruart, Michael A. Kiebler, Dusan Bartsch
Forebrain-specific, conditional silencing of Stauf2 alters synaptic plasticity, learning, and memory in rats.
Genome Biology 2017, 18, 222; <https://doi.org/10.1186/s13059-017-1350-8>.
- 5 Tejaswini Sharangdhar, Yoichiro Sugimoto, Jacqueline Heraud-Farlow, Sandra M. Fernández-Moya, **Janina Ehses**, Igor Ruiz de los Mozos, Jernej Ule, Michael A. Kiebler
A retained intron in the 3'-UTR of *Calm3* mRNA mediates its Stauf2- and activity-dependent localization to neuronal dendrites.
EMBO reports 2017, 18, 1762; <https://doi.org/10.15252/embr.201744334>.
- 6 Sandra M. Fernández-Moya, **Janina Ehses**, Michael A. Kiebler
The alternative life of RNA – sequencing meets single molecule approaches.
FEBS letters 2017, 591, 1455; <https://doi.org/10.1002/1873-3468.12639>.

-
- 7 Tjasa Lepko, Melanie Pusch, Tamara Müller, Dorothea Schulte, **Janina Ehses**, Michael A. Kiebler, Julia Hasler, Hagen B. Huttner, Roosmarijn E. Vandenbroucke, Charysse Vandendriessche, Miha Modic, Ana Martin-Villalba, Sheng Zhao, Enric Llorens-Bobadilla, Anja Schneider, Andre Fischer, Christopher T. Breunig, Stefan H. Stricker, Magdalena Götz, Jovica Ninkovic
Choroid plexus-derived miR-204 regulates the number of quiescent neural stem cells in the adult brain.
EMBO Journal **2019**, *38*, e100481; <https://doi.org/10.15252/emj.2018100481>.
- 8 Karl E. Bauer, Inmaculada Segura, Imre Gaspar, Volker Scheuss, Christin Illig, Georg Ammer, Saskia Hutten, Eugénia Basyuk, Sandra M. Fernández-Moya, **Janina Ehses**, Edouard Bertrand, Michael A. Kiebler
Live cell imaging reveals 3'-UTR dependent mRNA sorting to synapses.
Nature Communications **2019**, *10*, 3178; <https://doi.org/10.1038/s41467-019-11123-x>.
- 9 Sandra M. Fernández-Moya, **Janina Ehses**, Anob Chakrabarti, Karl E. Bauer, Rico Schieweck, Flora Lee, Jernej Ule, Michael A. Kiebler
RNA structure drives Stau2-dependent RNP assembly and localization in neurons.
Manuscript in preparation.

There is nothing more wonderful than being a scientist, nowhere I would rather be than in my lab, staining up my clothes and getting paid to play. – Marie Curie

1 Introduction

1.1 Neuronal RNA granules and the mRNP code

Posttranscriptional gene regulation represents one important cellular mechanism to ensure neuronal development and synaptic function (Gebauer et al., 2020; Schieweck et al., 2020; Wang et al., 2016). This is warranted by a network of thousands of RNA-binding proteins (RBPs) (Hentze et al., 2018; Schieweck et al., 2020). RBPs regulate many processes in the complex life of an RNA, mostly through binding to the 3'-untranslated region (3'-UTR) of the mRNA (Andreassi and Riccio, 2009). Intron retention, alternative splicing and alternative polyadenylation (APA) are co-transcriptionally governed by RBPs, resulting in a significant expansion of the proteome (Fernández-Moya et al., 2017; Schieweck et al., 2020; Schreiner et al., 2014). In addition to generating alternative proteins isoforms, this also leads to lengthening of 3'-UTRs particularly in the brain, thereby increasing the regulatory potential through RBPs (Di Giammartino et al., 2011; Miura et al., 2013; Tushev et al., 2018; Wang and Yi, 2014; Wei et al., 2020). Combinatorial binding of RBPs to a given mRNA results in formation of ribonucleoprotein particles (RNPs) that determine the fate of the mRNA (Iadevaia and Gerber, 2015). Recent evidence suggests that initial RNP assembly takes place in the nucleus (Duss et al., 2019; Kress et al., 2004; Rodgers and Woodson, 2019). Once exported from the nucleus RNP composition is dynamically altered to ensure controlled localization, translation and degradation of mRNAs (Heraud-Farlow and Kiebler, 2014; Kiebler and Bassell, 2006; Tauber et al., 2020).

In neurons, several distinct cytoplasmic RNPs exist that differ in their molecular composition and function. These include translationally repressed processing-bodies (P-bodies) and transport RNPs (Kiebler and Bassell, 2006). P-bodies are sites of RNA and RBP storage that are found both in the soma and in distal dendrites of neurons (Cougot et al., 2008; Hubstenberger et al., 2017; Standart and Weil, 2018). They contain proteins, mainly RBPs, that are involved in microRNA (miRNA) mediated gene silencing, deadenylation and decapping; and their homeostasis is governed by the translational repressor DEAD-box helicase 6 (Ddx6) (Hubstenberger et al., 2017; Di Stefano et al., 2019). In human cell lines and progenitor cells, mRNAs enriched in P-bodies are AU-rich and code for regulatory proteins, such as chromatin modifiers or RBPs (Courel et al., 2019; Di Stefano et al., 2019). Neuronal dendritic P-bodies are responsive to neuronal activity (Cougot et al., 2008) and they transiently interact with transport RNPs (Zeitelhofer et al., 2008). Transport RNPs are microtubule associated RNA granules that move bidirectionally along dendrites (Bauer et al., 2019; Doyle and Kiebler, 2011; Köhrmann et al., 1999). The directed transport along cellular processes ensures delivery of mRNAs to the sites of local translation, *e.g.* at synapses, axonal growth cones and endfeet of radial glia cells (Bauer et al., 2019; Holt et al., 2019; Pilaz et al., 2016; Shigeoka et al., 2016). Transport RNPs share a subset of protein components with P-bodies that ensure translational repression during RNA transport (Fritzsche et al., 2013; Kiebler and Bassell, 2006). However, in comparison to the larger P-bodies, they contain only few mRNAs (Doyle and Kiebler, 2011; Mikl et al., 2011; Tauber et al., 2020).

The cellular localization of the mRNA is regulated through assembly of RBPs into distinct RNA granules (Heraud-Farlow and Kiebler, 2014; Meer et al., 2012). The interdependent expression, activity and localization of these RBPs therefore determines the ultimate fate and function of the mRNA (Dassi, 2017; Schieweck et al., 2020). However, assembly of RBPs and mRNAs is also dependent on the presence and accessibility of RBP binding sites on the mRNA, termed the *RNA signature* (Doyle and Kiebler, 2011). Further, the RNA itself is a critical element for RNP condensation (Garcia-Jove Navarro et al., 2019) and this process can be regulated by RNA structure that determines accessibility of RBP binding sites (Langdon et al., 2018; Sanchez de Groot et al., 2019). The individual combination of RBP binding sites on the mRNA can result in synergistic or antagonistic actions of RBPs (Iadevaia and Gerber, 2015). Association of miRNAs with target mRNAs for example is highly regulated by other RBPs (Kosik, 2006), as it has been shown in cell lines for Pumilio2 (Pum2), Mov10, FMRP and HuR

(Iadevaia and Gerber, 2015; Kenny et al., 2014; Li et al., 2018; Sternburg et al., 2018). How these interdependent RBP networks and their influence on miRNA mediated gene silencing contribute to gene expression homeostasis in neurons is still largely unknown and are the main aim of this thesis (Heraud-Farlow and Kiebler, 2014; Kosik, 2006).

1.2 RNA interference

Following initial observations in plants (Napoli et al., 1990), the discovery of double-stranded RNA (dsRNA) at the center of a process called RNA interference (RNAi) 1998 in *C. elegans* opened an entirely new and important chapter in research of gene regulation (Fire et al., 1998). By now, we know that RNAi is highly conserved in eukaryotes and the processing of such dsRNA results in formation of small non-coding RNAs (ncRNAs) that mediate gene repression through hybridization with the cognate target RNA (Bartel, 2018). In mammals, miRNAs are the predominant form of short ncRNAs with 19 – 22 nt in length. Prediction shows that each human miRNA binds hundreds of different target mRNAs resulting in the miRNA pathway to target ~60% of protein-coding transcripts (Agarwal et al., 2015; Friedman et al., 2009). This makes miRNAs key regulators of all cellular processes, from embryonic development to refinement of synaptic plasticity during learning and memory formation (Nawalpuri et al., 2020).

Canonical miRNAs originate from endogenously transcribed stem loop regions from longer primary miRNA (pri-miRNA) transcripts. Specifically, pri-miRNA is cleaved by the Microprocessor, consisting of the endonuclease Drosha and its partner dsRBP, DGCR8, to produce the ~70 precursor miRNA (pre-miRNA) stem-loop (Lee et al., 2002, 2003). The pre-miRNA is subsequently exported from the nucleus via the Exportin5 pathway (Lund et al., 2004). In the cytosol, cleavage of the pre-miRNA stem-loop into a miRNA duplex is achieved by the RNase III enzyme Dicer under assistance of the dsRBPs TRBP and PACT (Fareh et al., 2016; Lee et al., 2013, 2006). The miRNA duplex is loaded into an Argonaute (Ago1-4) protein and the passenger strand (miRNA*) is expelled. This results in formation of the minimal RNA induced silencing complex (RISC), consisting of the miRNA guide strand and Ago protein. Generally, complementarity of the seed-region at position 2-8 of the miRNA confers target specificity of RISC. Through extended base-pairing towards the 3'-end of the miRNA the association of RISC at the target RNA and therefore gene repression can be further

strengthened (McGeary et al., 2019). For a detailed review on biogenesis and function of metazoan miRNAs see (Bartel, 2018).

1.2.1 The RNA induced silencing complex

The silencing of target RNAs by RISC is generally performed via two distinct pathways. In cases, where perfectly complementary base-pairing between the miRNA and its target takes place, endonucleolytically active Ago proteins directly slice the target transcript (Meister et al., 2004; Peters and Meister, 2007). In contrast, the prevalent pathway in animals is activated through imperfect base-pairing of the miRNA to the target, precluding catalytic activity of Ago. Here, silencing of target RNAs is achieved through recruitment of protein partners, that mediate translational repression, deadenylation, decapping and mRNA degradation (Jonas and Izaurralde, 2015). The default pathway in most post-embryonic cells involves miRNA mediated inhibition of translation, followed by prominent RNA degradation (Djuranovic et al., 2011). The flexible adaptor protein GW182/Tnrc6 interacts with the poly-A binding protein (PABP) and recruits cytoplasmic deadenylase complexes (CCR4-NOT and PAN2-PAN3), resulting in deadenylation of the mRNA. A network of direct physical interactions then results in decapping of the deadenylated mRNA through Dcp2 (Chen et al., 2014; Jonas and Izaurralde, 2015). The decapping process is supported by several cofactors, including the RNA helicase Ddx6 and the enhancers of decapping Edc3 and 4 (Chen et al., 2014; Mathys et al., 2014; Rouya et al., 2014). Finally, the major cytoplasmic 5'-3'-exoribonuclease 1 (Xrn1) degrades decapped and deadenylated mRNAs. Interestingly, exonucleolytic mRNA degradation can also be performed co-translationally in polysomes (Tat et al., 2016). However, the miRNA mediated gene silencing can be stalled and reversed at multiple steps. This includes uncoupling of Ddx6-mediated translational repression from mRNA degradation (Freimer et al., 2018). Further, translational repression seems to be preferred over irreversible mRNA degradation in oogenesis, early embryogenesis and, interestingly, in neurons (Nawalpuri et al., 2020). In neurons, reversible translation repression is a central concept hypothesized to enable fast spatiotemporally controlled gene expression through local translation, ensuring synaptic plasticity (Kiebler and Bassell, 2006).

1.2.2 Regulation of neuronal RISC

The activity of RISC can be modulated through external signals, such as neuronal activity, at several levels. This includes changes in expression levels, posttranslational modification and localization of one or more RISC components. For instance, increased expression of Ago2,

GW182 and Ddx6 has been observed in injured axons (Wu et al., 2013). In dendrites, neuronal activity driven phosphorylation of Ago2 at residue S387 strengthens its interaction with GW182 (Rajgor et al., 2018). This results in increased miRNA-mediated gene silencing and dendritic spine shrinkage. It has further been shown that RNAi components Dicer and GW182 are required for dendritic arborization (Davis et al., 2008; Nawalpur and Muddashetty, 2020). In addition to changes in RISC protein components, altered miRNA levels also play an important role in neuronal physiology. The maintenance of neuronal long-term potentiation (LTP) and dendritic spine enlargement for example are dependent on the expression of miR-26a and miR-384-5p (Gu et al., 2015). By now several miRNAs have been shown to localize to synapses, where they impact dendritic growth and spine morphology (Antoniou et al., 2018; Rajgor et al., 2018; Schratt et al., 2006). Recent evidence suggests that maturation of some of these miRNAs occurs locally in dendrites and that this may be regulated by neuronal activity (Antoniou et al., 2018; Bicker et al., 2013; Sambandan et al., 2017; Zampa et al., 2018). A prominent example here is the brain-specific miR-134, that represses expression of LIM domain kinase 1 (Limk1) (Rajgor et al., 2018; Schratt et al., 2006). Limk1 is important for activity-dependent dendritic spine homeostasis. Excitingly, the RBP required for dendritic localization and proper function of the pre-miR-134 has been identified, the DEAH-box helicase DHX36 (Bicker et al., 2013). This opens the question, whether transport and maturation of other miRNAs is regulated by RBPs. For a detailed review of the function and regulation of neuronal RISC please see (Nawalpur et al., 2020).

Silencing of gene expression by RISC is also dependent on interactions with other RBPs. As introduced in the beginning, mRNAs are bound and regulated by multiple RBPs in a competitive or cooperative manner (Iadevaia and Gerber, 2015). For example FMRP and Mov10 collectively regulate accessibility of miRNA binding sites (Kenny et al., 2014). Furthermore, RISC recruitment to the mRNA target (Kim et al., 2009) and miRNA biogenesis itself can be regulated by RBPs (Treiber et al., 2017). For instance processing of synaptic pre-miR-138 can be regulated by the RBP Matrin3 (Weiss et al., 2019). Most of the known interactions between RBP and RISC have been generated in cell lines. However, neuronal RISC differs from cell lines, *e.g.* translational repression is generally preferred over RNA degradation. It is therefore important to understand how RISC integrates into the neuronal RBP network. The following two paragraphs focus on two key RBPs that are expressed in neurons and have been partially linked to miRNA-mediated gene silencing.

1.3 The Staufen protein family

The family of Staufen (Stau) proteins are multifunctional *trans*-acting factors that specifically bind to double-stranded RNA via five dsRNA-binding domains (dsRBDs) (Lazzaretti et al., 2018; Masliah et al., 2013; Ramos et al., 2000) (Fig. 1.3). Stau was first described as essential localization factor for maternal RNAs in the *Drosophila* oocyte (St Johnston et al., 1991). The function in RNA localization and the Stau protein itself are both highly conserved across species (Allison et al., 2004; Bauer et al., 2019; Köhrmann et al., 1999; LeGendre et al., 2013; Liu, 2006; Ramasamy et al., 2006; Sharangdhar et al., 2017; St Johnston et al., 1991). Vertebrates carry two paralogs of Stau, Stau1 and Stau2, that both give rise to several splice isoforms (Duchaîne et al., 2002; Mallardo et al., 2003). There are important differences regarding the two Stau paralogs, that also localize to distinct dendritic particles in neurons (Duchaîne et al., 2002): (i) while Stau1 is ubiquitously expressed, Stau2 expression is highly enriched in neuronal tissue (Duchaîne et al., 2002) in comparison to the *Drosophila* ortholog; (ii) dsRBD1 is missing in Stau1; and (iii) dsRBD5 is inverted in mammalian Stau2, but not Stau1, in comparison to the *Drosophila* ortholog. The dsRBD5 is reported to have compromised RNA-binding capability and is not involved in Stau mediated *oskar* RNA transport in *Drosophila* oocytes. However, Stau contributes to *oskar* translation initiation at the posterior pole (Micklem et al., 2000). Interestingly, dsRBD5 is both necessary and sufficient to bind the *Drosophila* scaffold protein Miranda (Irion and St Johnston, 2007; Jia et al., 2015). Functionally, this protein-protein interaction is responsible for asymmetric localization of Stau during asymmetric division of *Drosophila* neuroblasts.

The contribution of the different dsRBDs to RNA-binding and in particular the specificity of Stau's ability in RNA binding has been a long-standing question. It has now been consistently shown that the conserved $\alpha\beta\beta\alpha$ structures in dsRBD3 and dsRBD4 are sufficient for RNA-binding (Bycroft et al., 1995; Duchaine et al., 2002; Lazzaretti et al., 2018; Ramos et al., 2000; Wickham et al., 1999). Additional contributions to RNA-binding by combinatorial binding of dsRBD1 and dsRBD2 have been recently implicated for mouse Stau2 (Heber et al., 2019). Previous data from *Drosophila*, however, only observed RNA-binding by dsRBD2, once the insertion was removed (Micklem et al., 2000). While dsRBPs clearly bind to RNA structures, it was not well understood if and how sequence-dependent RNA recognition would indeed contribute to RNA target specificity (Masliah et al., 2013). Similar to the combined shape and sequence-specific readout detected for RNA-binding of the dsRBP ADAR1 (Stefl et al., 2010),

the base-directed contact of Stau1 to *ARF1* dsRNA has been recently described (Lazzaretti et al., 2018; Yadav et al., 2020). Here, in addition to RNA backbone interactions, dsRBD3 and dsRBD4 are both in direct contact with guanines and cytosines in the minor groove of the A-form RNA. The overall structure of full length Stau1 has only been recently resolved (Visentin et al., 2020). The different dsRBDs of Stau1 are organized like beads on a string, connected by flexible linkers that enable structural plasticity. The possibility for Stau1 to adapt to multiple conformations may explain its diverse and sometimes contradicting functionality *in vivo*.

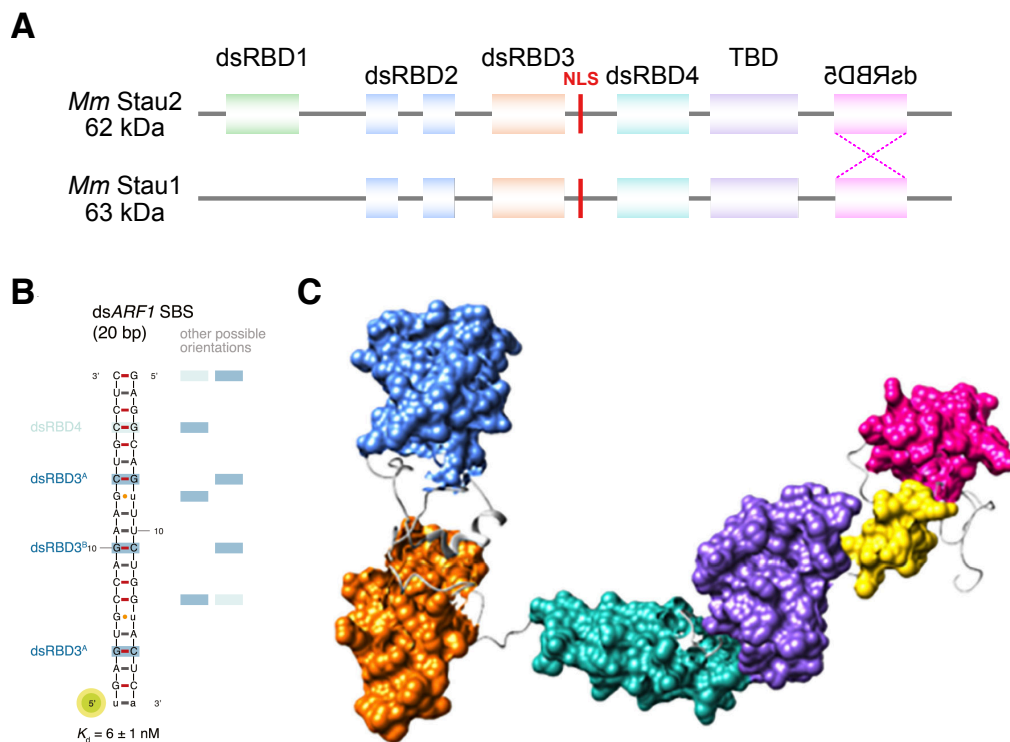


Figure 1.1: The Staufen protein family. (A) The double-stranded RNA-binding protein Staufen has two mammalian orthologs, Stau1 and Stau2 (shown here *mus musculus*). Both orthologs harbor a nuclear localization signal (NLS) and a tubulin binding domain (TBD). Stau2 contains five double-stranded RNA-binding domains (dsRBD), with dsRBD5 being inverted and incapable of RNA binding. By comparison, Stau1 is lacking dsRBD1, but contains correctly orientated dsRBD5. Alternative splicing at the 5'- and/or 3'-end produces shortened isoforms. (B) Stau1 dsRBD3 and 4 interact with the sugar-phosphate backbone and specific RNA bases (highlighted as blue boxes) of the target RNA duplex. Schematic representation of the *ARF1* RNA duplex bound by dimerized human Stau1 from (Lazzaretti et al., 2018). (C) The dsRBDs of Stau1 are connected via flexible linkers forming a beads-on-a-string structure. Conformational rearrangements of dsRBD3 (orange) and 4 (turquoise) may explain target RNA binding plasticity of Staufen proteins. Structure model of the full length human Stau1 55 kDa isoform based on small-angle X-ray scattering and Ensemble Optimization Method from (Visentin et al., 2020).

The profound lack of knowledge about the primary sequence specificity of Stau RNA-binding seriously complicated target prediction for Stau. Here, *in silico* modelling of Staufen recognition sites (SRS) based on biochemically detected Stau target RNAs have given first insight into characteristics of bound RNA structures (Heraud-Farlow et al., 2013; Laver et al., 2013). Stau2 targets show an enrichment of SRSs in the 3'-UTRs and those 3'-UTRs are also significantly longer compared to unbound 3'-UTRs. The development of the hiCLIP (RNA hybrid and individual-nucleotide resolution UV cross-linking and immunoprecipitation) technology enabled the first real breakthrough in elucidating Stau target binding on the molecular level (Sugimoto et al., 2015). Using hiCLIP, RNA duplexes bound by Stau1 in the physiological *in vivo* environment could be defined (Sugimoto et al., 2015). Consistent with the results before, the majority of RNA duplexes was detected in the 3'-UTRs of target mRNAs with loop lengths even longer than 500 nucleotides (20%). These long intramolecular duplexes suggest that Stau1 plays a role in compacting the 3'-UTR, possibly enabling interaction of proteins bound to distal parts of the mRNA. Further, Stau-bound RNA duplexes can also be formed intermolecularly (Sugimoto et al., 2015). One interesting example here is base pairing of an Alu element in the 3'-UTR of an mRNA with a long non-coding RNA (lncRNA), preceding Stau1-mediated RNA decay (Gong and Maquat, 2011). Even with the recent technical advances in RNA structure elucidation, the flexible structure of Stau and its limited sequence specificity still make it somewhat hard to delineate and predict a consensus RNA motif for Stau binding.

Mammalian Stau1 and Stau2 differ from *Drosophila* Stau as they harbor an additional tubulin-binding domain (TBD) and a nuclear localization sequence (NLS) (Macchi et al., 2004; Martel et al., 2006; Wickham et al., 1999). Further, alternative splicing of Stau2 at both the C- and N-terminus generates two additional isoforms (59 kDa and 52 kDa) that carry truncated versions of dsRBD1 and dsRBD5 and harbor an additional nuclear export sequence (NES) (Miki and Yoneda, 2004). This leads to isoform specific nuclear localization of Stau2 and distinct export mechanisms. The nuclear export of all isoforms depends on the RNA-binding capability of dsRBD3, as an RNA-binding mutant resulted in accumulation of Stau2 in the nucleolus (Macchi et al., 2004). In addition, the nuclear export of the Stau2 62 kDa isoform requires RNA-dependent interaction with the miRNA-export factor Exportin5 (Macchi et al., 2004), whereas the 59 kDa isoform is exported via Exportin1/Crm1 (Miki and Yoneda, 2004). It is hypothesized that the NLS is concealed upon RNA-binding by dsRBD3 and dsRBD4 (Macchi et al., 2004). Therefore, RNA-binding would promote nuclear export and prevent reimport

into the nucleus. This suggests that Stau2 RNP assembly starts in the nucleus, as it has been described for other RBPs (Giorgi and Moore, 2007; Kiebler et al., 2005).

1.3.1 Neuronal Staufen2

Much information about the molecular characteristics of Stau were gathered from studies on either mammalian Stau1 or orthologs from other species. I, however, am interested in the mechanism of action and function of the neuronally enriched Stau2. These are most likely distinct, since both, Stau1 and Stau2, are present in separate dendritic particles (Duchaîne et al., 2002), bind to distinct RNA target sets (Furic et al., 2007) and vary in their dsRBD composition (Macchi et al., 2004).

In addition to Stau2 function in early neurogenesis, a growing suit of evidence implicates Stau2 function in the mature nervous system, including neuronal maturation, synaptic plasticity and memory formation (Heraud-Farlow and Kiebler, 2014; Schieweck et al., 2020). For instance, in primary neuronal cultures deficiency for Stau2 results in transport and localization defects for *Regulator of G-protein signaling 4 (Rgs 4)*, the intron-retained *Calmodulin 3 (Calm3)* and, as shown by others, *Microtubule-associated protein 1b (Map1b)* mRNA via their 3'-UTRs (Bauer et al., 2019; Lebeau et al., 2011; Sharangdhar et al., 2017). In the case of *Map1b*, this results in reduction of the encoded protein regulating metabotropic Glutamate receptor (mGluR)-dependent long-term depression (LTD), a process important for learning and memory (Lebeau et al., 2011). This goes in line with a recent *in vivo* study observing impaired LTD and preferred LTP, thereby misbalancing synaptic plasticity in a transgenic rat model with forebrain specific depletion of Stau2 (Berger et al., 2017). Behavioral tests in Stau2 deficient rats and mice complemented these electrophysiological phenotypes. These animals show reduced locomotion and deficits in (spatial) novel object identification, spatial working memory and associative learning and memory (Berger et al., 2017; Popper et al., 2018). On the morphological level, Stau2 has been implicated in dendritic spine formation. In primary hippocampal rat cultures, selective downregulation of Stau2 resulted in rearrangement of the dendritic actin cytoskeleton network and reduction and malformation of dendritic spines (Goetze et al., 2006). Together, these findings strongly link Stau2 to proper nervous system function and highlight the importance for understanding the molecular function of Stau2 in gene expression homeostasis (Schieweck et al., 2020).

The identification of protein and RNA interactors of Stau2 from embryonic day 17 (E17) rat brain by the Kiebler lab in 2013 prepared the grounds for dissecting the molecular function of Stau2 in neurons (Fritzsche et al., 2013; Heraud-Farlow et al., 2013). Among other RNAs, Stau2 bound to (Heraud-Farlow et al., 2013; Sharangdhar et al., 2017), stabilized RNA levels (Heraud-Farlow et al., 2013) and mediated directed dendritic transport (Bauer et al., 2019) of *Rgs4* mRNA. *Rgs4* mRNA localizes to distal dendrites (Ehse et al., 2020; Heraud-Farlow et al., 2013), where the encoded protein shortens G-protein coupled receptor (GPCR) signaling by acting as a GTPase activating protein resulting in faster GTP hydrolysis on the G_{α} -protein (Gerber et al., 2016). *Rgs4* is therefore a prime candidate for dissecting RNA recognition of Stau2 and to understand how Stau2 orchestrates molecular mechanisms such as RNP assembly. Interestingly, seven other RNAs involved in the GPCR signaling pathway were also bound by Stau2 (Heraud-Farlow et al., 2013). This includes *Calm3* mRNA. More yet, Stau2-dependent regulation of dendritic localization (and nuclear export) of *Calm3* was mediated by a retained intron within the 3'-UTR (Sharangdhar et al., 2017). It is interesting to note that certain pre-miRNAs were also enriched in Stau2 immunoprecipitations from E17 rat brain (Heraud-Farlow et al., 2013), including pre-miR-26a. Further, unpublished preliminary data by Jacki Heraud-Farlow show a repressive function of Stau2 on pre-miR-26a maturation (J. Heraud-Farlow, PhD thesis, University of Vienna). Together, these data imply that the dsRBP Stau2 is able to bind to the short stem-loop structure formed by pre-miRNAs and potentially regulate their maturation, as it has been observed for other dsRBPs (Treiber et al., 2017).

The second study performed in parallel by the Kiebler lab focused on the identification of potential protein interactors present in Stau2 particles from E17 rat brains (Fritzsche et al., 2013). Here, several translational repressors co-precipitated with Stau2, including the well-known RBPs Pum2 and FMRP. Among these repressors were also proteins involved in RISC or RISC associated proteins. Specifically, Ago2, Ddx6 and Mov10 were enriched in Stau2 RNPs. The interaction between Stau2 and those RISC components was, however, mostly RNA dependent. Interestingly, Stau2 interacted with interferon-inducible double-stranded RNA-dependent protein kinase activator A (Prkra/PACT) protein in a manner independent of RNase treatment. In a complex together with TRBP and Dicer, PACT is required for small ncRNA biogenesis (Lee et al., 2006; Pullagura et al., 2018). Collectively these data indicate that the mRNA in Stau2 RNPs is translationally repressed, which might (at least in part) be achieved through RNAi. This is interesting, as Stau2 has been shown to associate with

ribosomes and the (rough) endoplasmic reticulum (Graber et al., 2017; Heraud-Farlow and Kiebler, 2014; Luo et al., 2002) and, further, Stau1-RNA binding has been linked to increased polysome association (Zheng et al., 2020). In addition, Stau2 target RNA levels decrease rather than increase upon knockdown of Stau2 (Heraud-Farlow et al., 2013). As Stau2 itself seems to promote expression of target genes, it is plausible that in addition to its function in RNA transport, Stau2 rather prevents strong activity of translational repressors and, therefore, balances gene expression. During transport, Stau2 RNPs are hypothesized to be translationally repressed and this repression is reversed upon arrival at the destination, *e.g.* the activated synapse, to enable local translation (Doyle and Kiebler, 2011; Kiebler and Bassell, 2006; Schieweck et al., 2020).

1.4 HuR/ELAVL1

Another group of protein interactors identified in the proteomic analysis of Stau2 granules consists of the Human-antigen (Hu) protein family (Fritzsche et al., 2013). While these proteins were also detected in the negative controls, Hu CLIP sites were found to be enriched in proximity to Stau1 binding sites determined by combined iCLIP and hiCLIP experiments (personal communication, A. Chakrabarti and J. Ule, Crick Institute, London; (Sugimoto et al., 2015)).

The mammalian family of Hu RBPs consists of four homologs of the *Drosophila* embryonic lethal abnormal vision (ELAV) protein, namely HuR (ELAVL1), HuB (ELAVL2), HuC (ELAVL3), and HuD (ELAVL4). These RBPs contain three RNA recognition motifs (RRMs) and bind to uracil-rich sequences interspersed with guanines and adenosines (Ravanidis et al., 2018). Whereas HuR is ubiquitously expressed, HuB-D protein expression is highly enriched in neurons and their binding to *HuR* 3'-UTR has been implicated in decreased expression of HuR in mature neurons (Mansfield and Keene, 2012; Zhao et al., 2020). Homozygous knockout of HuR is embryonically lethal and HuR depletion in adult mice results in lethality within ten days (Ghosh et al., 2009; Katsanou et al., 2009), highlighting the importance of HuR for cellular function. HuR has a neuroprotective function as illustrated by conditional loss-of-function studies. Specifically, neuron-specific knockout of HuR leads to increased inflammation and apoptosis, resulting in phenotypes resembling motor neuron and neurodegenerative diseases (Skliris et al., 2015; Sun et al., 2018).

Although HuR is predominantly found in the nucleus, it can shuttle to the cytoplasm and this translocation is required for adult neurogenesis in mice (Wang et al., 2019). In the nucleus, HuR participates in splicing regulation and alternative polyadenylation (Ravanidis et al., 2018). Interestingly, collective RNA-binding by the Hu family members in central nervous system underlies the extension of neuronal 3'-UTR isoforms by promotion of alternative polyadenylation (Wei et al., 2020). In the cytoplasm, HuR has been found to be enriched in cytoplasmic P-bodies, where predominantly AU-rich RNAs are found (Hubstenberger et al., 2017). It is, however, also present in Stau2 transport particles (Fritzsche et al., 2013). It was long thought that the main function of HuR would be the stabilization of RNAs by competing with RNA decay factors (such as AUF1/hnRNPd) for binding to AU-rich elements (Brennan and Steitz, 2001; Lal et al., 2004). Recent studies, however, suggest that this picture is more complex as HuR is also implicated in RNA destabilization and translational control through distinct cooperative and antagonistic mechanisms (Chang et al., 2010; Ehses et al., 2020; Kim et al., 2009; Li et al., 2018). In addition, HuR has been shown to facilitate membrane localization of newly-translated CD47 (leukocyte surface antigen CD47) protein by binding to the 3'-UTR of the translated *CD47* mRNA, thereby promoting cell survival (Berkovits and Mayr, 2015). This mechanism depends on alternative polyadenylation of *CD47* mRNA that acts as a scaffold for protein-protein interactions proposing a truly novel mechanism of protein localization. Together, this data places HuR as a major regulator of post-transcriptional gene regulation and show the importance to further dissect its role in neuronal physiology. It will be intriguingly to further elucidate its interactions with other RBPs in gene expression homeostasis and see how HuR promotes neuronal health and survival.

2 Aims

The overall goal of my PhD thesis was to investigate the influence of RBPs on the function of the RNA induced silencing complex in neurons. I decided to tackle this objective by choosing two complementary strategies, on one hand the exploration of a single target RNA, and on the other hand a genome-wide approach from the RBP direction. Based on previous data by the Kiebler Lab, I chose the *Stau2* target RNA *Rgs4* for the target-based project and studied how its regulation by miRNA/RISC is controlled through other RBPs, in this case AU-rich element binding protein HuR (**Chapter A**). In the second project, I exploited quantitative mass spectrometry (by R. Schieweck) in combination with RNA sequencing data from *Stau2* deficient neurons to study the global interdependency of RBPs with a focus on the miRNA pathway. Specifically, I aimed at defining the molecular interaction of *Stau2* and *Ago2* and the role of this interaction for neuronal physiology (**Chapter B**). In order to understand how *Stau2* might regulate RNA structure and therefore accessibility of miRNA binding sites, I collaborated with S. M. Fernández Moya, to unravel the underlying RNA characteristics important for *Stau2* binding (**Chapter C**). Ultimately, the insights from the two complementary approaches were combined to get a better understanding of the role of RNA structure and miRNA-loaded Ago in the neuronal RBP network.

Overall, I tried to address the following key questions in my thesis:

- (i) How do RBPs interact with each other on a single target RNA?
- (ii) How is RNAi regulated in the neuronal RBP network?
- (iii) How does the RNA structure contribute to neuronal RNP assembly?

3 Chapter A

This chapter contains the research article published in *RNA Biology* (2020) with the title

Synergistic regulation of *Rgs4* mRNA by HuR and miR-26/RISC in neurons

by

Janina Ehses, Sandra M. Fernández-Moya, Luise Schröger and Michael A. Kiebler*

* corresponding author

Author contributions:

Janina Ehses, Sandra M. Fernández-Moya and Michael A. Kiebler designed the study. Janina Ehses performed and analyzed experiments. Luise Schröger contributed to *in vitro* RNA affinity purification experiments. Janina Ehses prepared all figures. Janina Ehses and Michael A. Kiebler wrote the manuscript.

Synergistic regulation of *Rgs4* mRNA by HuR and miR-26/RISC in neurons

Janina Ehses , Sandra M. Fernández-Moya , Luise Schröger , and Michael A. Kiebler 

BioMedical Center, Medical Faculty, Ludwig Maximilians University of Munich, Martinsried, Germany

ABSTRACT

The negative regulator of G-protein signalling 4 (*Rgs4*) is linked to several neurologic diseases, *e.g.* schizophrenia, addiction, seizure and pain perception. Consequently, *Rgs4* expression is tightly regulated, resulting in high mRNA and protein turnover. The post-transcriptional control of gene expression is mediated via RNA-binding proteins (RBPs) that interact with mRNAs in a combinatorial fashion. Here, we show that in neurons the RBP HuR reduces endogenous *Rgs4* expression by destabilizing *Rgs4* mRNA. Interestingly, in smooth muscle cells, *Rgs4* is stabilized by HuR, indicating tissue-dependent differences in HuR function. Using *in vitro* RNA-based pulldown experiments, we identify the functional AU-rich element (ARE) within the *Rgs4* 3'-UTR that is recognized and bound by HuR. Bioinformatic analysis uncovered that this ARE lies within a highly conserved area next to a miR-26 binding site. We find that the neuronal-enriched miR-26 negatively influences *Rgs4* expression in neurons. Further, HuR and miR-26 act synergistically in fluorescent reporter assays. Together, our data suggest a regulatory mechanism, in which an RBP selectively destabilizes a target mRNA in cooperation with a miRNA and the RISC machinery.

ARTICLE HISTORY

Received 14 April 2020
Revised 22 June 2020
Accepted 9 July 2020

KEYWORDS



Mirna; RBP; cooperative binding; mRNA stability; neuronal RNA; *Rgs4*; HuR; ELAVL1; miR-26


Introduction

The negative regulator of G-protein signalling 4 (*Rgs4*) plays an important role in synaptic plasticity as well as in many diseases of the nervous system, including schizophrenia, addiction, seizure, pain and neurodegenerative disorders [1–5]. *Rgs4* encodes a GTPase-activating protein of the G protein-coupled receptor (GPCR) pathway, modulating receptor-mediated neuronal signalling at the synapse [5,6]. Both *Rgs4* protein as well as *Rgs4* mRNA show a high turnover rate, suggesting extensive post-transcriptional and post-translational regulation [7,8]. In contrast to the protein level, where *Rgs4* regulation has been studied extensively [5], knowledge about the regulation of *Rgs4* mRNA in neurons is scarce. Post-transcriptional gene regulation enables spatially and temporally fine-tuned protein production and is key in the nervous system, where targeted local protein synthesis at single synapses can take place [9,10]. The control of this process is likely to be mediated by the combinatorial binding of sequence- or structure-specific RNA-binding proteins (RBPs) and microRNAs (miRNAs) [11] preferentially to the 3'-untranslated region (3'-UTR) of target mRNAs. miRNAs are small noncoding RNAs that complementarily bind and repress target mRNAs by associating with Argonaute (Ago) proteins [11] and recruiting the RNA induced silencing complex (RISC). In neurons, *Rgs4* is post-transcriptionally regulated by the double-stranded RBP Stauf2. Endogenous *Rgs4* mRNA is reduced upon silencing of Stauf2 both *in vitro* [12] and *in vivo* [13], suggesting a role of Stauf2 in the regulation of *Rgs4* mRNA levels. In addition, Stau2 regulates dendritic transport of an *Rgs4* 3'-UTR reporter in primary hippocampal neurons [14].

While certain RBPs are enriched in nervous tissue, *e.g.* FMRP, Stauf2 or Pumilio2 [15], the vast majority of RBPs are ubiquitously expressed. HuR/ELAVL1 is a ubiquitously expressed RBP with a crucial role in the nervous system [16–19] as well as in muscle [7,20,21]. *Rgs4* mRNA is a physiological target of HuR [7]. Overexpression of *Rgs4* can rescue vascular phenotypes observed in smooth muscle cells deficient for HuR [21]. In those cells, HuR stabilizes *Rgs4* mRNA [7]. HuR binds to transcripts containing AU-rich elements (AREs), thereby mainly stabilizing the mRNA. There are cases, however, where HuR exerts the opposite effect [22,23]. Depending on its mode of action, it might act in a cooperative or competitive manner. Competition for binding with miRNAs due to steric hindrance or RNA structure-mediated effects has been reported [22,24,25].

To evaluate the role of HuR in the regulation of *Rgs4* mRNA expression in neurons, we used RNA interference by expressing a short hairpin RNA (shRNA) against HuR. The resulting downregulation of endogenous HuR expression in mature neurons caused an upregulation of *Rgs4* mRNA. Fluorescent reporter assays and *in vitro* RNA affinity purification allowed us to define the binding sites for both miR-26 and HuR in the *Rgs4* 3'-UTR, which are both located within the same predicted, highly conserved RNA hairpin structure. Detailed analysis of both factors allowed us to unravel a synergistic action of the RBP HuR together with the miR-26/RISC complex in the regulation of *Rgs4* mRNA in mature neurons. Our proposed mechanism highlights the fine-tuned interplay between *trans*-acting factors, *e.g.* the RBP and the miRNA/RISC, depending on the RNA target structure.

CONTACT Michael A. Kiebler  mkiebler@lmu.de  Department of Cell Biology, BioMedical Center, Ludwig Maximilians University of Munich, Planegg-Martinsried 82152, Germany

 Supplemental data for this article can be accessed [here](#).

© 2020 The Author(s). Published by Informa UK Limited, trading as Taylor & Francis Group. This is an Open Access article distributed under the terms of the Creative Commons Attribution License (<http://creativecommons.org/licenses/by/4.0/>), which permits unrestricted use, distribution, and reproduction in any medium, provided the original work is properly cited.

Results

HuR destabilizes *Rgs4* mRNA

We tested the influence of HuR expression on *Rgs4* mRNA levels in primary cortical neurons through knock-down (KD) of endogenous HuR by shRNA. The shRNA against HuR enables specific knock-down of HuR (Fig. 1A, Sup. Fig. 1B) but not of the neuron-specific Hu proteins, HuB/C/D (Sup. Fig. 1A). Contrary to published data from smooth muscle cells [7], *Rgs4* mRNA levels increased twofold upon knock-down of HuR (Fig. 1B). Downregulation of a different RBP, Pumilio2, did not result in altered *Rgs4* mRNA levels (Sup. Fig. 1C,D). We further determined if the *Rgs4* mRNA upregulation is due to effects of HuR on mRNA stability rather than transcription or splicing. As shown in Fig. 1C, treating neurons with the transcription inhibitor Actinomycin D resulted in a strong drop of *Rgs4* mRNA. This effect, however, could be rescued when HuR was knocked down (Fig. 1C, Sup. Fig. 1E). In order to rule out a major effect of HuR on *Rgs4* splicing, we tested whether a different isoform is detected upon HuR knock-down by RT-PCR. We only detected the major

annotated isoform *mmuRgs4-201* (Sup. Fig. 1F). Together, this data suggests that *Rgs4* mRNA is rapidly degraded, resulting in a high turnover rate and that HuR is important for *Rgs4* destabilization in neurons. Therefore, we decided to investigate whether this relation is also reflected by the expression pattern of HuR protein and *Rgs4* mRNA.

HuR protein and *Rgs4* mRNA show divergent expression with neuronal maturation

We tested the expression pattern of HuR protein and *Rgs4* mRNA during neuronal maturation in cell culture. During maturation of neurons, neuronal processes grow out, build synaptic protrusions and finally connect to each other through fully functioning synapses [26]. Expression of the Hu proteins HuB/C/D has been well described in neurons [27,28]. The neuronal role of HuR, however, has only been recently investigated [16,17]. HuR protein expression decreased with neuronal maturation in our primary cortical neuron culture (Fig. 1D). In contrast to HuR protein, we found that *Rgs4* mRNA levels increased with neuronal

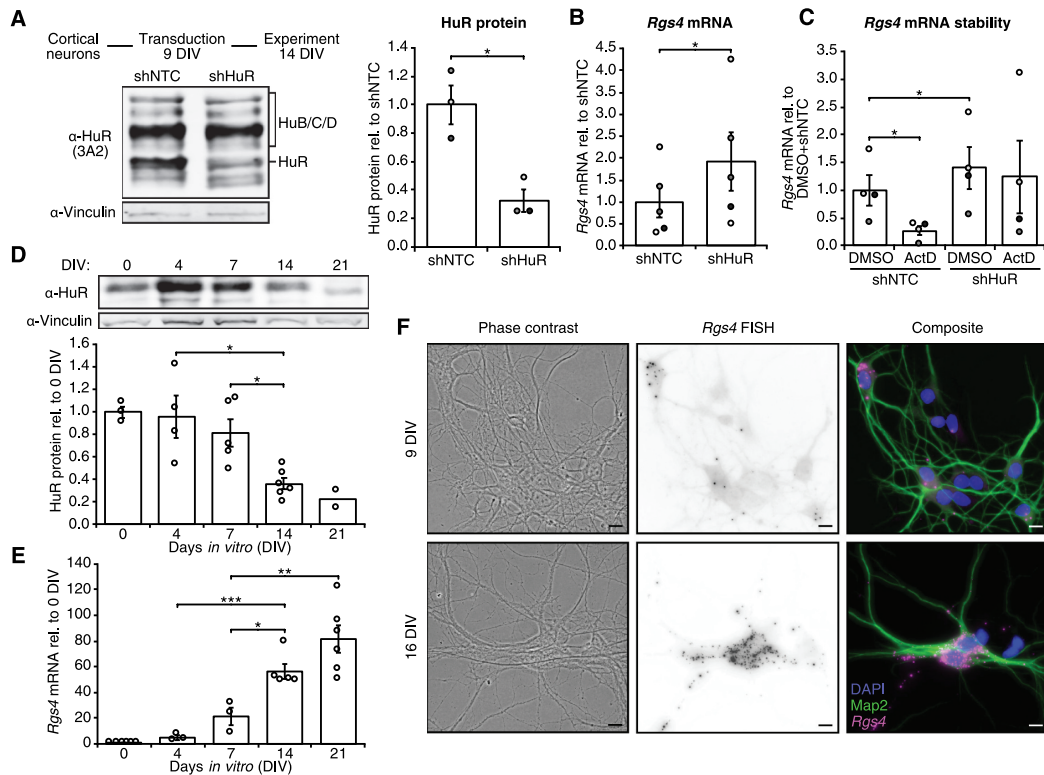


Figure 1. HuR destabilizes *Rgs4* mRNA in primary neurons. (A) Transduction of cortical neurons with shNTC or shHuR for 5 days. Left panel, experimental outline and Western blot against HuR of 14 DIV rat cortical neurons transduced at 9 + 5 DIV with lentiviruses expressing shNTC or shHuR. Right panel, quantification of HuR Western blot signal, normalized to shNTC. Paired Student's *t*-test. (B) Quantification of endogenous *Rgs4* mRNA by qRT-PCR in 14 DIV cortical neurons transduced at 9 + 5 DIV with lentiviruses expressing shNTC or shHuR, normalized to shNTC. Paired Student's *t*-test. (C) Analysis of *Rgs4* mRNA stability in 14 DIV cortical neurons transduced at 9 + 5 DIV with lentiviruses expressing shNTC or shHuR and treated with DMSO or ActD for 90 min at 14 DIV. *Rgs4* mRNA levels were quantified by qRT-PCR and normalized to DMSO+shNTC. Paired Student's *t*-test. (D) Quantification of Western blot HuR protein signal of rat cortical neurons at different DIV, normalized to 0 DIV. Unpaired Student's *t*-test. (E) Quantification of *Rgs4* mRNA qRT-PCR signal of rat hippocampal neurons at different DIV, normalized to 0 DIV. Unpaired Student's *t*-test. (F) Representative phase-contrast and pseudo-coloured fluorescence images of cortical neurons at 9 DIV and 16 DIV showing *Rgs4* FISH signal (magenta), staining for Map2 (green) and DAPI (blue). Scale bar 10 μm. All error bars are SEM from ≥ 3 independent biological replicates; asterisks represent *p*-values (**p* < 0.05, ***p* < 0.01, ****p* < 0.001). NTC non-targeting control; ActD Actinomycin D; DIV days *in vitro*; FISH fluorescent *in situ* hybridization.

maturation, measured both by qRT-PCR in hippocampal neurons (Fig. 1E) and by fluorescent *in situ* hybridization (FISH) against *Rgs4* in cortical neurons (Fig. 1F). Having established the relation between HuR and *Rgs4* mRNA in the endogenous context, we set out to define a possible HuR binding site in *Rgs4* mRNA.

HuR represses *Rgs4* expression through the *Rgs4* 3'-UTR

The coding sequence (CDS) of *Rgs4* consists of 618 bases; the 3'-UTR of 2,200 bases. We used the AREsite2 web database (<http://rna.tbi.univie.ac.at/>) to predict possible binding sites of HuR (Fig. 2A). Next, we used a fluorescent reporter assay consisting of eGFP only (Ctrl), a fusion protein of eGFP and *Rgs4* CDS and eGFP with the *Rgs4* 3'-UTR to define whether HuR affects *Rgs4* CDS reporter or 3'-UTR reporter expression (Fig. 2B). As shown in Fig. 2C, overexpression of tagRFP-HuR led to a decrease of *Rgs4* 3'-UTR reporter, but not Ctrl or CDS reporter expression. Consistent with this, knock-down of HuR by shRNAs resulted in the opposite effect, an increase of *Rgs4* 3'-UTR reporter, but not Ctrl or CDS reporter expression (Fig. 2D). Next, we defined the binding region of HuR in the *Rgs4* 3'-UTR using either full-length (FL) or three different fragments of the *Rgs4* 3'-UTR in an *in vitro* RNA purification experiment (trapping by RNA *in vitro* affinity

purification; TRAP). For TRAP, the RNA of interest is tagged with two MS2 stem loops (2MS2) and transcribed *in vitro*. After immobilizing the RNA on amylose beads via a maltose binding and MS2 coat fusion protein (MBP-MCP), beads were incubated with lysate from adult rat cortices (Fig. 2E). Here, HuR protein was fourfold enriched when using the *Rgs4* 3'-UTR FL RNA, but not by either CDS or MS2 only control RNA (Fig. 2F,G). Furthermore, the enrichment of HuR seems to be due to the binding of HuR to fragment 3, since fragment 1 and 2 did not show strong enrichment of HuR. Please note that binding of HuR was stronger in fragment 3 compared to *Rgs4* FL 3'-UTR. This could be due to altered RNA folding or binding of additional RBPs. The RBP Ago2 yielded a different enrichment pattern in the TRAP assay with prominent enrichment in fragment 2 (Fig. 2F). Quantification of the signals of neuron-specific Hu proteins HuB/C/D, which all run slower than HuR, showed slight enrichment (1.4-fold) with the *Rgs4* FL 3'-UTR as well as with fragment 1 and 3 (Sup. Fig. 2A,B). Together, we were able to show that binding of HuR takes place in the 3'-end of the *Rgs4* 3'-UTR; however, several AREs were predicted to be present in this fragment. Therefore, we decided to analyse the 3'-UTR for additional predictable features, e.g. miRNA binding sites and sequence conservation.

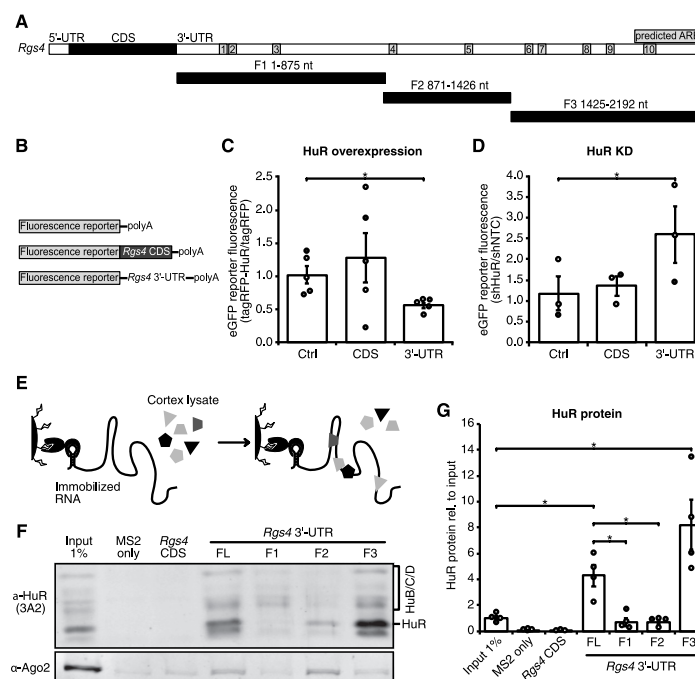
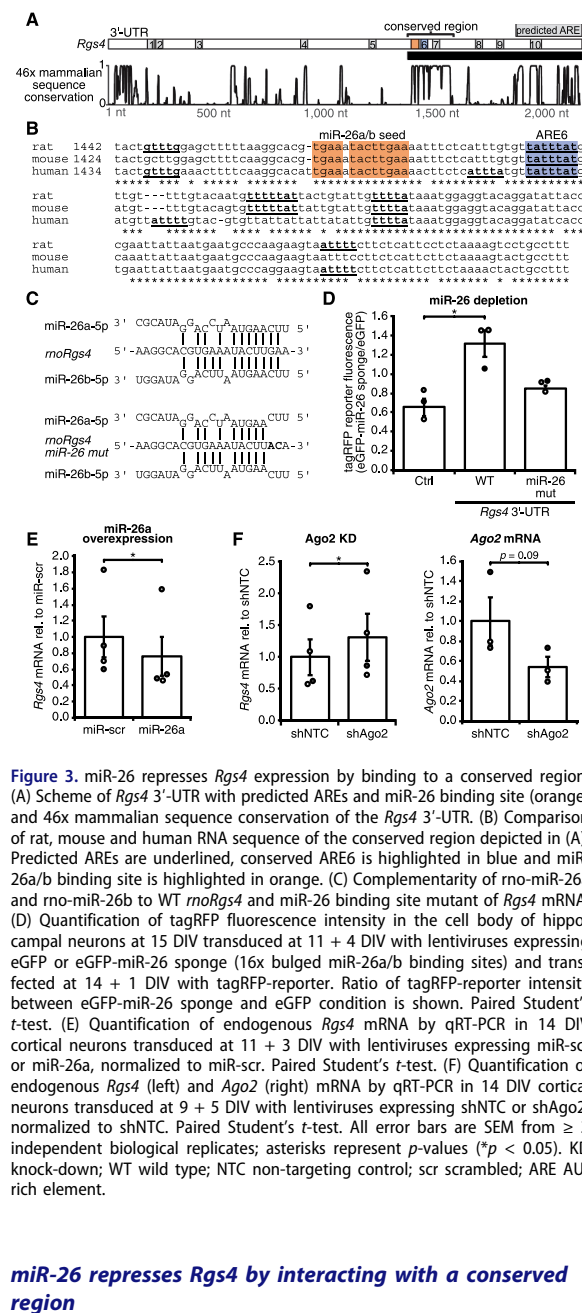


Figure 2. HuR represses *Rgs4* expression by binding to the 3' end of *Rgs4* 3'-UTR. (A) Scheme of *moRgs4* mRNA with predicted ARE sites and 3'-UTR fragments used in (F,G). (B) Scheme of fluorescence reporter constructs used in (C,D). (C) Quantification of eGFP fluorescence intensity in the cell body of hippocampal neurons at 15 DIV co-transfected at 14 + 1 DIV with eGFP-reporter and tagRFP or tagRFP-HuR. Ratio of eGFP-reporter intensity between tagRFP-HuR and tagRFP condition is shown. Paired Student's *t*-test. (D) Quantification of eGFP fluorescence intensity in the cell body of hippocampal neurons at 15 DIV transduced at 10 + 5 DIV with lentiviruses expressing shNTC or shHuR and transfected at 14 + 1 DIV with eGFP-reporter. Ratio of eGFP-reporter intensity between shHuR and shNTC condition is shown. Paired Student's *t*-test. (E) Scheme of *in vitro* RNA affinity purification (TRAP) of RBPs based on immobilization of *in vitro* transcribed RNA via 2xMS2 stem loops. (F,G) Representative Western blot against HuR and Ago2 (F) and quantification (G) of HuR enrichment in TRAP using 2xMS2 only, 2xMS2+ *Rgs4* CDS, 2xMS2+ *Rgs4* 3'-UTR and different 2xMS2+ *Rgs4* 3'-UTR fragments as depicted in (A) as bait RNA, normalized to input. Paired Student's *t*-test. All error bars are SEM from ≥ 3 independent biological replicates; asterisks represent *p*-values ($*p < 0.05$). KD knock-down; NTC non-targeting control; DIV days *in vitro*; ARE AU-rich element.

4 J. EHSE ET AL.



miR-26 represses *Rgs4* by interacting with a conserved region

In order to narrow down the HuR binding site(s), we analysed the sequence conservation in the *Rgs4* 3'-UTR of over 46 different mammalian genomes. As shown in Fig. 3A, a highly conserved region in the third fragment was standing out, containing two conserved possible AREs, ARE6 (UAUUUAU) and 7 (UUUUUA). Mainly positive effects of HuR on target expression levels have been previously reported [29]. In an interdependent mechanism together with the miRNA let-7, Gorospe et al. reported HuR to have a repressive effect on *c-myc* [22]. We asked whether the repressive effect of HuR on *Rgs4* mRNA was caused by other factors that associated with *Rgs4* mRNA. Using

the prediction software TargetScanMouse7.2, we analysed *Rgs4* for predicted miRNA binding sites. Interestingly, the webserver found a conserved miR-26 8mer binding site within the conserved region of the *Rgs4* 3'-UTR, in close proximity to the predicted ARE6 (Fig. 3B). miR-26 is a family of neuronal-enriched miRNAs [30,31], consisting of miR-26a and miR-26b, both shown to be important for neurogenesis [31], maintenance of long-term potentiation and dendritic spine enlargement [32]. As shown in Fig. 3C, miR-26a/b exhibit extended predicted binding to *Rgs4* mRNA in extension to the 8mer binding site, proposedly further strengthening the interaction. Introduction of two point mutations in the miR-26 binding site in *Rgs4* reduces complementarity and should abrogate miR-26 binding (Fig. 3C). We used a fluorescent reporter assay with tagRFP only (Ctrl), tagRFP fused to *Rgs4* 3'-UTR, or the *Rgs4* 3'-UTR miR-26 mutant to investigate the effect of miR-26 on *Rgs4* expression. Coexpression of a miR-26a/b sponge construct fused to eGFP depleted the levels of free miR-26. As depicted in Fig. 3D, depletion of miR-26 led to an upregulation of the WT *Rgs4* 3'-UTR reporter, but not the miR-26 mutant reporter, suggesting that miR-26 negatively regulates *Rgs4* expression by binding to the conserved region. We next tested whether this effect could also be reproduced for endogenous *Rgs4*. Indeed, overexpression of miR-26a in cortical neurons led to a reduction of *Rgs4* mRNA levels, as measured by qRT-PCR (Fig. 3E). Furthermore, knock-down of Ago2, an essential RISC component, resulted in *Rgs4* mRNA upregulation (Fig. 3F). Overexpression of miR-26a or knock-down of Ago2 did not alter *HuR* mRNA levels (Sup. Fig. 3A,B). In sum, miR-26 is repressing *Rgs4* expression through interaction with a binding site within a conserved region of the *Rgs4* 3'-UTR. This opens the question whether HuR and miR-26 synergistically act in reducing *Rgs4* mRNA levels.

HuR and miR-26 show an interdependent mechanism of *Rgs4* regulation

To explore the working model that HuR destabilized *Rgs4* mRNA by an interdependent effect with miR-26, we examined the conserved region for predicted secondary structures. Using thermodynamic structure prediction (RNAfold), we found the HuR and the miR-26 binding site to be in close proximity within the same RNA hairpin structure (Fig. 4A, Sup. Fig. 4A). We hypothesize a model where both miR-26 and HuR association with the RNA are needed to open the hairpin structure and enable sufficient repression of *Rgs4*. Using the TRAP assay, we evaluated the binding of HuR to WT, ARE6 mutant or miR-26 mutant *Rgs4* 3'-UTR RNAs. Neither of the mutants led to major changes of the predicted hairpin structures or significantly changed the minimal free energy of miR-26 binding to *Rgs4* mRNA (Fig. 4A, Sup. Fig. 4A,B). As shown in Fig. 4B, both mutating the HuR binding site (ARE6 mut) and the miR-26 binding site (miR-26 mut) significantly reduced HuR association with *Rgs4* 3'-UTR supporting our hypothesis of an interdependent mechanism. Binding of HuB/C/D to *Rgs4* 3'-UTR was unaffected by the mutations (Sup. Fig. 4C). Finally, we aimed at validating our results from the *in vitro* binding assay in hippocampal neurons using fluorescent reporter assays. Fig. 4D shows that overexpression of tagRFP-HuR led to a significant reduction

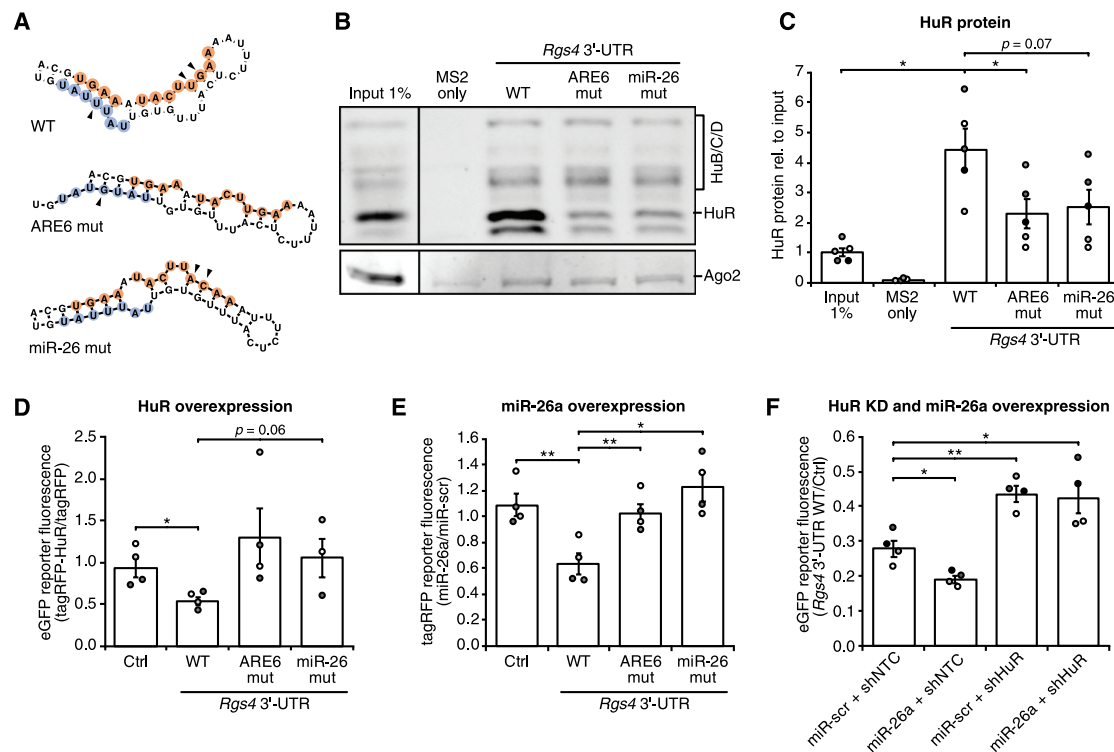


Figure 4. HuR and miR-26 synergistically repress *Rgs4* mRNA. (A) Predicted *in silico* folding of *Rgs4* conserved region (upper panel). The miR-26 binding site (orange) and the ARE6 (blue) are highlighted, with mutated sites marked by black arrows. (B,C) Representative Western blot against HuR and Ago2 (B) and quantification (C) of HuR enrichment from adult rat cortex lysate in *in vitro* RNA affinity purification using 2xMS2 only, 2xMS2+ *Rgs4* 3'-UTR WT, 2xMS2+ *Rgs4* 3'-UTR ARE6 mut and 2xMS2+ *Rgs4* 3'-UTR miR-26 mut as bait RNA, normalized to input. Paired Student's *t*-test. (D) Quantification of eGFP fluorescence intensity in the cell body of hippocampal neurons at 15 DIV co-transfected at 14 + 1 DIV with eGFP-reporter and tagRFP or tagRFP-HuR. Ratio of eGFP-reporter intensity between tagRFP-HuR and tagRFP condition is shown. Paired Student's *t*-test. (E) Quantification of tagRFP fluorescence intensity in the cell body of hippocampal neurons at 15 DIV co-transfected at 14 + 1 DIV with tagRFP-reporter and miR-scr or miR-26a. Ratio of tagRFP-reporter intensity between miR-26a and miR-scr condition is shown. Paired Student's *t*-test. (F) Quantification of eGFP fluorescence intensity in the cell body of hippocampal neurons at 15 DIV transduced at 10 + 5 DIV with lentiviruses expressing shNTC or shHuR and co-transfected at 14 + 1 DIV with eGFP-reporter and miR-scr or miR-26a. Ratio of eGFP-reporter intensity between *Rgs4* 3'-UTR WT and Ctrl reporter is shown. Paired Student's *t*-test. All error bars are SEM from ≥ 3 independent biological replicates; asterisks represent *p*-values (* $p < 0.05$, ** $p < 0.01$). ARE AU-rich element; WT wild type; KD knock-down; Scr scrambled.

of WT *Rgs4* 3'-UTR eGFP-reporter expression, but not of *Rgs4* 3'-UTR eGFP-reporter containing either HuR or miR-26 binding site mutants. Complementing this experiment, we used the tagRFP-reporter assay to test for the effect of miR-26a overexpression on WT, ARE6 and miR-26 *Rgs4* 3'-UTR tagRFP-reporter expression. Overexpression of miR-26a resulted in significant downregulation of WT *Rgs4* 3'-UTR tagRFP-reporter expression, but not of the *Rgs4* 3'-UTR tagRFP-reporter containing the HuR or miR-26 binding site mutants (Fig. 4E).

HuR is necessary for the repressive effect of miR-26a on *Rgs4* mRNA

To substantiate the observed interdependent mechanism from the mutation studies, we tested whether miR-26a represses *Rgs4* 3'-UTR reporter, when HuR protein has been depleted. While sole overexpression of miR-26a led to reduction of eGFP-*Rgs4* 3'-UTR reporter expression, the effect was

abolished when HuR levels were depleted (Fig. 4F). Furthermore, we investigated, whether the effects of HuR and miR-26a are additive using the eGFP reporter assay. In this case overexpression of both HuR and miR-26a would result in stronger repression of *Rgs4* 3'-UTR reporter expression, compared to overexpression of either HuR or miR-26a. However, we did not detect further repression, when both HuR and miR-26a were overexpressed (Sup. Fig. 4D). Together, our results from the mutation and the HuR/miR-26a combination studies substantiate the model of an interdependent mechanism of HuR and miR-26 in repressing *Rgs4* mRNA expression.

Mutation of miR-26 and HuR binding sites increases dendritic *Rgs4* mRNA levels

We finally aimed to investigate whether miR-26 and HuR could affect dendritic *Rgs4* mRNA levels. For this, we used the MS2 reporter system, previously applied to study live

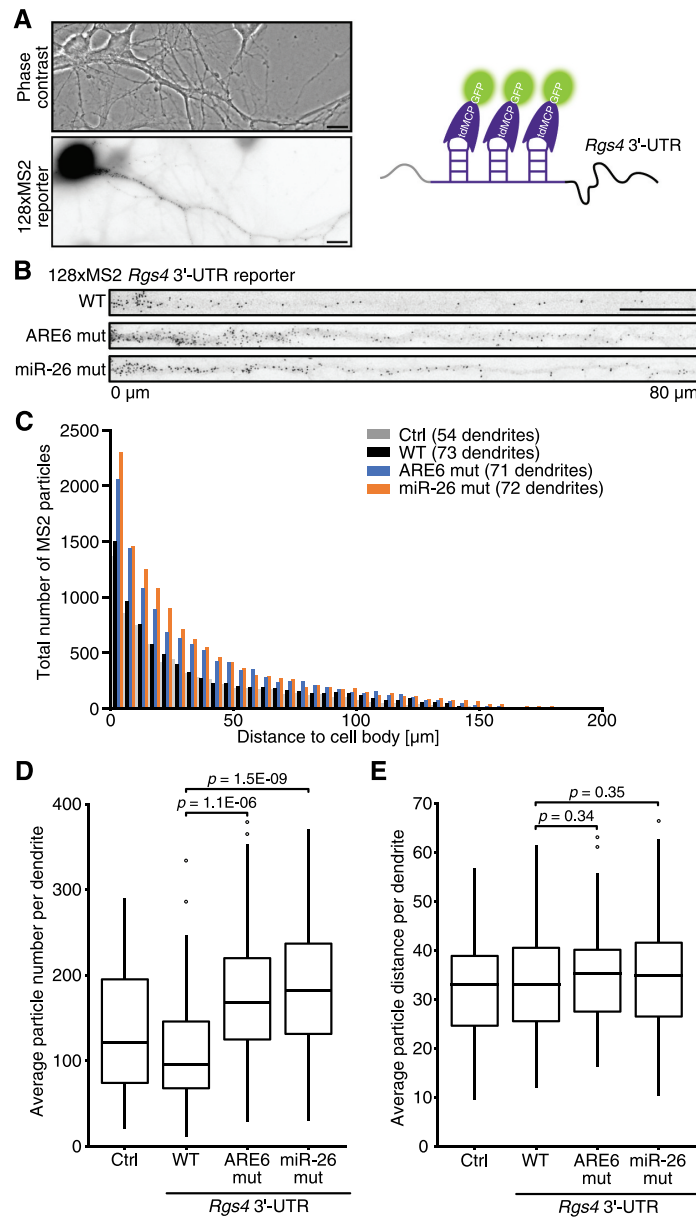


Figure 5. Mutation of miR-26 and HuR binding sites increases dendritic *Rgs4* RNA levels. (A) Phase contrast and 128xMS2 GFP reporter fluorescence in a rat hippocampal neuron at 14 + 1 DIV expressing both tdMCP-GFP and 128xMS2+ *Rgs4* 3'-UTR reporter RNA (left panel). Scheme of tdMCP-GFP bound to MS2 + *Rgs4* reporter RNA (right panel). (B) Deconvoluted and straightened images of dendrites expressing both tdMCP-GFP and 128xMS2+ *Rgs4* 3'-UTR WT, ARE6 mut or miR-26 mut reporter mRNA. Straightened images are cropped to 80 μm for better particle visibility. (C) Histogram displaying MS2 particle distance to cell body and total number of MS2 particles from hippocampal neurons transfected with tdMCP-GFP and 128xMS2+ Ctrl, 128xMS2+ *Rgs4* 3'-UTR WT, ARE6 mut or miR-26 mut reporter mRNA at 14 + 1 DIV. Binning on x-axis is 5 μm. (D) Boxplot of the average number of MS2 particles per dendrite. Unpaired Student's *t*-test. (E) Boxplot of the average distance of MS2 particles per dendrite. Unpaired Student's *t*-test. Data are obtained from 3 independent biological replicates; Dendrites: Ctrl *n* = 54, WT *n* = 73, ARE6 mut *n* = 71, miR-26 mut *n* = 72; scale bar 10 μm. ARE AU-rich element; WT wild type; tdMCP-GFP tandem MS2 coat protein fused to GFP; DIV *days in vitro*.

dynamics of *Rgs4* 3'-UTR [14]. The system is based on a reporter containing a LacZ open reading frame and a repetition of 128xMS2 stem loops in front of a 3'-UTR of interest. Hippocampal neurons were co-transfected with the 128xMS2 reporter and tandem MS2 coat protein-GFP

(tdMCP-GFP) (Fig. 5A). Binding of the tdMCP-GFP to the MS2 stem loops in the 128xMS2 reporter visualized the RNA reporter and allowed the quantification of dendritic MS2 particles (Fig. 5B). We measured the distance of dendritic MS2 particles from the cell body and counted the total

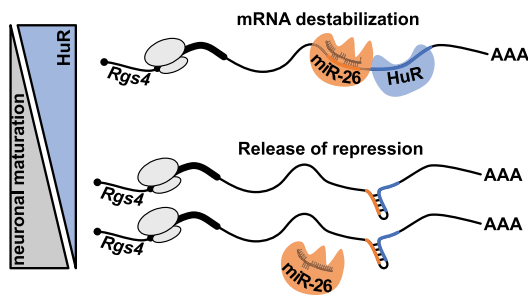


Figure 6. Proposed model of synergistic action of HuR and miR-26/RISC in neurons. Both, miR-26/RISC and HuR, are needed to open up the hairpin structure in *Rgs4* 3'-UTR and enable stable binding of both factors. This results in destabilization of *Rgs4* mRNA. The decrease of HuR protein with neuronal maturation or binding of additional RBPs to the mRNA favours the hairpin structure and miR-26/RISC can no longer bind. This results in increased mRNA levels of *Rgs4*, coding for a protein important for regulation of neuronal activity. See text for further details.

number of dendritic MS2 particles for 128xMS2 reporter with either no 3'-UTR (Ctrl), WT, ARE6 mutant and miR-26 mutant *Rgs4* 3'-UTR (Fig. 5C). As visualized in Fig. 5D, the average particle number per dendrite was significantly higher for the *Rgs4* 3'-UTR mutant reporters compared to WT. However, the distribution of MS2 particles along the dendrite was not affected by mutating either the ARE6 or the miR-26 binding site (Fig. 5E, Sup. Fig. 5A). This data on *Rgs4* 3'-UTR RNA reporter expression and localization suggests that HuR and miR-26 destabilize dendritic *Rgs4* mRNA, while not directly affecting *Rgs4* localization. This was important, as HuR is predominantly located in the nucleus under basal conditions, with scarce localization to dendrites [33,34].

In conclusion, our data suggest that miR-26/RISC and HuR co-regulate *Rgs4* 3'-UTR, resulting in destabilization of the mRNA. This is consistent with our working model of a dynamic RNA conformation, where binding of miR-26/RISC and HuR acts as a switch in opening an RNA hairpin structure. This enables a strong repression of *Rgs4* mRNA by downstream effectors. In mature neurons, however, the absence of HuR together with the binding of additional RBPs could favour the hairpin structure ('closed conformation'), thereby preventing miR-26/RISC binding. This, in turn, results in increased mRNA levels of *Rgs4*, coding for a protein that plays a critical role in the regulation of synaptic plasticity.

Discussion

In our study, we provide strong experimental evidence that miR-26 and HuR destabilize *Rgs4* mRNA in a synergistic manner. In contrast to previous studies in smooth muscle cells, where *Rgs4* mRNA was stabilized by HuR [7] and *Rgs4* overexpression rescued the phenotype observed in HuR knock-down cells [21], we find the opposite effect of HuR on *Rgs4* mRNA in neurons (Fig. 1). Furthermore, we identified the ARE bound by HuR to be within a conserved region in the 3' end of the *Rgs4* 3'-UTR (Figs. 2 and 4). Analysis of the conserved region revealed

a functional miR-26a/b binding site in close proximity to the ARE (Fig. 3). So far, HuR mainly exerts a stabilizing effect on target mRNAs, often by competing with miRNA binding [23,25]. There is, however, also evidence that HuR can destabilize mRNAs by cohesive action with miRNAs [24]. Based on the data presented in Fig. 4, we conclude that there is indeed evidence for synergism of miR-26 and HuR in repressing *Rgs4* mRNA. Mutation of both the miR-26 binding site and the ARE results in reduced binding of HuR in the TRAP assay. Further, we show that the miR-26 binding site mutant abolishes HuR and the ARE mutant abolishes miR-26 repressive effect on the *Rgs4* 3'-UTR reporter expression. Finally, in an experiment independent of mutations in the 3'-UTR sequence, we show that HuR is necessary for miR-26 to repress the *Rgs4* 3'-UTR reporter (Fig. 4F). Our data support a model, where both miR-26 and HuR can bind to the *Rgs4* 3'-UTR in order to facilitate repression of *Rgs4* mRNA. We, therefore, hypothesize that reduced HuR levels in mature neurons (Fig. 1) lead to deregulation of *Rgs4* mRNA by both miR-26 and HuR. This would result in increased *Rgs4* expression, important for proper neuronal function [5]. However, we cannot (yet) reliably define an order of events. In our presented model, the synergistic repressive effect of HuR and miR-26 on *Rgs4* mRNA arises from binding to an RNA sequence predicted to form a hairpin structure (Fig. 6). This assumption is based on RNA folding prediction, as we cannot yet provide experimental support for the predicted secondary RNA structure. Extensive future work is therefore needed to experimentally validate the change in RNA structure. An elegant study by Kim *et al.* (2009) illustrated a similar interaction mode of HuR and let-7 loaded Ago/RISC on *c-myc* mRNA [22].

Further support of our model comes from a genome-wide study by Li *et al.* (2018), which recently showed both antagonistic and agonistic interaction modes between HuR and the miRNA machinery [24]. They used high throughput sequencing of RNA after crosslinking and immunoprecipitation (CLIP) to map HuR or Ago2 binding sites and studied the effect of HuR knock-down on mRNA occupancy of Ago2 in human embryonic kidney cells. In addition to future studies addressing the combinatorial function of different RBPs as well as the miRNA/RISC machinery in brain through CLIP, it will be intriguing to get insight into the RBP-dependent dynamics of RNA structures in living cells [35]. To our current knowledge, the regulation of the AU-rich transcriptome in the brain has been studied solely through the neuron-specific Hu proteins HuB/C/D [36–39]. Only recently, the neuronal function of the ubiquitously expressed HuR has been explored [17–19,40,41]. It will, therefore, be interesting to see in the future, whether the data on post-transcriptional regulation by HuR from non-neuronal cells and tissues hold true for the complex nervous system. As our data show, there is no uniform mechanism of mRNA regulation by HuR, highlighting the importance of mechanistic studies on the single target level.

Materials and methods

Plasmids

The expression plasmid for MBP-MS2BP (Addgene 11,246) [42,43] and the pUBC-NLS-ha-tdMCP-GFP [14] and pRSV-

LacZ-128xMS2 [14] plasmids have been described. Generation of pRSV-LacZ-128xMS2, pCMV-tagRFP-STOP (ptagRFP-C, Evrogen) or pCMV-eGFP-STOP [44] (pEGFP-C1, Clontech) reporter plasmids was performed by insertion of the CDS (position 110–727 nt) or 3'-UTR (position 728–2919 nt) of rat *Rgs4* mRNA (NM_017214.1) in between the stop codon of the respective open reading frame of LacZ, tagRFP or eGFP and the poly A signal. Fragments of the *Rgs4* 3'-UTR were cloned by insertion of fragments of rat *Rgs4* mRNA (NM_017214.1), corresponding to position 728–1602 nt (F1), 1698–2153 nt (F2), 2152–2919 nt (F3), into pCMV-eGFP-STOP reporter as described above. Site-directed mutagenesis was performed on pRSV-LacZ-128xMS2-*Rgs4* 3'-UTR, pCMV-tagRFP-*Rgs4* 3'-UTR and pCMV-eGFP-*Rgs4* 3'-UTR reporter plasmids to generate *Rgs4* 3'-UTR ARE6 and *Rgs4* 3'-UTR miR-26 mutant reporter plasmids using the following primers (5'-3'): *Rgs4*_ARE6_F: ctatttggttatGtatgtgtttt; *Rgs4*_ARE6_R: caaaacaacataCataacacaa-atgag; *Rgs4*_miR-26_F: cactggaacttACaaatttctc; *Rgs4*_miR-26_R: gagaattGTa-agtatttcacgtg. The *in vitro* RNA transcription plasmid pcDNA3-T7-Ctrl-2xMS2 has been previously described [43]. The plasmids pcDNA3-T7-2xMS2 containing *Rgs4* CDS, 3'-UTR, 3'-UTR fragments and mutants were generated by subcloning the insert from respective above mentioned pCMV-eGFP-STOP reporter plasmids in between the T7-promotor and the 2xMS2 sequence by EcoRV/BamHI. pCMV-tagRFP-HuR was generated by inserting the coding sequence of HuR, corresponding to position 153–1133 nt of rat *HuR* mRNA (NM_001108848), into ptagRFP-C (evrogen). The plasmid pSup-eGFP-H1-pri-miR-26a used in the tagRFP-assay was generated by PCR-amplification and cloning of the primary rno-miR-26a sequence after the H1 promoter into the pSuperior.neo+GFP (oligo engine) using primer annealing 60 nt up- and downstream of the genomic locus of the rno-miR-26a stem-loop. Generation of pSup-eGFP-H1-miR-scr was performed by annealing and direct ligation of the following phosphorylated oligos after the H1 promoter into pSuperior.neo+GFP: miR-scr_F: gatcccggtgaacacgtctatcacccattcaagagatggggcgtatagacgtgttacactttt; miR-scr_R: ag-cttaaaagtgtaacacgtctatcacccattcttgaatggggcgtatagacgtgttacacggg. For combining HuR and miR-26a overexpression in eGFP-reporter assays, the following expression plasmids were generated: pSup-tagBFP-H1-miR-scr and pSup-tagBFP-H1-pri-miR-26a, by exchanging the eGFP open reading frame by tagBFP in the above-described pSup-eGFP plasmids. For generation of the lentiviral plasmids pFu3a-H1-pri-miR-26a-pCamK2a-tagRFP and pFu3a-H1-miR-scr-pCamK2a-tagRFP, the H1-shNTC sequence of the previously described pFu3a-H1-shNTC-pCamK2a-tagRFP [14] was exchanged by the H1-pri-miR-26a or H1-miR-scr sequence from above described pSup-eGFP-H1. Generation of the lentiviral plasmids pFu3a-pCamK2a-eGFP-STOP and pFu3a-pCamK2a-eGFP-STOP-16xmiR-26sponge was performed by first exchanging the H1-shNTC-pCamK2a-tagRFP by pCamK2a-eGFP-STOP. For pFu3a-pCamK2a-eGFP-STOP-16xmiR-26sponge, the following phosphorylated oligos were annealed, ligated and separated by 2% agarose gel electrophoresis (5'-3'): miR26a_sponge_F: ccggcagcctatcctCCTacttgaa; miR26a_sponge_R: ccgggtcaagtaagGagtagatgctg; 5'linker_sponge_F: agat-ctcagctcaagcttgcaattcc; 5'linker_sponge_R: ccggggaattcgaagcttgagctcgatct, 3'linker_sponge_F: ccggcgtcagcgtaccgcccgggatcc; 3'linker_sponge_R: ggatcc-cgggcccgggtaccgtcagc. A band of ~500 bp

was excised, gel purified and pasted into the 3'-UTR of eGFP into pFu3a-pCamK2a-eGFP-STOP via BamH/XhoI. To generate the lentiviral shRNA plasmids pFu3a-H1-shHuR-pCamK2a-tagRFP, pFu3a-H1-shAgo2-pCamK2a-tagRFP and pFu3a-H1-shPum2-pCamK2a-tagRFP, the H1-shNTC sequence of pFu3a-H1-shNTC-pCamK2a-tagRFP was exchanged by H1-shHuR, H1-shAgo2 or H1-shPum2 after subcloning the shRNAs into pSuperior.neo+GFP. The oligo sequences for shRNA generation were (5'-3'): shHuR_F: gatccccgaagaggcaatta-ccagttcattcaagatgaaactggtaattgcctctctttt; shHuR_R: tcgagaaaagaagaggcaatta-ccagttcattccttgaatgaaactggtaattgcctctcttggg; shAgo2_F: gatccctgtcgtgaattgggatcat-tgtacaatgatcccaattcacgaacattt; shAgo2_R: tcgagaaaatgttcgtgaattgggatcattgtac-aatgatcccaattcacgaacagg; shPum2_F: gatccccaccaagttggctggattcttcaagagaatc-cagaccaattgggtttt; shPum2_R: gaaaaaaccaagttggctggattcttcaagagaatc-cagacca-cttgggtgggatc. The lentiviral packaging plasmids, psPAX2 and pcDNA3.1-VSV-G, have previously been described [12].

Lentivirus production

Lentiviral particles for shNTC, shHuR, shAgo2, miR-scr, miR-26a, eGFP-Stop and eGFP-miR-26-sponge were generated from HEK-293 T cells co-transfected with psPAX2, pcDNA3.1-VSV-G and the respective pFu3a plasmids using calcium phosphate coprecipitation. After 48 h virus production, supernatants were filtered (0.45 µm PVDF Millex-HV; Millipore), concentrated by ultracentrifugation (65,000xg, 140 min, SW 32 Ti rotor; Beckman Coulter) and resuspended in Opti-MEM™ (Life Technologies) [12].

Neuronal cell culture, treatment, transduction and transfection

All animals in this study were used according to the German Welfare for Experimental Animals (LMU Munich, *Regierung von Oberbayern*). Rat hippocampal neuron cell cultures from embryos at day 17 (E17) of timed pregnant Sprague-Dawley rats (Charles River Laboratories) were generated as described previously [45]. Briefly, E17 hippocampi were dissected, trypsinized and cells dissociated and plated on poly-L-lysine-coated coverslips and cultured in NMEM+B27 medium (Invitrogen) with 5% CO₂ at 37°C. For cortical cultures, E17 cortices were trypsinized and dissociated, the cell suspension sequentially filtered through 100-, 70- and 40-µm cell strainers and then plated at a density of 100,000 cells/cm² on poly-L-lysine coated 60 mm dishes. For protein and RNA analysis, cortical neurons were transduced with lentiviral suspension at 9 days *in vitro* (DIV) and lysed at 14 DIV. Analysis of RNA stability was performed by incubation of lentivirus-treated cortical neurons at 14 DIV with 2 µM Actinomycin D (ActD; Sigma) or an equivalent amount of DMSO in NMEM+B27 for 90 min. Hippocampal neurons were transduced with lentiviral suspension at 10–11 DIV, followed by transient transfection by calcium phosphate coprecipitation [46] at 14 DIV and fixation with 4% paraformaldehyde (PFA) at 15 DIV. Transient co-transfection of hippocampal neurons by calcium phosphate precipitation was performed at 14 DIV, followed by fixation with 4% PFA at 15 DIV.

Fluorescent reporter assays

For fluorescent reporter assays with mere overexpression of miR-26a, HuR or both, hippocampal neurons grown on coverslips were transiently co-transfected at 14 DIV with the respective overexpression plasmids and the fluorescent reporter constructs. Neurons were fixed with 4% PFA 24 h post-transfection at 15 DIV. For fluorescent reporter assays with knock-down of HuR or depletion of miR-26, hippocampal neurons grown on coverslips were transduced with lentiviruses at 10 DIV for HuR knock-down and at 11 DIV for miR-26a depletion. At 14 DIV, neurons were transfected with the fluorescent reporter constructs (and miR-26a overexpression constructs to combine shHuR and miR-26a overexpression) followed by fixation with 4% PFA 24 h post-transfection at 15 DIV. Coverslips were mounted on microscope slides with Fluoromount™ Aqueous Mounting Medium (Sigma), imaged and analysed as described in the microscopy and image analysis section.

Protein purification

The MBP-MCP fusion protein was affinity purified as described [42] using amylose resin (New England Biolabs) in MBP-buffer (20 mM Tris at pH 7.2, 50 mM NaCl; 1 mM EDTA) and step elution with 10 mM maltose. Further purification was performed by linear NaCl elution from a heparin column using an Äkta purifier (GE Healthcare). Eluted fractions were combined, concentrated and washed with binding buffer (BB: 20 mM Tris, pH 7.5, 150 mM NaCl, 1.5 mM MgCl₂, 8.7% glycerol and 0.05% NP40) using Amicon Ultra centrifugal filters (Merck).

In vitro RNA affinity purification

In vitro RNA affinity purification was performed as previously described [43] with minor variations. Briefly, RNA containing 2xSM2 stem loops was *in vitro* transcribed by run-off transcription from linearized (XhoI) pCDNA3.1-T7-MS2 plasmids using the T7 RiboMAX Express Large-Scale RNA Production System (Promega). Synthesized RNAs were purified using NucAway spin columns (Invitrogen). Twenty microlitres of amylose resin (New England Biolabs) was washed four times with BB and incubated with 100 pmol recombinant MBP-MCP in 1 ml BB for 30 min. The resin was blocked with 0.5 mg/ml bovine serum albumin in 1 ml BB for 30 min and washed three times with binding buffer (BB). Twenty picomoles *in vitro* transcribed bait RNA was heated to 65°C for 10 min, let cool to room temperature over 10 min and immobilized on the resin 1 ml BB + 11 mg/ml heparin (Sigma) for 1 h. One adult rat cortex was lysed in 1 ml BB + cOmplete Protease Inhibitor Cocktail Tablets (Roche) using bead homogenization on a FastPrep-24 instrument (MP Biomedicals) with lysing matrix D (MP Biomedicals). The lysate was diluted to 1:20 with BB + cOmplete Protease Inhibitor and cleared twice by centrifugation at 15,600xg and 4°C for 10 min. The RNA loaded resin was washed once with BB + 11 mg/ml heparin, before the resin was incubated for 30 min with 500 µl lysate and 500 µl BB + 22 mg/ml heparin, 2 mM dithiothreitol and 40 U/ml murine RNase Inhibitor (New England Biolabs). The resin was washed four times with BB + 11 mg/ml heparin. Proteins were eluted by incubation with 15 µl 3x SDS sample buffer at 65°C for 12 min. All steps, except

lysis, RNA folding and elution, were conducted at room temperature and constant agitation.

Western blotting

Neurons were washed twice with warm Hanks' Balanced Salt Solution (HBSS, Gibco) and then lysed in 3x SDS sample buffer. Samples were treated with 50 U Benzoylase Nuclease (Merck) for 10 min and heated to 65°C for 12 min. Proteins of equivalent number of neurons were resolved on 10% SDS-PAGE and subjected to immunoblotting with mouse anti-HuR (3A2) (1:500, sc-5261, Santa Cruz), mouse anti-Ago2 (2E12-1 C9) (1:500, WH0027161M1, Sigma) goat anti-Vinculin (1:500, sc-7649, Santa Cruz). After incubation with IRDye labelled secondary donkey anti-mouse (IRDye 800CW) and donkey anti-goat (IRDye 680RD) (both 1:15,000, Li-Cor), membranes were imaged on an Odyssey CLx Imaging System (Li-Cor) and quantified using Image Studio Lite software (Li-Cor).

RNA extraction, cDNA synthesis and qRT-PCR

Neurons were washed twice with warm HBSS (Gibco), before total RNA from cortical neurons was extracted using TRIzol (Invitrogen) and total RNA from hippocampal neurons grown on coverslips was extracted using RNeasy Mini Kit (Qiagen). cDNA was generated from 1 µg of DNase treated total RNA, using Superscript III reverse transcriptase (Invitrogen) according to the manufacturer's instructions with a minor variation. A mixture of 1.5 µM random primer mix (New England Biolabs) and 2.5 µM (dT)₂₀ was used during cDNA synthesis. Quantitative real-time PCR (qRT-PCR) was performed in duplicates from a 1:50 dilution of the stock cDNA using a home-made SYBR Green Master Mix [44], with the LightCycler 96 System (Roche). Only primers with an optimized efficiency of 95–105% were used. The 2^{-ΔΔCt} method implemented in the LightCycler Software (Roche) was used to calculate differences in RNA levels relative to peptidylprolyl isomerase A (PPIA) mRNA. The sequences of the qRT-PCR primers were (5'–3'): Ppia_F: gtaacccaccgtgtctt; Ppia_R: ctgctgtcttggactttg; Rgs4_F: agtcccaaggccaagaagat; Rgs4_R: aacatgttccggctgtctc; HuR_F: tcggttggcgaaatcaca; HuR_R: ctacgagcgagtggtacag; Ago2_F: acaagctggtttcgcctac; Ago2_R: ttgctgatctcct-ctgccc; Pum2_F: atgggagcagctcttgact; Pum2_R: gatgagcacaatcactgagag. Reverse transcription PCR (RT-PCR) was performed from a 1:50 dilution of the cDNA using *Taq* DNA Polymerase (NEB) according to the manufacturer instructions. The sequences of the RT-PCR primers were (5'–3'): Rgs4_RT_F: aatagaaccaccgtgtctc; Rgs4_RT_R: aacatgttccggctgtctc.

FISH and immunostaining

For FISH and immunostaining neurons were washed twice with warm HBSS and then fixed with warm 4% PFA in HBSS for 10 min. The fluorescence *in situ* hybridization (FISH) against *Rgs4* mRNA using Cy5-tyramide signal amplification was performed as described [12,47]. For immunostaining, fixed cells were washed with HBSS and permeabilized with 0.1% Triton X-100 in DPBS for 5 min. The following primary

antibodies were used: mouse anti-HuR (3A2) (1:500, sc-5261, Santa Cruz Biotechnology) and mouse anti-Map2 (HM-2) (1:500, M4403, Sigma). The following secondary antibodies were used: donkey anti-mouse AF488- or AF647-conjugated antibodies (both Invitrogen). Coverslips were mounted on microscope slides with Prolong Diamond antifade mounting medium (Invitrogen).

Microscopy and image analysis

Images were acquired using Zeiss Zen software on a Zeiss Z1 Axio Observer microscope including a 63x Plan-Apochromat oil immersion objective (1.40 NA), a COLIBRI.2 LED and an HXP 120 C light source and the Axiocam 506 mono camera. Neurons were selected for cell morphology and viability as well as for expression of plasmids and images were taken of the dendritic plane. For FISH experiments, z-stacks of neurons were acquired (50 images with 0.26 μm step-size), and a z-projection of the maximum intensity was performed in ImageJ. For cell body, fluorescence intensity quantification of eGFP- or tagRFP-reporter signal, the measure function in the Zeiss Zen software was used and a region of interest was drawn by hand based on the phase-contrast image. The mean intensity of each condition was calculated and normalized to the fluorescent reporter levels in the control conditions (miR-scr or tagRFP) with one exception. For experiments with overexpression or knock-down of both miR-26a and HuR, the mean intensity of the reporter fluorescence was normalized to the control eGFP reporter. For 128xMS2 experiments, z-stacks of neurons were acquired (30 images with 0.26 μm step-size). Images were then deconvoluted using the Zeiss Zen software deconvolution module, with default settings of the constrained iterative method and analysed in ImageJ. A z-projection of the maximum intensity was performed in ImageJ, and for 128xMS2 particle quantification, one dendrite per cell was selected and straightened using the segmented line tool with 40-pixel width. Particles were manually detected using the multi-point tool and the ROI manager. The distance was measured by extracting the x position for each particle in μm . The average number and average distance of particles per dendrite were calculated. For all experiments, ≥ 20 dendrites or cell bodies per condition from at least three independent experiments were selected for quantification.

RNA structure and binding site predictions

The thermodynamic structure prediction of the conserved region corresponding to nucleotide position 1442 to 1631 of the 3'-UTR sequence of rat *Rgs4* mRNA (NM_017214.1) was predicted using the RNAfold server within the ViennaRNA web services (<http://rna.tbi.univie.ac.at/>) [48]. Standard options were used, but no GU pairs at the end of helices were allowed. Accessibility of the miRNA interaction site within *Rgs4* 3'-UTR conserved region was predicted with IntaRNA web interface within the Freiburg RNA tools (<http://rna.informatik.uni-freiburg.de/IntaRNA>) [49]. Prediction of ARE in the mouse

Rgs4 3'-UTR was performed using AREsite2 within the ViennaRNA web services (<http://rna.tbi.univie.ac.at/>) [50].

Statistical analysis

Microsoft Excel and R software were used for data processing, plotting and statistical analysis [51,52]. Figures represent mean \pm standard error of the mean (SEM) of at least three independent biological replicates. Asterisks represent p-values obtained by one-way ANOVA and either paired or unpaired two-sided Student's t-test using the mean values per experiment ($*p < 0.05$, $**p < 0.01$, $***p < 0.001$), as indicated.

Acknowledgments

We thank Christin Illig for preparing primary neuron cultures; Renate Dombi, Ulrike Kring, Daniela Rieger and Marlene Brunner for technical assistance; Karl Bauer for assistance with R and image analysis; Jacqueline Heraud-Farlow for initial experiments and Rico Schieweck, Max Harner and Karl Bauer for critical comments on the manuscript. We thank Stefan Hüttelmaier for pcDNA3.1-2xMS2 and pMal-MCP plasmids and advice. This work was supported by grants from the DFG (Großgeräteantrag INST86/1581-1FUGG, SPP1738, FOR2333, SFB870) and the FWF (I 590-B09, F4314-B09 SFB RNA-seq) (all to M.A.K.); and the Friedrich-Baur-Stiftung (to S.F.M).

Author contributions

M.A.K., J.E. and S.F.M. conceived the project. J.E. and L.S. performed experiments and J.E. conducted data analysis. J.E. and M.A.K. wrote the manuscript, with feedback from all authors.

Disclosure statement

No potential conflicts of interest were disclosed.

Funding

This work was supported by the Austrian Science Fund [I 590-B09]; Austrian Science Fund [F43-B09]; Deutsche Forschungsgemeinschaft [INST86/1581-1FUGG]; Deutsche Forschungsgemeinschaft [FOR2333]; Deutsche Forschungsgemeinschaft [SPP1738]; Deutsche Forschungsgemeinschaft [SFB870]; Friedrich-Baur-Stiftung [SFM].

ORCID

Janina Ehse  <http://orcid.org/0000-0003-0634-769X>
Sandra M. Fernández-Moya  <http://orcid.org/0000-0002-5894-4296>
Luise Schröger  <http://orcid.org/0000-0002-6213-4202>
Michael A. Kiebler  <http://orcid.org/0000-0002-8850-6297>

References

- [1] Namvar S, Fathollahi Y, Javan M, *et al.* The antiepileptogenic effect of low-frequency stimulation on perforant path kindling involves changes in regulators of G-protein signaling in rat. *J Neurol Sci.* 2017;375:450–459.
- [2] Chen Y, Liu Y, Cottingham C, *et al.* Neurabin scaffolding of adenosine receptor and RGS4 regulates anti-seizure effect of endogenous adenosine. *J Neurosci.* 2012;32:2683–2695.
- [3] Avrampou K, Pryce KD, Ramakrishnan A, *et al.* RGS4 maintains chronic pain symptoms in rodent models. *J Neurosci.* 2019;39:8291–8304.

- [4] Ding J, Guzman JN, Tkatch T, *et al.* RGS4-dependent attenuation of M4 autoreceptor function in striatal cholinergic interneurons following dopamine depletion. *Nat Neurosci.* 2006;9:832–842.
- [5] Gerber KJ, Squires KE, Hepler JR. Roles for regulator of G protein signaling proteins in synaptic signaling and plasticity. *Mol Pharmacol.* 2016;89:273–286.
- [6] Berman DM, Kozasa T, Gilman AG. The GTPase-activating protein RGS4 stabilizes the transition state for nucleotide hydrolysis. *J Biol Chem.* 1996;271:27209–27212.
- [7] Li F, Hu DY, Liu S, *et al.* RNA-binding protein HuR regulates RGS4 mRNA stability in rabbit colonic smooth muscle cells. *AJP Cell Physiol.* 2010;299:C1418–C1429.
- [8] Davydov IV, Varshavsky A. RGS4 is arginylated and degraded by the N-end rule pathway in vitro. *J Biol Chem.* 2000;275:22931–22941.
- [9] Wu B, Eliscovich C, Yoon YJ, *et al.* Translation dynamics of single mRNAs in live cells and neurons. *Science.* 2016;352:1430–1435.
- [10] Wang DO, Kim SM, Zhao Y, *et al.* Synapse- and stimulus-specific local translation during long-term neuronal plasticity. *Science.* 2009;324:1536–1540.
- [11] Bartel DP. *Metazoan MicroRNAs.* *Cell.* 2018;173:20–51.
- [12] Heraud-Farlow JE, Sharangdhar T, Li X, *et al.* Staufeu2 regulates neuronal target RNAs. *Cell Rep.* 2013;5:1511–1518.
- [13] Berger SM, Fernández-Lamo I, Schöning K, *et al.* Forebrain-specific, conditional silencing of Staufeu2 alters synaptic plasticity, learning, and memory in rats. *Genome Biol.* 2017;18:222.
- [14] Bauer KE, Segura I, Gaspar I, *et al.* Live cell imaging reveals 3'-UTR dependent mRNA sorting to synapses. *Nat Commun.* 2019;10:3178.
- [15] Fritzsche R, Karra D, Bennett K, *et al.* Interactome of Two Diverse RNA Granules Links mRNA Localization to Translational Repression in Neurons. *Cell Rep.* 2013;5:1749–1762.
- [16] Skliris A, Papadaki O, Kafasla P, *et al.* Neuroprotection requires the functions of the RNA-binding protein HuR. *Cell Death Differ.* 2015;22:703–718.
- [17] Sun K, Li X, Chen X, *et al.* Neuron-specific HuR-deficient mice spontaneously develop motor neuron disease. *J Immunol.* 2018;201:157–166.
- [18] Carelli S, Giallongo T, Rey F, *et al.* HuR interacts with lincBRN1a and lincBRN1b during neuronal stem cells differentiation. *RNA Biol.* 2019;16:1471–1485.
- [19] Wang Y, Guo Y, Tang C, *et al.* Developmental cytoplasmic-to-nuclear translocation of RNA-binding protein HuR is required for adult neurogenesis. *Cell Rep.* 2019;29:3101–3117.e7.
- [20] Phillips BL, Banerjee A, Sanchez BJ, *et al.* Post-transcriptional regulation of Pabpn1 by the RNA binding protein HuR. *Nucleic Acids Res.* 2018;46:7643–7661.
- [21] Liu S, Jiang X, Lu H, *et al.* HuR (Human Antigen R) regulates the contraction of vascular smooth muscle and maintains blood pressure. *Arterioscler Thromb Vasc Biol.* 2020;40:943–957.
- [22] Kim HH, Kuwano Y, Srikantan S, *et al.* HuR recruits let-7/RISC to repress c-Myc expression. *Genes Dev.* 2009;23:1743–1748.
- [23] Meisner N-C, Filipowicz W. Properties of the regulatory RNA-binding protein HuR and its role in controlling miRNA repression. *Adv Exp Med Biol.* 2011;700:106–123.
- [24] Li Y, Estep JA, Karginov FV. Transcriptome-wide Identification and Validation of Interactions between the miRNA Machinery and HuR on mRNA Targets. *J Mol Biol.* 2018;430:285–296.
- [25] Iadevaia V, Gerber AP. Combinatorial Control of mRNA Fates by RNA-Binding Proteins and Non-Coding RNAs. *Biomolecules.* 2015;5:2207–2222.
- [26] Dotti CG, Sullivan CA, Banker GA. The establishment of polarity by hippocampal neurons in culture. *J Neurosci.* 1988;8:1454–1468.
- [27] Moore MJ, Proudfoot NJ. Pre-mRNA Processing Reaches Back to Transcription and Ahead to Translation. *Cell.* 2009;136:688–700.
- [28] Darnell RB. RNA protein interaction in neurons. *Annu Rev Neurosci.* 2013;36:243–270.
- [29] Loffreda A, Rigamonti A, Barabino SML, *et al.* RNA-binding proteins in the regulation of miRNA activity: A focus on neuronal functions. *Biomolecules.* 2015;5:2363–2387.
- [30] Ludwig N, Leidinger P, Becker K, *et al.* Distribution of miRNA expression across human tissues. *Nucleic Acids Res.* 2016;44:3865–3877.
- [31] Dill H, Linder B, Fehr A, *et al.* Intronic miR-26b controls neuronal differentiation by repressing its host transcript, *ctdsp2*. *Genes Dev.* 2012;26:25–30.
- [32] Gu Q-H, Yu D, Hu Z, *et al.* miR-26a and miR-384-5p are required for LTP maintenance and spine enlargement. *Nat Commun.* 2015;6:6789.
- [33] Grammatikakis I, Abdelmohsen K, Gorospe M. Posttranslational control of HuR function. *Wiley Interdiscip Rev RNA.* 2017;8:e1372.
- [34] Tiruchinapalli DM, Caron MG, Keene JD. Activity-dependent expression of ELAV/Hu RBPs and neuronal mRNAs in seizure and cocaine brain. *J Neurochem.* 2008;107:1529–1543.
- [35] Spitale RC, Crisalli P, Flynn RA, *et al.* RNA SHAPE analysis in living cells. *Nat Chem Biol.* 2013;9:18–20.
- [36] Ince-Dunn G, Okano H, Jensen KB, *et al.* Neuronal Elav-like (Hu) proteins regulate RNA splicing and abundance to control glutamate levels and neuronal excitability. *Neuron.* 2012;75:1067–1080.
- [37] Scheckel C, Drapeau E, Frias MA, *et al.* Regulatory consequences of neuronal ELAV-like protein binding to coding and non-coding RNAs in human brain. *Elife.* 2016;5:e10421.
- [38] Ogawa Y, Kakumoto K, Yoshida T, *et al.* Elavl3 is essential for the maintenance of Purkinje neuron axons. *Sci Rep.* 2018;8:2722.
- [39] Sosanya NM, Huang PP, Cacheaux LP, *et al.* Degradation of high affinity HuD targets releases Kv1.1 mRNA from miR-129 repression by mTORC1. *J Cell Biol.* 2013;202:53–69.
- [40] Zybura-Broda K, Wolder-Gontarek M, Ambrozek-Latecka M, *et al.* HuR (Elavl1) and HuB (Elavl2) stabilize matrix metalloproteinase-9 mRNA during seizure-induced Mmp-9 expression in neurons. *Front Neurosci.* 2018;12:1–15.
- [41] Popovitchenko T, Thompson K, Viljetic B, *et al.* The RNA binding protein HuR determines the differential translation of autism-associated FoxP subfamily members in the developing neocortex. *Sci Rep.* 2016;6:28998.
- [42] Kohn M, Lederer M, Wachter K, *et al.* Near-infrared (NIR) dye-labeled RNAs identify binding of ZBP1 to the noncoding Y3-RNA. *RNA.* 2010;16:1420–1428.
- [43] Braun J, Misiak D, Busch B, *et al.* Rapid identification of regulatory microRNAs by miTRAP (miRNA trapping by RNA in vitro affinity purification). *Nucleic Acids Res.* 2014;42:e66.
- [44] Sharangdhar T, Sugimoto Y, Heraud-Farlow J, *et al.* A retained intron in the 3'-UTR of *Calm3* mRNA mediates its Staufeu2- and activity-dependent localization to neuronal dendrites. *EMBO Rep.* 2017;18:1762–1774.
- [45] Goetze B, Tuebing F, Xie Y, *et al.* The brain-specific double-stranded RNA-binding protein Staufeu2 is required for dendritic spine morphogenesis. *J Cell Biol.* 2006;172:221–231.
- [46] Zeitelhofer M, Vessey JP, Xie Y, *et al.* High-efficiency transfection of mammalian neurons via nucleofection. *Nat Protoc.* 2007;2:1692–1704.
- [47] Heraud-Farlow JE, Sharangdhar T, Kiebler MA. Fluorescent in situ hybridization in primary hippocampal neurons to detect localized mRNAs. In: Hauptmann G editor. *In situ hybridization methods.* Springer: New York. 2015. p. 321–337. DOI:10.1007/978-1-4939-2303-8_16
- [48] Gruber AR, Lorenz R, Bernhart SH, *et al.* The Vienna RNA Websuite. *Nucleic Acids Res.* 2008;36:W70–W74.
- [49] Mann M, Wright PR, Backofen R. IntaRNA 2.0: enhanced and customizable prediction of RNA–RNA interactions. *Nucleic Acids Res.* 2017;45:W435–W439.
- [50] Fallmann J, Sedlyarov V, Tanzer A, *et al.* AREsite2: an enhanced database for the comprehensive investigation of AU/GU/U-rich elements. *Nucleic Acids Res.* 2015;44:D90–D95.
- [51] Team RC. R: a language and environment for statistical computing. Vienna: R Foundation for Statistical Computing; 2014.
- [52] Wickham H. *ggplot2.* New York: Springer; 2009. DOI:10.1007/978-0-387-98141-3

Supplementary Information

Synergistic regulation of *Rgs4* mRNA by HuR and miR-26/RISC in neurons

Authors

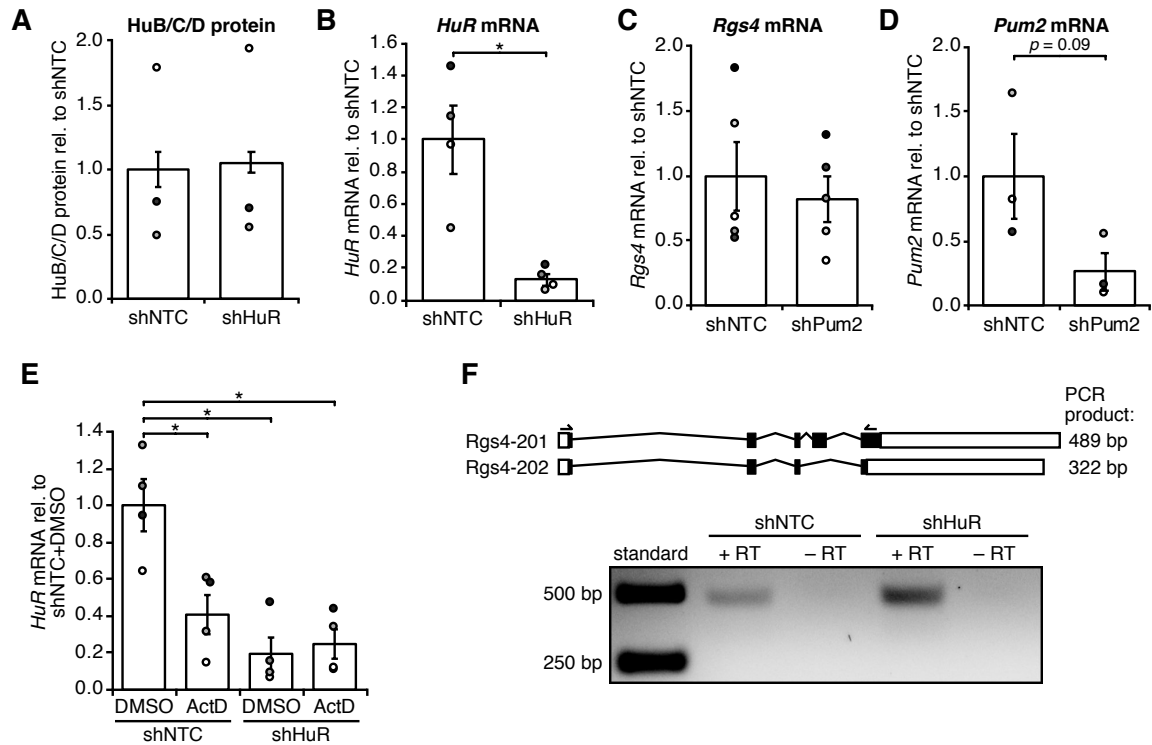
Janina Ehses ^a, Sandra M. Fernández-Moya ^a, Luise Schröger ^a, Michael A. Kiebler ^a

^a BioMedical Center, Medical Faculty, Ludwig Maximilians University of Munich, Martinsried, Germany

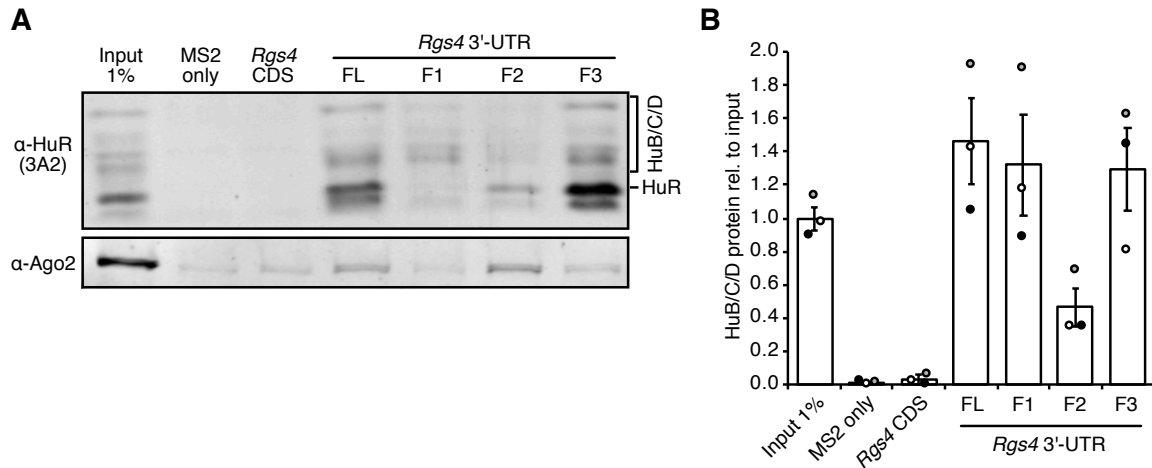
Corresponding Author:

Michael A. Kiebler (mkiebler@lmu.de)

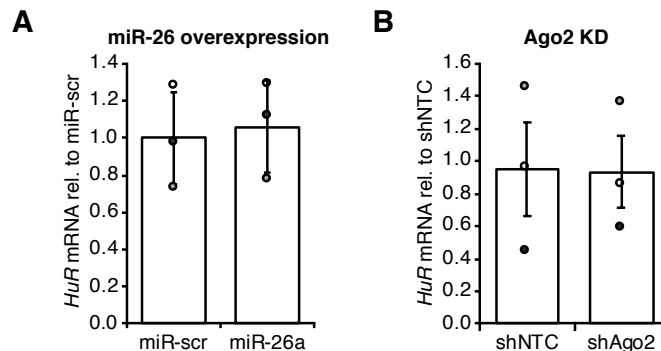
Department of Cell Biology, BioMedical Center, Ludwig Maximilians University of Munich, Großhaderner Str. 9, 82152 Planegg-Martinsried, Germany



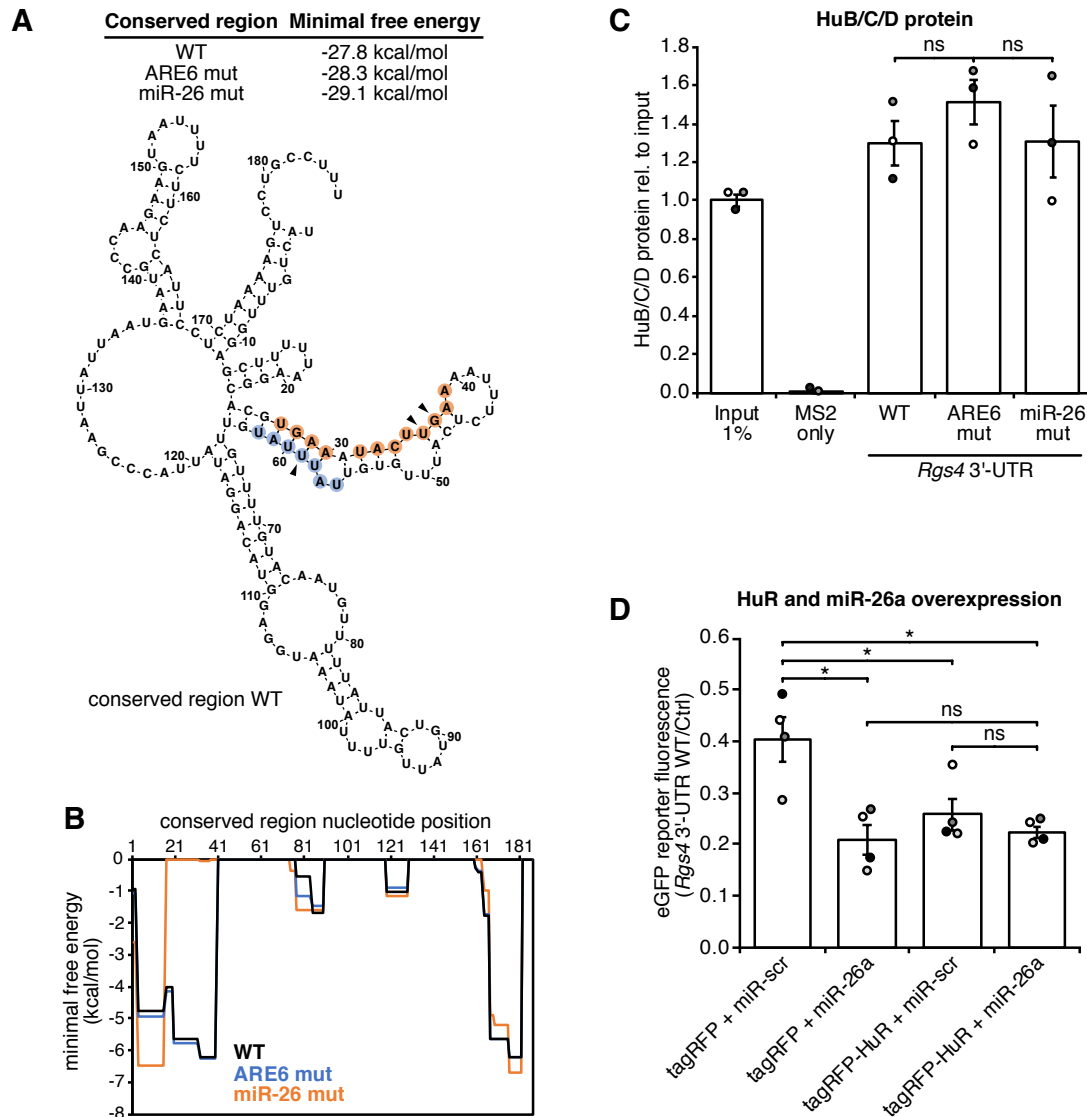
Supplementary Figure 1. Increase of *Rgs4* mRNA upon HuR knock-down is HuR specific. (A) Quantification of HuB/C/D western blot signal from 14 DIV cortical neurons transduced at 9+5 DIV with lentiviruses expressing shNTC or shHuR, normalized to shNTC. Paired Student's *t*-test. (B) Quantification of endogenous *HuR* mRNA by qRT-PCR from 14 DIV cortical neurons transduced at 9+5 DIV with lentiviruses expressing shNTC or shHuR, normalized to shNTC. Paired Student's *t*-test. (C) Quantification of endogenous *Rgs4* mRNA by qRT-PCR from 14 DIV cortical neurons transduced at 9+5 DIV with lentiviruses expressing shNTC or shPum2, normalized to shNTC. Paired Student's *t*-test. (D) Quantification of endogenous *Pum2* mRNA by qRT-PCR from 14 DIV cortical neurons transduced at 9+5 DIV with lentiviruses expressing shNTC or shPum2, normalized to shNTC. Paired Student's *t*-test. (E) Analysis of *HuR* mRNA stability in 14 DIV cortical neurons transduced at 9+5 DIV with lentiviruses expressing shNTC or shHuR and treated with DMSO or ActD for 90 min at 14 DIV. *HuR* mRNA levels were quantified by qRT-PCR and normalized to DMSO+shNTC. Paired Student's *t*-test. (F) RT-PCR with cDNA from 14 DIV rat cortical neurons transduced at 9+5 DIV with lentiviruses expressing shNTC or shHuR using primers detecting both annotated *mmuRgs4* splice isoforms (Ensemble, mm10). All error bars are SEM from ≥ 3 independent biological replicates; asterisks represent *p*-values ($*p < 0.05$). KD knock-down; NTC non-targeting control; ActD Actinomycin D; bp base pair; DIV days *in vitro*.



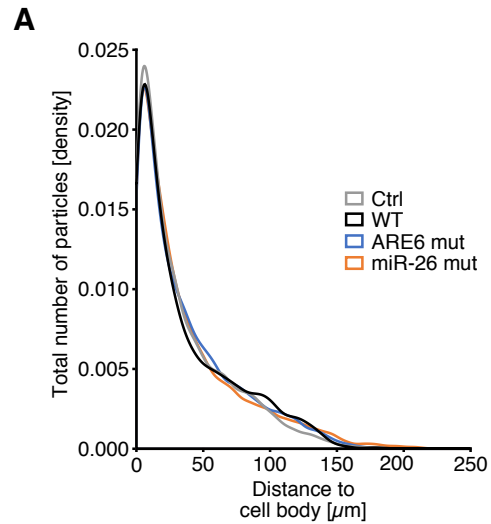
Supplementary Figure 2. HuB/C/D protein is less enriched in *Rgs4* *in vitro* RNA purification. (A,B) Representative western blot against HuR (HuB/C/D) and Ago2 (A) and quantification (B) of HuB/C/D enrichment from adult rat cortex lysate in *in vitro* RNA affinity purification using 2xMS2 only, 2xMS2+*Rgs4* CDS, 2xMS2+*Rgs4* 3'-UTR, and different 2xMS2+*Rgs4* 3'-UTR fragments as bait RNA, normalized to input. All error bars are SEM from ≥ 3 independent biological replicates. WT wild type.



Supplementary Figure 3. *HuR* mRNA is not affected by miR-26 overexpression or Ago2 KD. (A) qRT-PCR analysis of endogenous *HuR* mRNA in 14 DIV cortical neurons transduced at 11+3 DIV with lentiviruses expressing miR-scr or miR-26a, normalized to miR-scr. (B) qRT-PCR analysis of endogenous *HuR* mRNA in 14 DIV cortical neurons transduced at 9+5 DIV with lentiviruses expressing shNTC or shAgo2, normalized to shNTC. Paired Student's *t*-test. All error bars are SEM from ≥ 3 independent biological replicates. KD knock-down; Scr scrambled; NTC non-targeting control; DIV *days in vitro*.



Supplementary Figure 4. HuB/C/D binding in *Rgs4* *in vitro* RNA purification is not affected by ARE6 or miR-26 mutations. (A) Minimal free energies of predicted folding (RNAfold) of the conserved region of WT *Rgs4* 3'-UTR and ARE6 and miR-26 binding site mutants. (B) Minimal free energy of bound miR-26a to *Rgs4* conserved region calculated by IntaRNA for the *Rgs4* WT conserved region, and ARE6 and miR-26 binding site mutants. (C) Quantification of HuB/C/D enrichment from adult rat cortex lysate in *in vitro* RNA affinity purification using 2xMS2 only, 2xMS2+*Rgs4* 3'-UTR WT, 2xMS2+*Rgs4* 3'-UTR ARE6 mut and 2xMS2+*Rgs4* 3'-UTR miR-26 mut as bait RNA, normalized to input. Paired Student's *t*-test. (D) Quantification of eGFP fluorescence intensity in the cell body of hippocampal neurons at 15 DIV co-transfected at 14+1 DIV with eGFP-reporter and tagRFP or tagRFP-HuR and miR-scr or miR-26a. Ratio of eGFP reporter intensity between *Rgs4* 3'-UTR WT and Ctrl reporter is shown. Paired Student's *t*-test. All error bars are SEM from ≥ 3 independent biological replicates; asterisks represent *p*-values ($*p < 0.05$). WT wild type; ARE AU-rich element; DIV days *in vitro*.



Supplementary Figure 5. Mutation of miR-26 and HuR binding sites does not change dendritic *Rgs4* RNA distribution. (A) Density plot of the total number of MS2 particles over distance from cell body from hippocampal neurons transfected with tdMCP-GFP and 128xMS2+Ctrl, 128xMS2+*Rgs4* 3'-UTR WT, ARE6 mut or miR-26 mut reporter mRNA at 14+1 DIV. ARE AU-rich element; WT wild type; tdMCP-GFP tandem MS2 coat protein fused to GFP; DIV *days in vitro*.

4 Chapter B

This chapter contains the manuscript with the title

The dsRBP Staufen2 governs RNP assembly of neuronal Argonaute proteins

by

Janina Ehses, Melina Schlegel, Luise Schröger, Rico Schieweck, Sophia Derdak, Max Harner, Martin Bilban and Michael A. Kiebler*

* corresponding author

Author contributions:

Janina Ehses and Michael A. Kiebler designed and supervised the study. Janina Ehses, Melina Schlegel and Luise Schröger performed and analyzed experiments. Rico Schieweck performed and analyzed polysome profiling experiments. Sophia Derdak performed and analyzed and Martin Bilban supervised small RNA Sequencing experiments. Janina Ehses prepared all figures. Janina Ehses and Michael A. Kiebler wrote the manuscript.

The dsRBP Staufen2 governs RNP assembly of neuronal Argonaute proteins

Janina Ehse¹, Melina Schlegel¹, Luise Schröger¹, Rico Schieweck¹, Sophia Derdak²
Max Harner¹, Martin Bilban³ and Michael A. Kiebler^{1,*}

¹ Biomedical Center (BMC), Department for Cell Biology (Anatomy III), Medical Faculty, Ludwig-Maximilians University of Munich, Planegg-Martinsried, Germany

² Medical University of Vienna, Core Facilities, Lazarettgasse 14, 1090 Vienna, Austria

³ Department of Laboratory Medicine and Core Facility Genomics, Medical University of Vienna, Vienna, Austria

* Corresponding author:

Michael A. Kiebler (mkiebler@lmu.de)

Department for Cell Biology

Biomedical Center (BMC)

Medical Faculty, LMU

Großhaderner Straße 9, 82152 Planegg-Martinsried, Germany

ORCID

Michael A. Kiebler: <https://orcid.org/0000-0002-8850-6297>

Janina Ehse: <https://orcid.org/0000-0003-0634-769X>

Luise Schröger: <https://orcid.org/0000-0002-6213-4202>

Keywords

Ago; RNP assembly; RISC; RNA-binding protein; neuronal branching; Staufen2; P-bodies; polysomes.

Highlights

- Ago1/2 and RISC effector proteins are upregulated upon Stau2 KD
- Stau2 regulates Ago1/2 assembly with polysomes and P-bodies
- Upregulation and relocalization of Ago1/2 correlates with global downregulation of translation
- Stau2 and Ago1/2 counterbalance neuronal branching

Abstract (190 words)

Mature microRNAs are bound by a member of the Argonaute (Ago1-4) protein family, forming the core of the RNA induced silencing complex (RISC). Association of RISC with target mRNA results in translational silencing or RNA degradation depending on the recruitment of downstream effector proteins. Ago proteins also exist in other types of ribonucleoprotein particles (RNPs). However, both the dynamics of RNP assembly and the underlying functional implications are largely unknown. Here, we are characterizing the role the double-stranded RNA-binding protein Staufen2, a potential Ago interactor, in Ago1/2-RNP formation. Stau2 depletion resulted in the upregulation of Ago1/2 and the RISC effector proteins Ddx6 and Dcp1a. This upregulation caused displacement of Ago2 from processing bodies, large RNPs implicated in RNA storage, and subsequent association with translating polysomes suggesting an impact of Stau2 in Ago1/2-RNP assembly. Consequently, Stau2 deficiency yielded decreased global translation and increased neuronal branching. As these phenotypes can be rescued by Ago1/2 knockdown, we are proposing a working model in which both RNA binding proteins, Stau2 and Ago, critically depend on each other and play a key role in neuronal homeostasis with direct phenotypic consequences if brought out of balance.

Ehse *et.al.*, Regulation of RISC by Stau2

Introduction

Posttranscriptional gene regulation is an important cellular mechanism, which is mediated through a network of thousands of RNA-binding proteins (RBPs)^{1,2}. It is the RNA that serves as platform for the combinatorial assembly of different RBPs. Their intertwined action actually determines the RNA fate^{1,3}. The association of RNAs and proteins results in formation of RNA granules, called ribonucleoprotein particles (RNPs), that show large heterogeneity in composition, size and function⁴. Depending on the composition and condensation grade of RNA and protein components within the particles, the dynamic of RNP assembly differs⁵. While transport RNPs have been shown to contain only few transcripts and mediate RNA localization and local translation⁶⁻⁸, larger assemblies such as stress granules or cytosolic processing (P-) bodies are thought to rather serve in RNA and RBP storage^{4,9}.

Specific RNA structures rather than primary binding sequences are preferentially recognized by double-stranded RBPs (dsRBPs), thereby regulating RNA condensation grade and RNA accessibility for other RBPs. The neuron-enriched Stau2 (Stau2) protein is an dsRBP that binds to the 3'-UTR of target RNAs¹⁰ and, as a part of transport RNPs, enables their directed dendritic transport^{11,12}. Stau2 regulates activity-dependent dendritic mRNA localization¹⁰ and is required for maintenance of general dendritic RNA content¹³. A large subset of Stau2 targets encodes for synaptic proteins, with a prominent enrichment of the G protein-coupled receptor pathway and dopamine and serotonin receptors¹⁴. Finally, *in vivo* and *in vitro* studies showed that defective or missing Stau2 might yield abnormal dendritic spines¹⁵ and deficits in long-term depression¹⁶. On the protein site, Stau2 has been shown to interact with several other RBPs, including some involved in RNA interference (RNAi) and translation repression, mainly in an RNA-dependent manner¹⁷. One core component of RNAi is the ubiquitously expressed RBP Argonaute (Ago1-4). During this process, small RNAs, such as microRNAs (miRNAs), are transcribed, processed and loaded onto Ago, where they serve as a guide strand to recognize a set of target mRNAs¹⁸. This RNA induced silencing complex (RISC) then leads to translation repression and/or RNA degradation of the target mRNA. On the mechanistic level, this is achieved by recruitment of downstream effector proteins such as GW182/Tnrc6, Ddx6 and CCR4-NOT¹⁹. In addition, direct RNA degradation can be achieved by the intrinsic slicer activity of Ago2²⁰. The importance of Ago2 and RISC is highlighted by the findings that

Ehses *et.al.*, Regulation of RISC by Stau2

loss of Ago2 in mice leads to embryonic lethality and Ago2 germline mutants to central nervous system abnormalities in humans^{20,21}. Both Ago and RISC effector proteins are enriched in P-bodies⁹, but also exist in the cytosol. Certain members even localize to distal dendrites, where they exert neuronal activity dependent functions, such as Ago2, Dicer or TRBP^{22,23}.

Proteins involved in RNAi have been shown to exist in neuronal Stau2 RNPs^{17,24}. Here, we aimed at unraveling the underlying network of Stau2 and RBPs involved in RNAi. The synergistic or antagonistic mechanisms between different RBPs have been extensively studied on the single target level²⁵. Cellular RNP remodeling, however, upon alteration of single RBP concentrations has rarely been looked at so far. We provide strong experimental evidence for the neuronal dsRBP Stau2 to regulate RISC protein expression, while global miRNA abundance is unaffected by Stau2. Further, Stau2 deficiency resulted in altered Ago1/2 RNP assembly, shifting Ago1/2 association from P-bodies to actively translating polysomes. Finally, analysis of global translation, mRNA levels and branching complexity in neurons, led us to speculate that Ago and Stau2 need to be properly balanced in order to ensure neuronal function and homeostasis. Importantly, our biochemical and cell biological study reveals a compensatory loop between two key RBPs providing new functional and mechanistic insight into neuronal Ago RNP assembly and RNAi.

Results

Ago1/2 and RISC effector proteins are upregulated in Stau2 depleted neurons

Recently, we have performed label-free quantitative mass spectrometry to characterize of proteome changes in primary cortical neurons upon depletion of Stau2 (Schieweck *et al.*, *under revision*). This allowed us to analyze in detail possible changes of RBP levels, which would give us first insights into the underlying dynamics of RNP remodeling². Using gene ontology (GO) analysis, we found a statistically significant enrichment of miRNA associated biological processes in the proteome of neurons deficient for Stau2 (**Fig. 1A**). Rewardingly, proteins significantly downregulated in Stau2 depleted neurons showed an overrepresentation for actin, neuronal and transport related biological processes (**EV Fig. 1A**), which is in line with previous findings (Schieweck *et al.*, *under revision*). The overrepresentation of miRNA related biological processes was caused by the concerted upregulation of the RISC

Ehse *et.al.*, Regulation of RISC by Stau2

effector proteins Ddx6, Dcp1a and Edc4 and especially Ago1 and Ago2 protein upon Stau2 depletion (**Fig. 1B**). As implicated by the GO analysis, those significantly upregulated RBPs are functionally connected with each other (**Fig. 1B**). This upregulation seemed to be predominantly regulated at the protein level, as a significant increase of *Ago1* and *Ago2* mRNA levels was not detected in cortical neurons deficient for Stau2 (**Fig. 1C**). Next, we asked the question if Stau2 possibly altered expression or translation of the upregulated miRNA associated genes via direct RNA binding. We compared the list of upregulated proteins with published Stau2 target RNA datasets from RNA-immunoprecipitation¹⁴ and individual-nucleotide resolution UV crosslinking and immunoprecipitation (iCLIP)¹⁰ experiments (both from embryonic neuronal tissue). Notably, the mRNAs coding for Ago1, Ago2, Ddx6, Dcp1a and Edc4 were not detected in those datasets, suggesting that Stau2 does not regulate their expression through direct RNA-binding (**Fig. 1D**). However, several lines of evidence suggest a possible link between Stau2 and the miRNA machinery: (i) Stau2 has been linked to processing of small interfering RNAs in coleopteran insects²⁶; (ii) nuclear export of the Stau2 62kDa isoform is dependent on the miRNA-export factor Exportin5²⁷; and (iii) mRNAs of miRNA processing factors *Drosha* and *Dicer* were upregulated in Stau2 deficient neurons (**EV Fig. 1C**).

To test whether Stau2 indeed regulates mature miRNA levels, we performed small RNA sequencing from Stau2 deficient cortical neurons (**EV Fig. 1D**). Of the total detected miRNA population, 43 miRNAs (8 %) were differentially regulated with a majority being downregulated (**EV Fig. 1E,F**). Interestingly, comparison of the mean expression levels of those significantly altered miRNAs revealed no total net change of miRNA abundance between Stau2 depleted and control neurons (**EV Fig. 1G**). This is in accordance with previous results from *C. elegans* deficient for Stau2²⁸. Based on these results, we conclude that the upregulation of Ago1/2 and its effector proteins is not caused by changes in global miRNA abundance.

Next, we investigated the coexistence of Stau2, Ago2 and Ddx6 in the same RNA granules, based on previous reports^{9,17,29}. In HEK-293 cells, Stau2 as well as the upregulated miRNA associated proteins are found to be enriched in LSM14-positive P-bodies⁹ (**Fig. 1E**). Furthermore, we analyzed the association between endogenous Stau2, Ago and Ddx6 in proximal and distal dendritic segments (**Fig. 1F**). In the proximal segment, Ago2 showed strong colocalization with Ddx6 (90 ± 5 %) while colocalization with Stau2 was subtler (23 ± 5 %) (**Fig. 1G**). These results are

Ehse *et.al.*, Regulation of RISC by Stau2

comparable to previous colocalization analysis and live cell imaging data showing transient interactions between Stau2 and Ago2²⁴. Interestingly, in distal dendrites this pattern changed and colocalization of Ago2 with Stau2 increased significantly to $45 \pm 6 \%$, while colocalization with Ddx6 remained high with a downwards trend ($74 \pm 4 \%$). This suggests that the interaction between Stau2 and Ago2 is localization-dependent and rather takes place in dendritic RNPs than in P-bodies in the soma.

Stau2 selectively regulates Ago1/2 localization to P-bodies

Next, we investigated whether Stau2 might affect Ago2 protein localization in primary hippocampal neurons. Since the interaction of Stau2 and Ago seemed to be localization-specific, we hypothesized that Stau2 deficiency could selectively affect Ago2 RNP assembly. Similar to endogenous Ago2, eGFP-Ago2 predominantly yielded a granular pattern and colocalized with endogenous Dcp1a and Ddx6 in control conditions (shNTC) in mature neurons (**Fig. 2A, EV Fig. 2A**). Upon depletion of Stau2 by RNA interference using an shRNA against Stau2 (**EV Fig. 2B**)¹⁴, eGFP-Ago2 disassembled from P-bodies and yielded a diffuse expression pattern. Quantification of the granule number per cell revealed a statistically significant shift from 46 ± 7 to 10 ± 4 eGFP-Ago2 particles per cell (**Fig. 2B,C**). Importantly, localization of the P-body markers Dcp1a and Ddx6 was not affected by Stau2 depletion (**Fig. 2D, EV Fig. 2C**). Together, these data suggest that Stau2 selectively regulates the disassembly of Ago2 RNPs, but not of other P-body enriched proteins.

Quantification of the eGFP-Ago2 intensity in the cell body (**Fig. 2E**) revealed a similar increase as detected for endogenous Ago2 in the mass spectrometry and Western Blot analyses (**Fig. 1A, EV Fig. 1B**), thereby further substantiating the posttranscriptional upregulation of Ago2. Another Ago protein family member, Ago1, was equally upregulated in Stau2 depleted neurons (**Fig. 1B**). Therefore, we also characterized Ago1 localization in dependence of Stau2 and detected a similar localization pattern for eGFP-Ago1 as for eGFP-Ago2 (**Fig. 2F,G**). This indicates that the regulation is not Ago2 specific, but possibly common for all Ago proteins. In addition, we examined the Stau2 dependent localization of the Ago2 interacting protein and translational repressor Mov10 (**EV Fig. 2D**). Mov10 is an RBP that has been reported to colocalize with Stau2¹⁷ and to regulate the association of Ago2 with miRNA binding sites³⁰. We did not, however, detect any changes in eGFP-Mov10 particle numbers upon Stau2 depletion. Together, these results tempted us to speculate that Stau2 regulates

Ehse *et.al.*, Regulation of RISC by Stau2

specifically the assembly of Ago1/2 into miRNA containing RNPs, but not of other RISC-associated proteins.

In order to ensure that the observed relocalization is not caused by mere overexpression of an exogenous Ago-dependent shRNA, we repeated the experiment by coexpressing shRNAs against the RBPs Pum2 and HuR, respectively (**EV Fig. 2E-H**). Rewardingly, there was no effect on eGFP-Ago1/2 localization. We next investigated whether the observed disassembly of Ago2 from P-bodies can also be reversed upon rescue of Stau2 protein levels (**Fig. 2 H, I**). First, overexpression of tagRFP-Stau2 significantly increased the average number of eGFP-Ago2 particles per cell (60 particles), compared to the control condition with untagged tagRFP (38 particles). Furthermore, overexpression of an sh-resistant tagRFP-Stau2^R 15 in the presence of shStau2 was sufficient to partially rescue eGFP-Ago2 localization to P-bodies.

Ago2 associates with translating polysomes upon Stau2 depletion

Ago proteins have been linked to RNA degradation and translation inhibition. While P-bodies are thought to be places of RNA storage³¹, RNAi mediated translation control seems to be independent of these granules³². In this context it is interesting to note that Ago2 can associate with polysomes at the endoplasmic reticulum and in the cytosol³³, where it inhibits³⁴ or promotes translation³⁵, respectively. As we observed disassembly of Ago2 from P-bodies upon Stau2 depletion, we were interested if cytoplasmic Ago2 would associate with polysomes. Therefore, we performed polysome profiling, a method where translating ribosomes are frozen on the mRNA by incubating neurons with the translation inhibitor cycloheximide, followed by lysis and fractionation on a sucrose gradient (**Fig. 3A**). Western Blot analysis of the profiling fractions revealed that both eGFP-Ago2 and Stau2 comigrate with polysomes (**Fig. 3B**). Interestingly, eGFP-Ago2 comigration significantly increased in Stau2 deficient neurons (**Fig. 3C**), while the ribosomal marker Rpl7a was not affected. Ribosome run-off of actively translating polysomes by pretreatment of neurons with the translation initiation inhibitor harringtonine resulted in a shift of Rpl7a as well as eGFP-Ago2 towards monosomes (**Fig. 3D,E**), compared to cycloheximide-treated neurons (**Fig. 3B,C**). This indicates that eGFP-Ago2 migration indeed depends on actively translating polysomes. Together, our data suggest that Stau2 depletion results in an increased association of Ago2 with actively translating polysomes. This observation

Ehres *et.al.*, Regulation of RISC by Stau2

matches the disassembly of Ago2 from P-bodies upon Stau2 depletion, since P-bodies are reported to be polysome-free⁹.

Ago1/2 and Stau2 act antagonistically on global translation

Ago1/2 and RISC inhibit translation¹⁸, however, in some cases they can also promote translation^{35,36}. Here we wanted to test, if increased association of Ago with polysomes upon Stau2 depletion would result in inhibition or rather in promotion of global translation. Therefore, we designed lentiviruses harboring shRNAs against Ago1 and Ago2 and tested the effect of Ago1/2 depletion, as well as Stau2 depletion (**EV Fig. 4A**), on global translation in cortical and hippocampal neurons using the puromycin assay³⁷. Puromycin binds to actively translating ribosomes, resulting in termination of translation and release of a puromycin labelled peptide that can be detected by puromycin antibodies. Downregulation of Ago1/2 protein levels resulted in upregulated global translation in hippocampal neurons detected by immunostaining against puromycin (**Fig. 4A,B**). On the contrary, depletion of Stau2 resulted in a decrease of global translation, measured by puromycin incorporation. Finally, coexpression of shAgo1/2 and shStau2 resulted in the rescue of control (shNTC) translation levels. These effects could also be reproduced in cortical neurons by Western Blot analysis (**EV Fig. 4B**). It is important to note that pretreatment of neurons with the translation inhibitor cycloheximide prevented puromycin incorporation (**Fig. 4C, EV Fig. 4C**), indicating that puromycylation depends on actively translating ribosomes. Together, we show the opposing action of Ago1/2 and Stau2 on global translation.

mRNA levels are oppositely affected by Ago1/2 and Stau2 depletion

A series of Stau2 mRNA targets contain miRNA binding sites, and are potentially regulated by Stau2 and Ago on the mRNA level. Here, we show that the effects of Stau2 and Ago1/2 can be opposite for different Stau2 target mRNAs, while GC content, ORF and UTR lengths were all comparable. RNA levels from cortical neurons transduced with the respective lentiviruses were measured by qRT-PCR. *Rgs4* mRNA levels were decreased upon depletion of Stau2 and increased in Ago1/2 depleted neurons (**Fig. 4D**). On the contrary, *Rhoa* mRNA levels were increased in Stau2 depleted neurons (**Fig. 4E**). *Rgs4* as well as *Rhoa* mRNA levels were rescued by double-knockdown of both Stau2 and Ago1/2. Interestingly, *Rgs4* mRNA has been found to be enriched in P-bodies, while *Rhoa* mRNA was depleted from P-bodies in

Ehse *et al.*, Regulation of RISC by Stau2

HEK293T cells⁹. We conclude that, independent of the direction, the effect of the RBPs Stau2 and Ago1/2 on mRNA expression is contrary. Finally, we tested if Stau2 alone promoted gene expression when tethered to a luciferase reporter. Here, we used the well-established MS2 system³⁸ to tether a fusion protein of Stau2 and MS2-coat binding protein to a luciferase RNA by incorporation of two MS2 stem loop structures. Interestingly, tethering of Stau2 to the mRNA was sufficient to promote luciferase reporter expression (**EV Fig. 4D**). Overexpression of tagRFP-Stau2 did not result in changes of MS2 reporter expression, suggesting that the promoting effect is not mediated by unspecific binding to the MS2 stem loops. However, both tagRFP-Stau2 and MCP-Stau2 were sufficient to promote *Rgs4* 3'-UTR reporter expression, a direct mRNA target of Stau2¹⁴. Together, this provides additional experimental evidence for an opposing function of Stau2 and Ago1/2 in neuronal posttranscriptional gene expression.

Stau2 and Ago balance neuronal branching

Together, our data suggest that Stau2 and Ago1/2 act in opposite ways on RNA expression as well as translation. This tempted us to hypothesize that a balanced expression of Stau2 and Ago1/2 is ultimately important for proper neuronal physiology. According to our GO-term analysis biological processes associated to dendrite morphology, dendrite development and actin cytoskeleton, were enriched in proteins downregulated upon Stau2 depletion (**EV Fig. 1A**). In addition, the Ago1/2 regulated Stau2 target *Rgs4* has been reported to negatively affect arborization complexity in primary cortical neurons³⁹. We therefore tested the effects of Stau2 and Ago1/2 on neuronal morphology by analyzing the complexity of neuronal branching in fully developed hippocampal neurons at 14 DIV⁴⁰, that were transfected with the respective shRNAs three days prior to analysis (**Fig. 5A**). We found neuronal branching to be drastically increased in Stau2 deficient neurons, while knockdown of Ago1/2 led to a reduction of branching complexity (**Fig. 5B,C**). These data fit to previous observations as knockdown of RNAi components GW182/Tnrc6 and Dicer similarly resulted in reduced dendritic arborization^{41,42}. Double knockdown of both, Stau2 and Ago1/2, was sufficient to rescue control dendritic complexity. Interestingly, knockdown of Ago1 or Ago2 alone did not led to a reproducible effect compared to control conditions (**EV Fig. 5A,B**). Either the knockdown efficiency of Ago1 or Ago2 alone was not sufficient to impact arborization complexity, or the proteins can compensate for each other.

Discussion

It is now widely accepted in the field that RBPs do not act as separate players, but rather as interdependent factors jointly determining the fate of an RNA^{2,25}. Depending on the combination of RNA sequence and structure elements that regulate RBP assembly, the action of individual RBPs can differ for different target RNAs. For example, the AU-rich binding protein family Elavl has been shown to act synergistically as well as antagonistically with miRNAs/Ago on target RNAs^{25,43,44}. Here, we have taken an alternative approach by investigating the consequences of depletion of a single RBP, Stau2, on the RBPome. Specifically, Ago and RISC associated proteins were upregulated under those conditions. Together with our findings on the Stau2-specific Ago disassembly from P-bodies and increased association with polysomes, our data suggest a Stau2 dependent regulation of miRNA containing RNP assembly and composition. We hypothesized whether this Stau2 dependent regulation could be caused by different molecular mechanisms, from (i) altered global miRNA abundance to (ii) changes in the phosphorylation state of Ago and (iii) altered accessibility of miRNA binding sites in Stau2 target RNAs. The expression of proteins involved in miRNA processing and RISC assembly is tightly coupled to global miRNA abundance. As Stau2 binds to dsRNA and especially complex, extended RNA structures^{10,45}, potential binding to precursor miRNAs could therefore alter global miRNA processing. Furthermore, Stau2 has been previously connected to the small RNA processing pathway^{26,27}. Secondly, it has been shown that phosphorylation of Ago2 regulates its affinity to RISC associated proteins (S387)⁴⁶ and target mRNAs (S/T824:34)^{47,48}, leading to a remodeling of miRNPs independent of direct Stau2 binding. Several phosphatases and kinases show altered expression levels upon Stau2 depletion (Schieweck *et al.*, *under revision*). Using phosphomutants of the two major Ago2 phosphorylation sites S387 and S/T824:34 (**EV Fig. 2I-L**) and by performing small RNA sequencing, we could exclude the first two proposed mechanisms. This led us to our third hypothesis, where Ago hijacks previously inaccessible miRNA binding sites in the Stau2 target RNA pool upon depletion of Stau2 (**Fig. 6**). In this model, Stau2 prevents RISC assembly on translating RNAs thereby modulating RNA fate, eventually resulting in increased translation and/or RNA stability. Our data on changes in global neuronal translation would support this hypothesis, as translation is decreased in Stau2 depleted neurons and could be rescued by knockdown of Ago1/2. Previously, Stau2 has been

Ehse *et.al.*, Regulation of RISC by Stau2

shown to generally stabilize target mRNAs¹⁴. These observations, however, cannot be translated to single mRNAs, as Stau2 seems to occasionally also destabilize mRNAs, e.g. *Rhoa* mRNA. Interestingly, in all tested Stau2 target mRNAs the effect of Stau2 and Ago1/2 knockdown was opposite and could be rescued by triple knockdown. We also observed this complementary pattern of Stau2 and Ago1/2 when examining neuronal branching, indicating that this complex RBP network is important for neuronal function. Possibly this antagonistic action also results in stabilization of the mRNA component in Stau2 containing transport RNPs, that are translationally silenced by Ago⁸. Our data showing increased colocalization of Ago2 and Stau2 in distal dendrites, where directed transport of RNAs is taking place, are supporting this model. Here, a finetuned equilibrium of Stau2 and Ago proteins would ensure spatiotemporal control of translation that critically contributes to neuronal function and synaptic plasticity. Together, our data suggest that Stau2 and Ago/RISC counterbalance each other on several levels: RNA stability, translation and neuronal morphology. Removing one layer of posttranscriptional gene regulation may therefore result in an unbalanced condition that is more prone to external perturbations.

Ehse *et al.*, Regulation of RISC by Stau2

Materials and Methods:

Plasmids

Plasmids expressing human Flag/HA-Ago1 (NM_012199.5, 214 – 2787 nt), Flag/HA-Ago2 (NM_012154.5, 128 – 2070 nt), Flag/HA-Ago2-S387A and Flag/HA-Ago2-824:34A were kindly provided by G. Meister⁴⁷ and subcloned into pEGFP-C3 (Clontech) or ptagRFP-C (Evrogen) under control of a CMV promoter. For luciferase assays 2x MS2 loops⁴⁹ or the 3'-UTR of rat *Rgs4* (position 728–2919 nt; NM_017214.1) were cloned 3' of the renilla open reading frame of the psiCHECK2 dual luciferase vector. The MS2 coat protein (MCP)⁴⁹ was cloned into ptagRFP-C (Evrogen) by replacing the tagRFP open reading frame and mouse Stau2 62kDa isoform¹⁰ was inserted N-terminal to MCP. The plasmids expressing sh-resistant pCMV-tagRFP-Stau2 62kDa¹⁰, pCMV-eGFP-Mov10 (NM001107711, 159 – 3173 nt)¹⁷, psPAX2¹⁴, and pcDNA3.1-VSV-G¹⁴ have been described previously. The pSUPERIOR.neo vector (oligoengine) was used for expression of shRNAs; plasmids expressing shStau2⁵⁰, shPum2⁵¹, shAgo2⁴³, shHuR⁴³ have been described previously. For lentivirus expression, pCMV-eGFP-Ago2, pCamk2a-tagRFP-H1-shRNA, or pCamk2a-tagBFP-H1-shRNA were subcloned into lentiviral vector Fu3a. The shRNA oligo sequences were (5'–3'):

shNTC_F: tccaaagttcgaatggtttcaagagaaaccattcgaactttgga;

shStau2_F: gatatgaaccaacctcaattcaagagattgaaggttggtcatatc;

shPum2_F: accaagttggtctggattctcaagagagaatccagaccaacttggt;

shHuR_F: gaagaggcaattaccagtttcaagagatgaaactggaattgcctcttc;

shAgo1_F: cgagaagagggtgctcaagaactgtgaagccacagatgggttcttgagcacctctctcg;

shAgo2_F: tttctggaattgggatcattgtacaatgatcccaaattcacgaaca.

Lentivirus Production

Lentiviral particles for shNTC, shStau2, shPum2, shAgo2, shAgo1 and eGFP-Ago2 were generated from HEK-293T cells co-transfected with packaging plasmids psPAX2 and pcDNA3.1-VSV-G and the respective lentiviral Fu3a plasmid using calcium phosphate coprecipitation. After 48 h virus production, supernatants were filtered (0.45 µm PVDF Millex-HV; Millipore), concentrated by ultracentrifugation (65,000 x g, 140 min, SW 32 Ti rotor; Beckman Coulter) and resuspended in Opti-MEM™ (Life Technologies)¹⁴.

Ehse *et al.*, Regulation of RISC by Stau2

Neuronal Cell Culture, Transduction and Transfection

All animals in this study were used according to the German Welfare legislation for Experimental Animals (LMU Munich, *Regierung von Oberbayern*). Rat hippocampal neuron cell cultures from embryos at day 17 (E17) of timed pregnant Sprague-Dawley rats (Charles River Laboratories) were generated as described previously¹⁵. Briefly, E17 hippocampi were dissected, trypsinized and cells dissociated and plated on poly-L-lysine coated coverslips and cultured in NMEM+B27 medium (Invitrogen) with 5% CO₂ at 37°C. For cortical cultures, E17 cortices were trypsinized and dissociated, the cell suspension sequentially filtered through 100-, 70-, and 40-µm cell strainers and then plated at a density of 100,000 cells/cm² on poly-L-lysine coated 60 mm or 100 mm dishes. For protein and RNA analysis, cortical neurons were transduced with lentiviral suspension at 9-10 days *in vitro* (DIV) and lysed at 13–14 DIV. For protein localization experiments, transient co-transfection of hippocampal neurons by calcium phosphate precipitation⁵² was performed at 14 DIV, followed by fixation with 4 % PFA at 15 DIV.

Polysome Profiling

Cortical neurons grown (5 million cells per condition) in 100 mm dishes were co-transduced at 10 DIV with eGFP-Ago2 and shNTC or shStau2, respectively. Fifty percent of the medium was refreshed at 11 DIV and 13 DIV. At 14 DIV, neurons were treated with 100 µg/mL cycloheximide (CHX, 355 µM) for 10 min, washed three times with warm HBSS supplemented with 100 µg/mL CHX and lysed in polysome buffer (50 mM Tris HCl pH 7.4, 150 mM NaCl, 5 mM MgCl₂, 1% sodium deoxycholate, 1% NP-40 (IGEPAL CA-630), 355 µM CHX, 2 mM dithiothreitol) at 4°C. For analysis of active translating polysomes, neurons were pretreated with 2 µg/mL harringtonine (3.7 µM) for 10 min prior to washes, and lysis as described above. Lysates were cleared at 13,000 x g for 5 min at 4°C and the supernatant layered on top of a sucrose gradient (5 mL gradient volume; 18 %–50 % (w/v) sucrose in 100 mM KCl, 5 mM MgCl₂, 20 mM Hepes KOH pH 7.4). Gradients were ultracentrifuged (35,000 rpm, 90 min, 4°C, SW 55 Ti rotor, Beckman Coulter) before separated into 10x 500 µL fractions using an automated fractionator (Piston Fractionator, Biocomp) using RNA absorbance detection at 254 nm. Protein extraction of 300 µL per fraction was performed using methanol/chloroform extraction⁵³, the proteins were resolubilized in SDS loading buffer and heated to 95°C for 3 min.

Ehse et.al., Regulation of RISC by Stau2

Ago1/2 and Mov10 protein localization

Analysis of eGFP-Ago or eGFP-Mov10 localization in dependence of Stau2, Pum2 or HuR depletion was performed in hippocampal neurons grown on coverslips. Neurons were transiently co-transfected at 14 DIV with the respective overexpression plasmids and shNTC, shStau2, shPum2 or shHuR expressing plasmids using calcium phosphate precipitation. Neurons were fixed with 4 % PFA 16–20 h post transfection at 15 DIV. Coverslips were immunostained against Stau2 or Pum2, mounted on microscope slides with Fluoromount™ Aqueous Mounting Medium (Sigma), imaged and analyzed as described in the microscopy and image analysis section.

Puromycylation assay

Cortical neurons (2 millions per condition) grown in 60 mm dishes, or hippocampal neurons grown on coverslips were transduced with lentiviruses expressing shNTC, shStau2, shAgo1, and/or shAgo2 at 8–9 DIV. The medium was refreshed after two days of lentivirus transduction. At 13–14 DIV, neurons were treated with 1 μ M puromycin for 5 min, washed 2x with warm HBSS and lysed in 3xSDS loading buffer (cortical neurons for Western Blot) or fixed with 4 % PFA for 10 min (hippocampal neurons for immunostaining). As a control, cells were pretreated with 100 μ g/mL cycloheximide for 10 min prior to addition of puromycin. Western Blot, immunostaining against puromycin, microscopy and image analysis were performed as described in the respective sections. Quantification of the puromycin intensity from Western Blot was performed by measuring the whole lane intensity normalized to α Tubulin, for each biological replicate two technical replicates were performed. For hippocampal neurons, the average cell body intensity was measured of ≥ 30 healthy neurons per experiment and condition.

Tethering assay

HeLa cells were cultured in DMEM+FCS medium at 37°C and 5 % CO₂. One day prior to transfection 4000 cells per well were plated in tissue culture treated 96-well plates. Cotransfection was performed in 3 technical replicates with MCP or tagRFP overexpression and psiCHECK™-2 dual luciferase vectors using Lipofectamine® 2000 (Thermo) according to manufacturer's instructions. 16 – 18 h after transfection, cells were washed once with prewarmed DPBS (Life Technologies) and lysed in 50 μ L

Ehse *et al.*, Regulation of RISC by Stau2

passive lysis buffer (Promega) per well. Lysis was completed by incubation for 1 h at RT, before 10 μ L lysate per well were transferred into a white 96-well plate (Greiner). Luciferase activity was assessed with freshly prepared firefly (4 mM Tricine, 534 μ M MgSO₄, 20 μ M EDTA, 33.3 mM DTT, 530 μ M ATP (PJK Biotech), 270 μ M Coenzyme A (PJK Biotech), 470 μ M D-luciferin (PJK Biotech), pH 7.8) and renilla luciferase buffer (550 mM NaCl, 1.1 mM EDTA, 110 mM KH₂PO₄, 440 μ g/mL BSA (Sigma), 13 μ M Coelenterazin (PJK Biotech), 0.5 mM NaN₃, pH 5.0). Luminescence was measured in a Centro XS3 LB 960 High Sensitivity Microplate Luminometer (Berthold) using the following parameters: Per well measurement; 50 μ L/well injection volume; 2 sec delay; repeated measurements; 10 sec integration time. Data were exported as raw files and the ratio of renilla to firefly luciferase activity was calculated. The empty psiCheck™-2 vector was used as normalization control.

Sholl analysis

Hippocampal neurons grown on coverslips were transiently transfected with plasmids expressing fluorescent reporters and shNTC, shStau2, shAgo1, and/or shAgo2 at 11 DIV. Three days after transfection, neurons were washed with warm HBSS and fixed with 4 % PFA for 10 min. Images were acquired according to Microscopy and image analysis section and the eGFP fluorescent reporter signal used as marker of dendritic branches of transfected neurons. Using ImageJ, the images were converted into 8 bit and a threshold was set for clear differentiation between dendrites and background. Unspecific background pixels were removed, a line between the center of the cell body and the furthest dendritic signal was drawn as basis for the Sholl analysis plugin in ImageJ (10 μ m ring step size) that automatically counted intersections between dendritic branches and individual concentric rings.

Western blotting

Samples were treated with 50 U Benzonase Nuclease (Merck) for 10 min and 3xSDS loading buffer was added, prior to heating to 65°C for 12 min. Proteins of equivalent number of neurons were resolved on 10 % SDS-PAGE, transferred to nitrocellulose (pore size 0.2 μ m) and subjected to immunoblotting with mouse anti-Ago2 (2E12-1C9) (1:500, WH0027161M1, Sigma), rabbit anti-Stau2 (1:500, selfmade), rabbit anti- α Tubulin (1:15,000, P1332Y, Abcam), rabbit anti-GFP (1:500, K3-184-2, A. Noegel), mouse anti-Puromycin (1:500, 12D10, Millipore), or rabbit anti-Rpl7a (1:1,000, Abcam)

Ehse *et.al.*, Regulation of RISC by Stau2

diluted in blocking solution (2 % BSA, 0.1% Tween20, 0.1 % sodium azide in TBS pH 7.5). After incubation with IRDye labelled secondary donkey anti-mouse, anti-rabbit, or anti-goat (IRDye 800CW or 680RD, Li-Cor), all diluted 1:15,000 in blocking solution, membranes were imaged on an Odyssey CLx Imaging System (Li-Cor). Band intensities were quantified using Image Studio Lite software (Li-Cor) and normalized to α Tubulin signal intensity.

RNA extraction, cDNA synthesis and qRT-PCR

Total RNA from cortical neurons was extracted using TRIzol (Invitrogen) or miRNeasy Mini Kit (Qiagen). cDNA was generated from 1 μ g of DNase treated total RNA, using Superscript III reverse transcriptase (Invitrogen) with minor variation to the manufacturer's instructions. A mixture of 1.5 μ M random primer mix (New England Biolabs) and 2.5 μ M (dT)₂₀ was used during cDNA synthesis. Quantitative real time PCR (qRT-PCR) was performed in duplicates from a 1:50 dilution of the stock cDNA using a home-made SYBR Green Master Mix¹⁰, with the LightCycler 96 System (Roche). Only primers with an optimized efficiency of 95 – 105% were used. The $2^{-\Delta\Delta C_t}$ method implemented in the LightCycler Software (Roche) was used to calculate differences in RNA levels relative to peptidylprolyl isomerase A (*Ppia*) mRNA. The sequences of the qRT-PCR primers were (5'–3'):

*Ppia*_F: gtcaaccccaccgtgttctt; *Ppia*_R: ctgctgtctttggaacttg;
*Rgs4*_F: agtcccaaggccaagaagat; *Rgs4*_R: aacatgttccggctgtctc;
*Rhoa*_F: aaggaccagtcccagaggt; *Rhoa*_R: tgtccagctgtgtccataa;
*Drosha*_F: ctacacggtggccgtttact; *Drosha*_R: caatgaaccgcttctgatga;
*Dicer*_F: gcaaggaatggactctgagc; *Dicer*_R: gtacacctgccagaccact;
*Stau2*_F: agttgcgactggaacaggac; *Stau2*_R: tggaccactccatcctttgt;
*Ago1*_F: caacatcactcaccgctttg; *Ago1*_R: gcaggtgctgggatagagac;
*Ago2*_F: acaagctggtttgcgctac; *Ago2*_R: ttctgatctcctcttgccg;
*Pum2*_F: atgggagcagctctttgact; *Pum2*_R: gatgagccaaatccactgagag.

Small RNA sequencing and data analysis

Cortical neurons (2 million cells per condition) were transduced at 10 DIV with lentiviruses expressing shNTC and shStau2, and the medium was refreshed two days after transduction. At 14 DIV, neurons were washed twice in warm HBSS, lysed in QIAzol (Qiagen) and stored at -80°C until total RNA was batch-isolated using

Ehse *et.al.*, Regulation of RISC by Stau2

miRNeasy Mini kit (Qiagen). Only RNA with an RNA integrity number (RIN) ≥ 9.5 , determined on a Bioanalyzer 2100 (Agilent), was subjected to library preparation. Sequencing libraries were prepared at the Core Facility Genomics, Medical University of Vienna using the QIAgen smallRNA Library Prep Kit with Unique Molecular Identifiers (UMIs) according to manufacturer's protocols. Libraries were QC-checked on a Bioanalyzer 2100 (Agilent) using a High Sensitivity DNA Kit for correct insert size and quantified using Qubit dsDNA HS Assay (Invitrogen). Pooled libraries were sequenced on a NextSeq500 instrument (Illumina) in 1x75bp single-end sequencing mode. Approximately 10 million reads were generated per sample.

Reads in fastq format were aligned to a database of rat miRNAs and quantified considering the UMIs using the QIAseq miRNA Library Kit-Primary Quantification analysis tool from QIAgen GeneGlobe (<https://geneglobe.qiagen.com/at/analyze/>); accessed: 2020/07/29. Raw counts were normalized and analyzed for differential miRNA abundance using DESeq2⁵⁴ version 1.22.2.

Immunostaining

For immunostaining neurons were washed twice with warm HBSS and then fixed with warm 4 % PFA in HBSS for 10 min. Fixed cells were washed thrice with HBSS and permeabilized with 0.1 % Triton X-100 in DPBS for 5 min and blocked for at least 30 min in blocking solution (2 % FCS, 2 % BSA, 0.2 % fish gelatin (Sigma) in DPBS). The following primary antibodies were used overnight in 10vol% blocking solution in DPBS: mouse anti-Ago2 (2E12-1C9) (1:500, WH0027161M1, Sigma), rabbit anti-Stau2 (1:500, selfmade), mouse anti-Stau2 (1:500, selfmade), mouse anti-Puromycin (1:500, 12D10, Millipore), mouse anti-Dcp1a (1:500, Sigma), rabbit anti-Ddx6 (1:500), mouse anti-Pum2 (1:10,000, Abcam). The following secondary antibodies were used for 2 h in 10vol% blocking solution in DPBS: donkey anti-mouse or rabbit AF488-, AF555- or AF647-conjugated antibodies (all Invitrogen). Coverslips were mounted on microscope slides with Fluoromount™ Aqueous Mounting Medium (Sigma).

Microscopy and image analysis

Images were acquired using Zeiss Zen software on a Zeiss Z1 Axio Observer microscope including a 63x Plan-Apochromat oil immersion objective (1.40 NA), a COLIBRI.2 LED and an HXP 120 C light source and the AxioCam 506 mono camera. Neurons were selected for cell morphology and viability as well as for expression of

Ehse *et.al.*, Regulation of RISC by Stau2

plasmids or lentiviruses and images were taken in the dendritic plane. For eGFP-Ago1/2 and eGFP-Mov10 protein localization experiments, z-stacks of whole neurons were acquired (30 planes with 0.26 μm step-size) and a z-projection of the maximum intensity was performed in ImageJ. The number of eGFP-Ago1/2, eGFP-Mov10, Dcp1a and Ddx6 particles per neuron were manually counted using the multipoint tool in ImageJ. For cell body fluorescence intensity quantification of eGFP-Ago2, or puromycin, Stau2 and Pum2 protein signal, the measure function in the Zeiss Zen software was used and a region of interest was drawn by hand based on the phase contrast image. Analysis of colocalization between endogenous Ago2, Stau2, Dcp1a and Ddx6 was performed by acquisition of z-stacks of whole neurons (35 planes with 0.22 μm step-size), followed by deconvolution using the Zeiss Zen software deconvolution module, with default settings of the constrained iterative method. Colocalization analysis was performed blind using ImageJ. For all experiments, ≥ 15 neurons per condition from at least three independent biological experiments were quantified.

Dataset comparison and gene ontology analysis

Gene ontology overrepresentation analysis was done using the statistical overrepresentation test of the PANTHER classification system (<http://www.pantherdb.org>)⁵⁵. Protein network analysis was done using STRING database (<https://string-db.org/>)⁵⁶. Comparison of Stau2 related MS datasets with P-body enriched genes were performed using R studio based on the Gene names.

Statistical analysis

Microsoft Excel, Prism5, and R software were used for data processing, plotting and statistical analysis^{57,58}. Figures represent mean \pm standard error of the mean (SEM) of at least three independent biological replicates. Asterisks represent p -values obtained by one-way ANOVA and either paired or unpaired two-sided Student's t-test using the mean values per experiment (* $p < 0.05$, ** $p < 0.01$, *** $p < 0.001$, **** $p < 0.0001$), if not stated otherwise.

Acknowledgements

We thank Christin Illig and Renate Dombi for excellent technical assistance; Ilaria Brentari for initial experiments on neuronal branching and members of the Kiebler lab

Ehnes *et.al.*, Regulation of RISC by Stau2

for helpful discussions and critical comments on the manuscript. This work was supported by the DFG (Großgeräteantrag INST86/1581-1FUGG, SPP1738, FOR2333, SFB870) and the FWF (I 590-B09, F4314-B09 SFB RNA-seq) (all to M.A.K).

Author contributions

J.E. and M.A.K. designed and conceptualized the project. J.E., M.S., L.S. and R.S. performed experiments and analyzed the data. S.D. performed and M.B. supervised small RNA sequencing experiments. J.E. and M.A.K. wrote the manuscript, with feedback from all authors.

Declaration of interest statement

No potential conflicts of interest were disclosed.

Ehse *et al.*, Regulation of RISC by Stau2**References**

1. Hentze, M. W., Castello, A., Schwarzl, T. & Preiss, T. A brave new world of RNA-binding proteins. *Nat. Rev. Mol. Cell Biol.* **19**, 327–341 (2018).
2. Schieweck, R., Ninkovic, J. & Kiebler, M. A. RNA-binding proteins balance brain function in health and disease. (2020).
3. Dassi, E. Handshakes and Fights: The Regulatory Interplay of RNA-Binding Proteins. *Front. Mol. Biosci.* **4**, 1–8 (2017).
4. Kiebler, M. A. & Bassell, G. J. Neuronal RNA Granules: Movers and Makers. *Neuron* **51**, 685–690 (2006).
5. Tauber, D., Tauber, G. & Parker, R. Mechanisms and Regulation of RNA Condensation in RNP Granule Formation. *Trends Biochem. Sci.* **45**, 764–778 (2020).
6. Mikl, M., Vendra, G. & Kiebler, M. A. Independent localization of MAP2, CaMKII α and β -actin RNAs in low copy numbers. *EMBO Rep.* **12**, 1077–1084 (2011).
7. Pilaz, L.-J., Lennox, A. L., Rouanet, J. P. & Silver, D. L. Dynamic mRNA Transport and Local Translation in Radial Glial Progenitors of the Developing Brain. *Curr. Biol.* **26**, 3383–3392 (2016).
8. Kiebler, M. A. & Bassell, G. J. Neuronal RNA Granules: Movers and Makers. *Neuron* **51**, 685–690 (2006).
9. Hubstenberger, A. *et al.* P-Body Purification Reveals the Condensation of Repressed mRNA Regulons. *Mol. Cell* **68**, 144–157.e5 (2017).
10. Sharangdhar, T. *et al.* A retained intron in the 3'-UTR of Calm3 mRNA mediates its Stau2- and activity-dependent localization to neuronal dendrites. *EMBO Rep.* **18**, 1762–1774 (2017).
11. Köhrmann, M. *et al.* Microtubule-dependent Recruitment of Stau2-Green Fluorescent Protein into Large RNA-containing Granules and Subsequent Dendritic Transport in Living Hippocampal Neurons. *Mol. Biol. Cell* **10**, 2945–2953 (1999).
12. Bauer, K. E. *et al.* Live cell imaging reveals 3'-UTR dependent mRNA sorting to synapses. *Nat. Commun.* **10**, 3178 (2019).
13. Tang, S. J., Meulemans, D., Vazquez, L., Colaco, N. & Schuman, E. A Role for a Rat Homolog of Stau2 in the Transport of RNA to Neuronal Dendrites. *Neuron* **32**, 463–475 (2001).
14. Heraud-Farlow, J. E. *et al.* Stau2 regulates neuronal target RNAs. *Cell Rep.* **5**, 1511–8 (2013).
15. Goetze, B. *et al.* The brain-specific double-stranded RNA-binding protein Stau2 is required for dendritic spine morphogenesis. *J. Cell Biol.* **172**, 221–231 (2006).
16. Berger, S. M. *et al.* Forebrain-specific, conditional silencing of Stau2 alters synaptic plasticity, learning, and memory in rats. *Genome Biol.* **18**, 222 (2017).
17. Fritzsche, R. *et al.* Interactome of Two Diverse RNA Granules Links mRNA Localization to Translational Repression in Neurons. *Cell Rep.* **5**, 1749–1762 (2013).
18. Bartel, D. P. Metazoan MicroRNAs. *Cell* **173**, 20–51 (2018).
19. Jonas, S. & Izaurralde, E. Towards a molecular understanding of microRNA-mediated gene silencing. *Nat. Rev. Genet.* **16**, 421–433 (2015).
20. Liu, J. *et al.* Argonaute2 is the catalytic engine of mammalian RNAi. *Science* **305**, 1437–41 (2004).
21. Lessel, D. *et al.* Germline AGO2 mutations impair RNA interference and human neurological development. *Nat. Commun.* **11**, 5797 (2020).

Ehse *et al.*, Regulation of RISC by Stau2

22. Nawalpur, B., Ravindran, S. & Muddashetty, R. S. The Role of Dynamic miRISC During Neuronal Development. *Front. Mol. Biosci.* **7**, (2020).
23. Antoniou, A. *et al.* The dynamic recruitment of TRBP to neuronal membranes mediates dendritogenesis during development. *EMBO Rep.* **19**, (2018).
24. Zeitelhofer, M. *et al.* Dynamic Interaction between P-Bodies and Transport Ribonucleoprotein Particles in Dendrites of Mature Hippocampal Neurons. *J. Neurosci.* **28**, 7555–7562 (2008).
25. Iadevaia, V. & Gerber, A. P. Combinatorial Control of mRNA Fates by RNA-Binding Proteins and Non-Coding RNAs. *Biomolecules* **5**, 2207–22 (2015).
26. Yoon, J.-S. *et al.* Double-stranded RNA binding protein, Stau2, is required for the initiation of RNAi in coleopteran insects. *Proc. Natl. Acad. Sci.* 201809381 (2018). doi:10.1073/pnas.1809381115
27. Macchi, P. *et al.* The Brain-specific Double-stranded RNA-binding Protein Stau2. *J. Biol. Chem.* **279**, 31440–31444 (2004).
28. Ren, Z., Veksler-Lublinsky, I., Morrissey, D. & Ambros, V. Stau2 Negatively Modulates MicroRNA Activity in *Caenorhabditis elegans*. *Genes & Genomes Genetics* **6**, 1227–1237 (2016).
29. Peredo, J., Villacé, P., Ortín, J. & De Lucas, S. Human Stau1 associates to MiRNAs involved in neuronal cell differentiation and is required for correct dendritic formation. *PLoS One* **9**, e113704 (2014).
30. Kenny, P. J. *et al.* MOV10 and FMRP regulate AGO2 association with microRNA recognition elements. *Cell Rep.* **9**, 1729–41 (2014).
31. Horvathova, I. *et al.* The Dynamics of mRNA Turnover Revealed by Single-Molecule Imaging in Single Cells. *Mol. Cell* **68**, 615–625.e9 (2017).
32. Freimer, J. W., Hu, T. J. & Blalock, R. Decoupling the impact of MicroRNAs on translational repression versus RNA degradation in embryonic stem cells. *Elife* **7**, 1–23 (2018).
33. Höck, J. *et al.* Proteomic and functional analysis of Argonaute-containing mRNA–protein complexes in human cells. *EMBO Rep.* **8**, 1052–1060 (2007).
34. Nottrott, S., Simard, M. J. & Richter, J. D. Human let-7a miRNA blocks protein production on actively translating polyribosomes. *Nat. Struct. Mol. Biol.* **13**, 1108–1114 (2006).
35. Vasudevan, S. & Steitz, J. A. AU-Rich-Element-Mediated Upregulation of Translation by FXR1 and Argonaute 2. 1105–1118 (2007). doi:10.1016/j.cell.2007.01.038
36. Rocchi, A. *et al.* Neurite-Enriched MicroRNA-218 Stimulates Translation of the GluA2 Subunit and Increases Excitatory Synaptic Strength. *Mol. Neurobiol.* **56**, 5701–5714 (2019).
37. Schmidt, E. K., Clavarino, G., Ceppi, M. & Pierre, P. SUNSET, a nonradioactive method to monitor protein synthesis. *Nat. Methods* **6**, 275–277 (2009).
38. Bertrand, E. *et al.* Localization of ASH1 mRNA Particles in Living Yeast. *Mol. Cell* **2**, 437–445 (1998).
39. Pallaki, P. *et al.* A novel regulatory role of RGS4 in STAT5B activation, neurite outgrowth and neuronal differentiation. *Neuropharmacology* **117**, 408–421 (2017).
40. Dotti, C. G., Sullivan, C. A. & Banker, G. A. The establishment of polarity by hippocampal neurons in culture. *J. Neurosci.* **8**, 1454–68 (1988).
41. Davis, T. H. *et al.* Conditional Loss of Dicer Disrupts Cellular and Tissue Morphogenesis in the Cortex and Hippocampus. *J. Neurosci.* **28**, 4322–4330 (2008).
42. Nawalpur, B. & Muddashetty, R. Distinct temporal expression of GW182 in

Ehse *et al.*, Regulation of RISC by Stau2

- neurons regulates dendritic arborization. *bioRxiv* 2020.12.05.412932 (2020). doi:10.1101/2020.12.05.412932
43. Ehse, J., Fernández-Moya, S. M., Schröger, L. & Kiebler, M. A. Synergistic regulation of Rgs4 mRNA by HuR and miR-26/RISC in neurons. *RNA Biol.* **00**, 1–11 (2020).
 44. Kim, H. H. *et al.* HuR recruits let-7/RISC to repress c-Myc expression. *Genes Dev.* **23**, 1743–1748 (2009).
 45. Sugimoto, Y. *et al.* hiCLIP reveals the in vivo atlas of mRNA secondary structures recognized by Stau1. *Nature* **519**, 491–494 (2015).
 46. Rajgor, D., Sanderson, T. M., Amici, M., Collingridge, G. L. & Hanley, J. G. NMDAR-dependent Argonaute 2 phosphorylation regulates miRNA activity and dendritic spine plasticity. *EMBO J.* **44**, 1–21 (2018).
 47. Quévillon Huberdeau, M. *et al.* Phosphorylation of Argonaute proteins affects mRNA binding and is essential for microRNA-guided gene silencing in vivo. *EMBO J.* **36**, 2088–2106 (2017).
 48. Golden, R. J. *et al.* An Argonaute phosphorylation cycle promotes microRNA-mediated silencing. *Nature* **542**, 197–202 (2017).
 49. Braun, J., Misiak, D., Busch, B., Krohn, K. & Hüttelmaier, S. Rapid identification of regulatory microRNAs by miTRAP (miRNA trapping by RNA in vitro affinity purification). *Nucleic Acids Res.* **42**, e66 (2014).
 50. Heraud-Farlow, J. E. & Kiebler, M. A. The multifunctional Stau proteins: conserved roles from neurogenesis to synaptic plasticity. *Trends Neurosci.* **37**, 470–479 (2014).
 51. Vessey, J. P. *et al.* Mammalian Pumilio 2 regulates dendrite morphogenesis and synaptic function. *Proc. Natl. Acad. Sci.* **107**, 3222–3227 (2010).
 52. Zeitelhofer, M. *et al.* High-efficiency transfection of mammalian neurons via nucleofection. *Nat. Protoc.* **2**, 1692–1704 (2007).
 53. Wessel, D. & Flügge, U. I. A method for the quantitative recovery of protein in dilute solution in the presence of detergents and lipids. *Anal. Biochem.* **138**, 141–143 (1984).
 54. Love, M. I., Huber, W. & Anders, S. Moderated estimation of fold change and dispersion for RNA-seq data with DESeq2. *Genome Biol.* **15**, 550 (2014).
 55. Mi, H., Muruganujan, A., Ebert, D., Huang, X. & Thomas, P. D. PANTHER version 14: more genomes, a new PANTHER GO-slim and improvements in enrichment analysis tools. *Nucleic Acids Res.* **47**, D419–D426 (2019).
 56. Szklarczyk, D. *et al.* STRING v11: protein–protein association networks with increased coverage, supporting functional discovery in genome-wide experimental datasets. *Nucleic Acids Res.* **47**, D607–D613 (2019).
 57. Team, R. C. R: A Language and Environment for Statistical Computing. (2014).
 58. Wickham, H. *ggplot2*. (Springer New York, 2009). doi:10.1007/978-0-387-98141-3

Ehse *et al.*, Regulation of RISC by Stau2

Figure 1. Stau2 depletion leads to upregulation of Ago1/2 and RISC effector proteins. (A) Gene ontology (GO) overrepresentation analysis (PANTHER, biological process) of all significantly upregulated proteins from primary rat cortical neurons deficient for Stau2 (Schieweck *et al. under revision*). (B) Volcano plot displaying protein levels measured by quantitative mass spectrometry and protein network analysis (STRING database) of highlighted significantly upregulated genes (orange). (C) Quantification of *Stau2*, *Ago1* and *Ago2* mRNA levels using qRT-PCR from cortical neurons at 14 DIV transduced with shNTC or shStau2 at 10 DIV, normalized to *Ppia* and shNTC. (D) Venn diagram comparing proteins significantly upregulated upon Stau2 KD, RNAs enriched in Stau2 RNA-IPs¹⁴, or Stau2 targets identified by iCLIP¹⁰. (E) Venn diagram comparing significantly altered proteins upon Stau2 KD (Schieweck *et al. under revision*) and proteins enriched in P-bodies⁹. (F) Representative phase contrast and pseudocolored deconvolved fluorescent images of hippocampal neurons at 15 DIV stained for Ago2, Ddx6 and Stau2. Scale bar is 10 μm and 5 μm for insets. (G) Quantification of colocalization between endogenous Ago2 particles and Ddx6 or Stau2 particles in proximal (first 15 μm) and distal (≥ 20 μm from cell body) dendritic regions. Error bars are \pm SEM from ≥ 3 independent biological experiments and ≥ 20 cells per replicate; asterisks represent *p*-values ($*p < 0.05$). Paired two-tailed Student's *t*-test. DIV days *in vitro*; NTC non-targeting control; TL translation; KD knock down; iCLIP individual-nucleotide resolution cross-linking and immunoprecipitation.

Figure 2. Stau2 regulates Ago1/2 localization to P-bodies. (A-E) Representative phase contrast and fluorescent images and quantification of hippocampal neurons co-transfected at 14+1 DIV with eGFP-Ago2 and shNTC or shStau2 constructs and immunostained against Dcp1a. (B) Histogram showing the frequency distribution of the number of eGFP-Ago2 particles per cells from four biological replicates. Bin center is displayed on X-axis. (C) Dot plot showing the average number of eGFP-Ago2 particles per cell. (D) Quantification of the average number of Dcp1a particles per cell. (E) Quantification of the eGFP-Ago2 fluorescence intensity in the cell body. (F,G) Quantification of eGFP-Ago1 particles from hippocampal neurons co-transfected at 14+1 DIV with eGFP-Ago1 and shNTC or shStau2 constructs as in B and C. (H,I) Representative fluorescent images and quantification of hippocampal neurons co-transfected at 14+1 DIV with eGFP-Ago2, shNTC or shStau2, and tagRFP or sh-resistant tagRFP-Stau2^R constructs. (I) Dot plot showing the average number of eGFP-

Ehse *et.al.*, Regulation of RISC by Stau2

Ago2 particles per cell. Error bars are \pm SEM from four independent biological experiments (shown as individual symbols) with ≥ 15 cells per replicate and condition; asterisks and hash keys represent p -values ($*p < 0.05$, $**p < 0.01$). Paired two-tailed Student's t -test. Scale bar is 5 μ m. DIV days *in vitro*; NTC non-targeting control.

Figure 3. Ago2 associates with translating polysomes in Stau2 depleted neurons. (A) Polysome profiles of post-nuclear lysates from cortical neurons treated with translation inhibitor cycloheximide (CHX) at 14 DIV and transduced at 10 DIV with lentiviruses expressing eGFP-Ago2 and shNTC or shStau2 and experiment outline. (B) Representative Western Blots of polysome profiles, immunoblotted for eGFP, Stau2 and Rpl7a (serving as ribosome marker). (C) Quantification of Western Blot eGFP-Ago2 protein intensities from three independent polysome profiling experiments, normalized to fraction 2 (F2). (D) Polysome profiles from cortical neurons transduced as in A pretreated with Harringtonine and experiment scheme. Harringtonine inhibits the first round of translation elongation after initiation. (E) Representative Western Blots of polysome profiles from cortical neurons treated with Harringtonine and transduced with shStau2 and eGFP-Ago2, immunoblots for eGFP and Rpl7a are shown. Error bars are \pm SEM from 3 independent biological experiments; asterisks represent p -values ($*p < 0.05$). Paired two-tailed Student's t -test. DIV days *in vitro*; NTC non-targeting control, CHX cycloheximide.

Figure 4. Stau2 and Ago1/2 oppositely regulate posttranscriptional gene regulation. (A) Representative fluorescent images of hippocampal neurons transduced with lentiviruses expressing shNTC, shStau2, or shAgo1/2 at 9-8 DIV and treated with puromycin for 5 min prior to fixation at 13-14 DIV. Puromycin fluorescent intensity is shown as pseudocolored grey values. (B) Dot plot of the cell body puromycin signal intensity from four biological replicates (≥ 40 cells per replicate and condition; cells shown as individual symbols). (C) Dot plot of the cell body puromycin signal intensity from two biological replicates treated with translation inhibitor CHX or with DMSO as control (≥ 35 cells per replicate and condition; cells shown as individual symbols). (D,E) The mRNA levels from 14 DIV cortical neurons, transduced with lentiviruses expressing shNTC, shStau2, or/and shAgo1/2 for 5 days, were quantified by qRT-PCR. RNA levels are normalized to *Ppia* and shNTC. Error bars are \pm SEM from independent biological experiments; asterisks represent p -values ($*p < 0.05$, $**p$

Ehse *et al.*, Regulation of RISC by Stau2

< 0.01 , $***p < 0.001$). Paired two-tailed Student's *t*-test. Scale bar is 10 μm . DIV days *in vitro*; NTC non-targeting control; CHX cycloheximide.

Figure 5. Balanced Stau2/Ago levels are important for neuronal branching. (A) Experiment outline and representative eGFP fluorescent images of hippocampal neurons transfected at 11 DIV with respective shRNA constructs and fixed at 14 DIV for Sholl analysis. (B) Quantification of intersections between neuronal branches and concentric rings. (C) Dot plot showing the sum of intersections over all concentric rings. Error bars are \pm SEM from five independent biological experiments (shown as individual dots) with ≥ 20 cells per replicate and condition; asterisks (to shNTC) and hash keys (to shStau2 + shAgo1/2) represent *p*-values ($*p < 0.05$, $**p < 0.01$, $***p < 0.001$). Paired two-tailed Student's *t*-test. DIV days *in vitro*; NTC non-targeting control.

Figure 6. Proposed model of Stau2 governed Ago1/2 RNP assembly. In wild type neurons, Ago proteins in the cell body colocalize with Ddx6 and Dcp1a in prominent particles, possibly processing bodies (P-bodies). Stau2 binds to structured elements in the 3'-UTR of neuronal mRNAs, that can be translationally silenced or active. In distal dendrites, colocalization of Ago and Stau2 is strong, possibly in translationally silenced transport RNPs. Stau2 depletion leads to mislocalization and destabilization of transported RNAs and remodeling of mRNPs. This in turn enables hijacking of Ago to previously inaccessible miRNA binding sites in actively translated mRNAs. The mRNA mislocalization together with altered mRNP formation possibly results in uncontrolled neuronal branching.

Ehse *et al.*, Regulation of RISC by Stau2

EV Figure 1. Stau2 KD does not affect global miRNA abundance. (A) Gene ontology (GO) overrepresentation analysis (PANTHER, biological process) of proteins significantly downregulated in primary cortical neurons depleted for Stau2. (B) Representative Western Blots and quantification of protein signal normalized to α Tubulin from cortical neurons transduced with shNTC or shStau2. (C) Quantification of *Drosha* and *Dicer* mRNA levels using qRT-PCR from cortical neurons at 14 DIV transduced with shNTC or shStau2 at 10 DIV, normalized to *Ppia* and shNTC. (D) Dot plot comparing miRNA expression levels (BaseMean) and fold change of small RNA Sequencing from 14 DIV cortical neurons transduced at 10 DIV with shNTC or shStau2. (E) Volcano plot highlighting differentially expressed miRNAs. (F) Bar graph displaying number of differentially regulated miRNAs categorized in groups based on up- or downregulation upon Stau2 depletion. (G) Box plot comparing the total miRNA abundance of all differentially regulated miRNAs in between shNTC and shStau2. Error bars are \pm SEM from ≥ 3 independent biological experiments; asterisks represent *p*-values ($*p < 0.05$). Paired two-tailed Student's *t*-test. DIV days *in vitro*; NTC non-targeting control.

EV Figure 2. Ago1/2 localization is Stau2 specific. (A-C) Hippocampal neurons co-transfected at 14+1 DIV with eGFP-Ago2 and shNTC or shStau2 constructs were immunostained against Stau2, Ddx6 and Dcp1a. (A) Quantification of colocalization between eGFP-Ago2 particles and endogenous Ddx6 or Dcp1a. (B) Quantification of the average Stau2 protein signal per cell body. (C) Histogram showing the frequency of number of endogenous Dcp1a particles per cell over four biological replicates. Bin center is displayed on X-axis. (D) Quantification of the number of eGFP-Mov10 particles per cell from cells co-transfected with shNTC or shStau2 at 14+1 DIV. (E-F) Quantification of Pum2 protein signal in the cell body (E) and eGFP-Ago particles per cell (F, G) from hippocampal neurons co-transfected at 14+1 DIV with eGFP-Ago2 or eGFP-Ago1 and shNTC or shPum2. (H) Quantification of the number of eGFP-Ago2 particles per cell from hippocampal neurons co-transfected with shNTC or shHuR at 14+1 DIV. (I-L) Quantification of the number of phosphomutant eGFP-Ago2-S/T824:34A (I, J) und eGFP-Ago2-S387A (K, L) particles per cell from hippocampal neurons co-transfected with shNTC or shStau2 at 14+1 DIV. Error bars are \pm SEM from ≥ 3 independent biological experiments (shown as individual symbols) with ≥ 15

Ehse *et.al.*, Regulation of RISC by Stau2

cells per replicate and condition; asterisks represent p -values ($*p < 0.05$). Paired two-tailed Student's t -test. DIV *days in vitro*; NTC non-targeting control.

EV Figure 4. Stau2 tethering to mRNA promotes gene expression. (A) RNA levels from 14 DIV cortical neurons transduced at 9 DIV with shNTC, shStau2, shAgo1, shAgo2 or a combination were quantified by qRT-PCR and normalized to *Ppia* and shNTC. (B) Representative Western Blot and quantification of cortical neurons transduced with lentiviruses expressing shNTC, shStau2, and/or shAgo1/2 at 9 DIV and treated with puromycin for 5 min prior to lysis at 14 DIV. As control neurons were treated with cycloheximide (CHX) prior to addition of puromycin. (C) Representative fluorescent images of hippocampal neurons treated with cycloheximide (CHX) or DMSO (Ctrl) for 5 min prior to treatment with puromycin for 5 min and fixation at 14 DIV. Puromycin fluorescent intensity is shown as pseudocolored grey values. (D) Luciferase activity in HeLa cells cotransfected with luciferase reporters and tagRFP or MCP proteins was quantified. Normalization to ctrl luciferase reporter levels and tagRFP condition was performed. Error bars are \pm SEM from ≥ 3 independent biological replicates; asterisks represent p -values ($*p < 0.05$, $**p < 0.01$, $***p < 0.001$, $****p < 0.0001$). Paired two-tailed Student's t -test. Scale bar is 20 μ m. DIV *days in vitro*; CHX cycloheximide; NTC non-targeting control; MCP MS2 coat protein.

EV Figure 5. Depletion of Ago1 or Ago2 alone is not sufficient to reduce branch complexity. (A) Quantification of intersections between neuronal branches and Sholl rings from hippocampal neurons transfected at 11 DIV with respective shRNA constructs and fixed at 14 DIV for Sholl analysis. (B) Dot plot showing the sum of intersections over all Sholl rings. Error bars are \pm SEM from five independent biological experiments (shown as individual dots in B) with ≥ 20 cells per replicate and condition; asterisks represent p -values ($*p < 0.05$). Paired two-tailed Student's t -test. DIV *days in vitro*; NTC non-targeting control.

Figure 1: Stau2 depletion leads to upregulation of Ago1/2 and RISC effector proteins

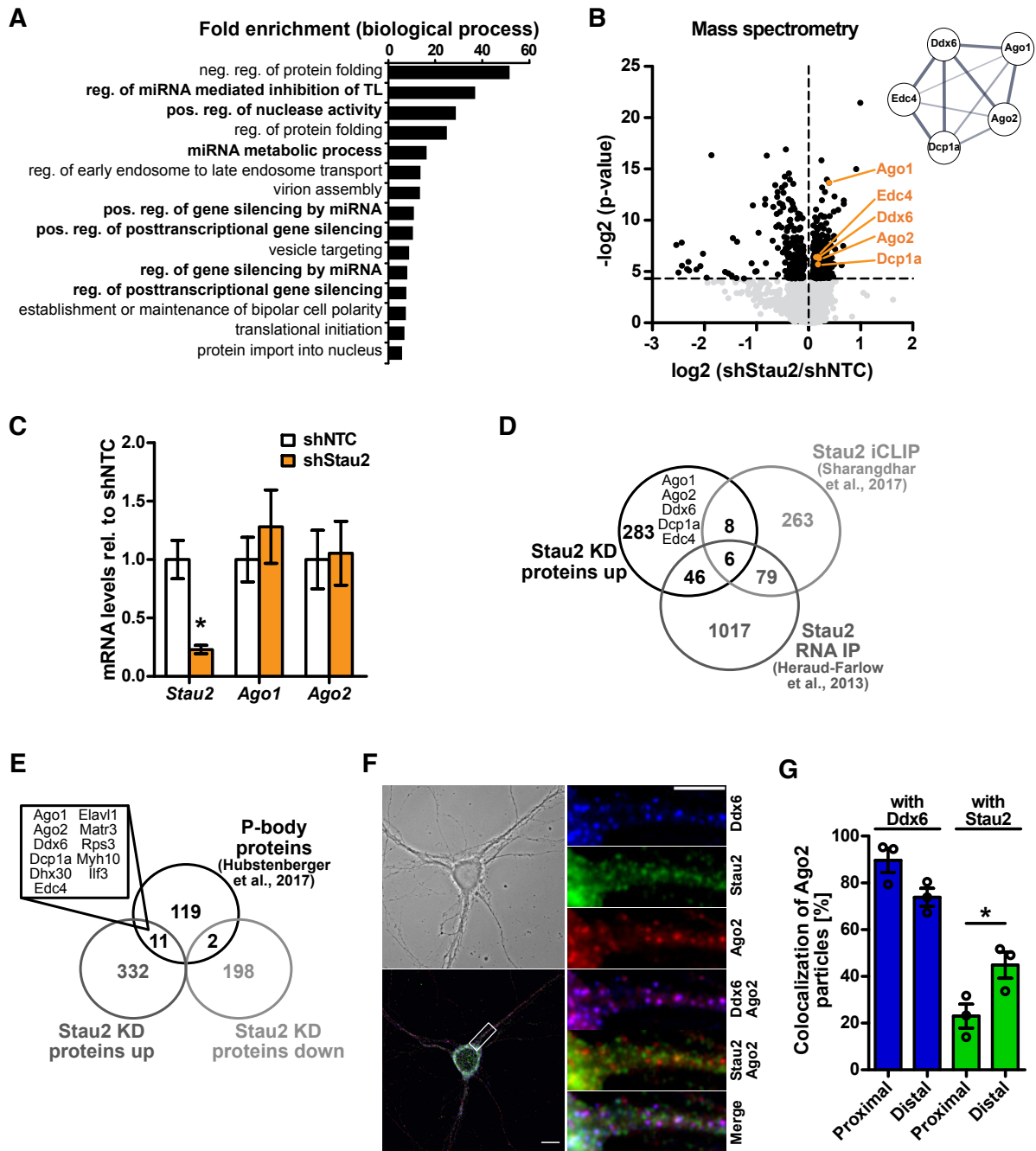


Figure 2: Stau2 regulates Ago1/2 localization to P-bodies

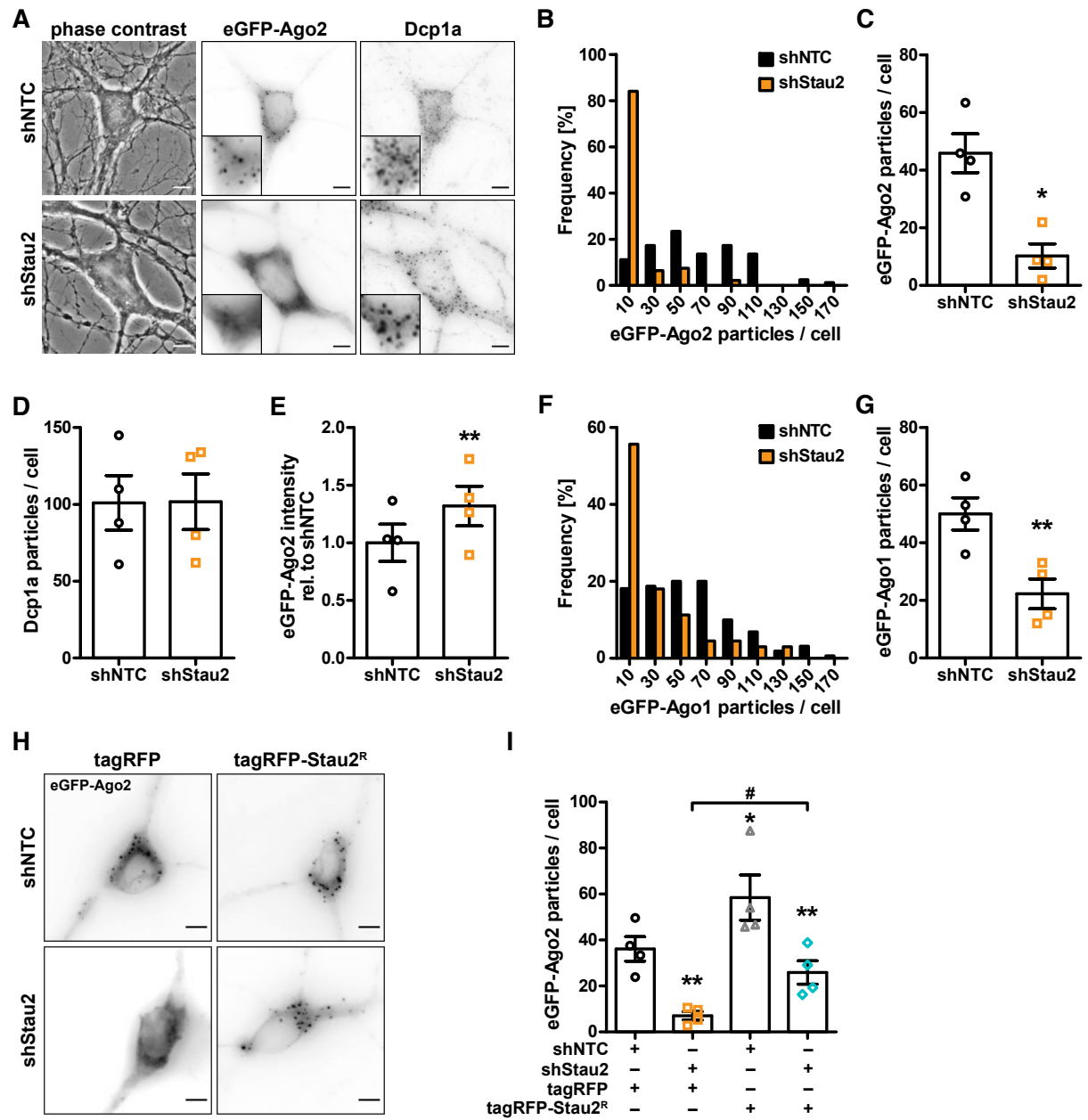


Figure 3: Ago2 associates with translating polysomes in Stau2 depleted neurons

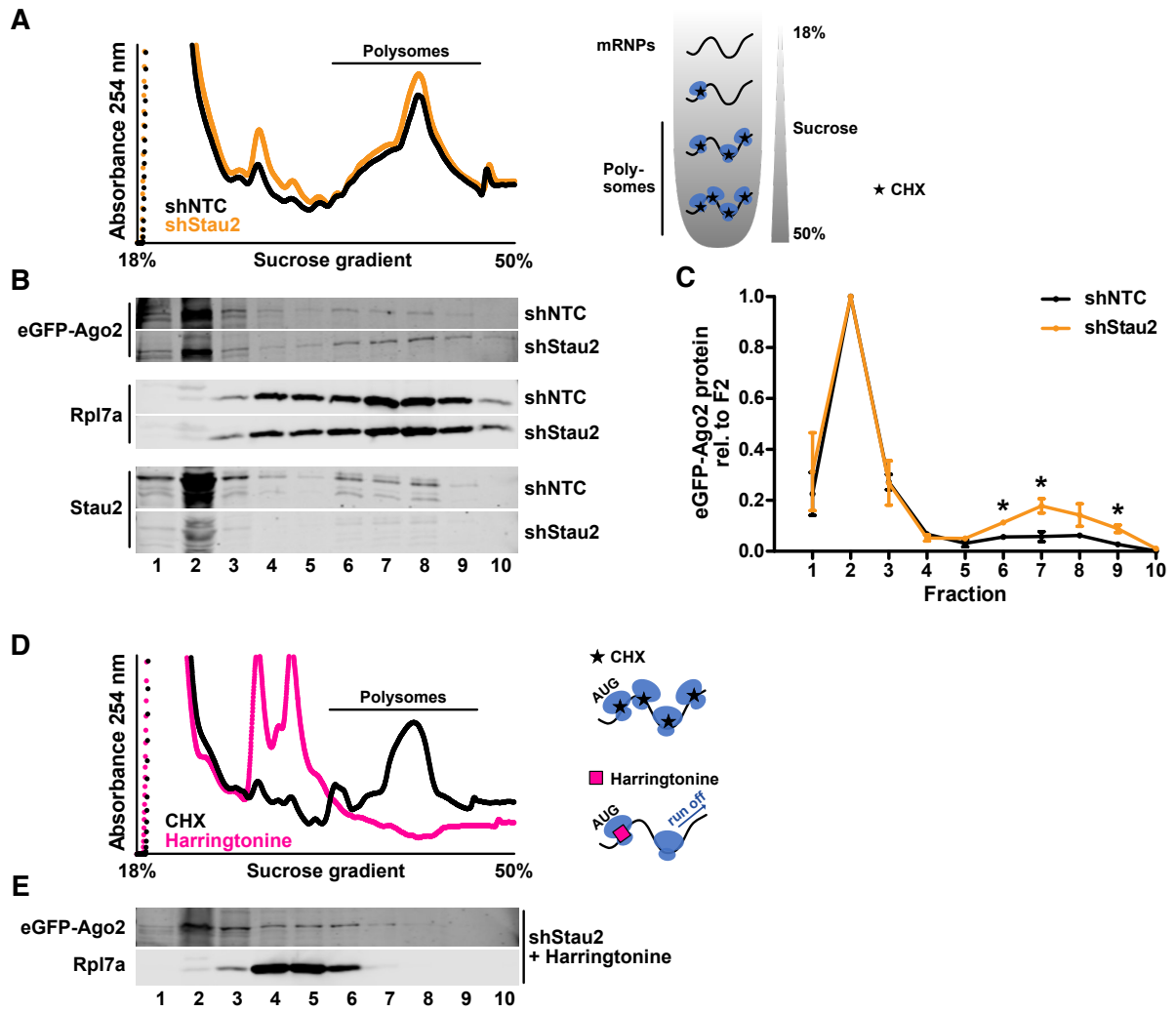


Figure 4: Stau2 and Ago1/2 oppositely affect posttranscriptional gene regulation

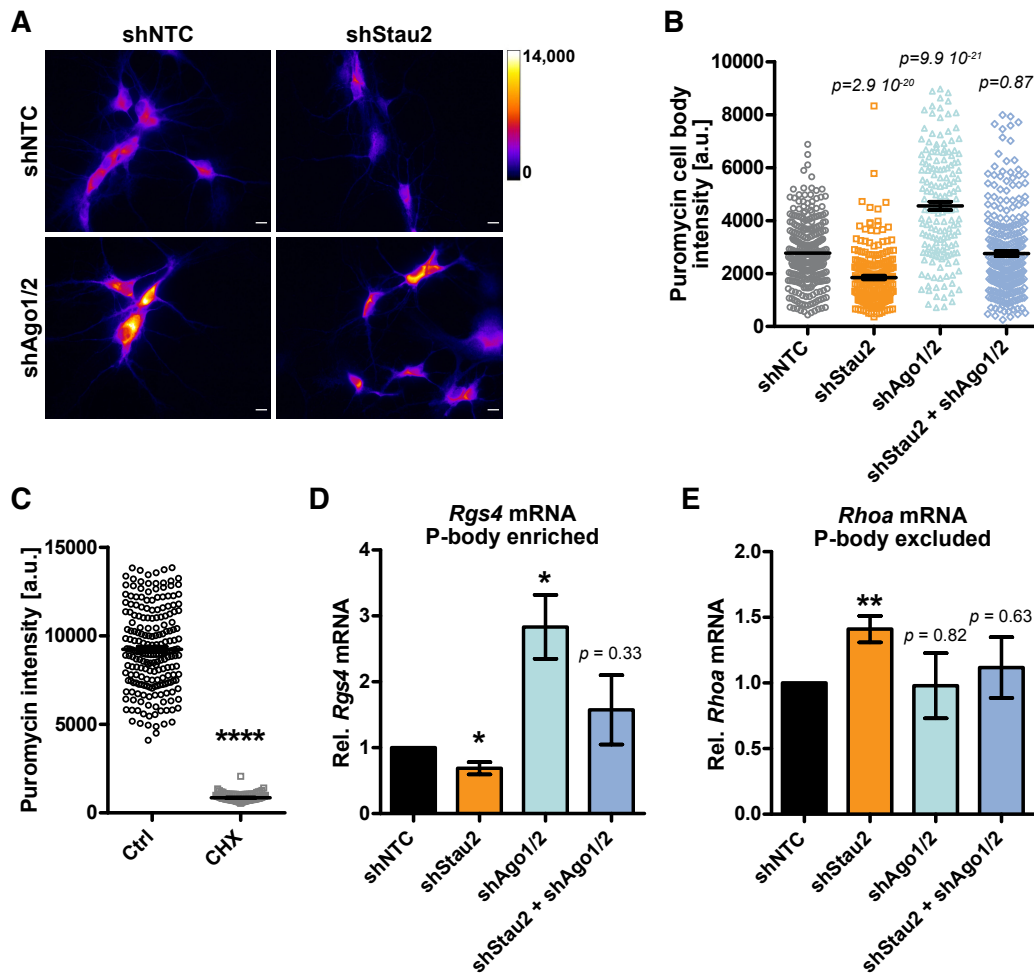


Figure 5: Balanced Stau2/Ago levels are important for neuronal branching

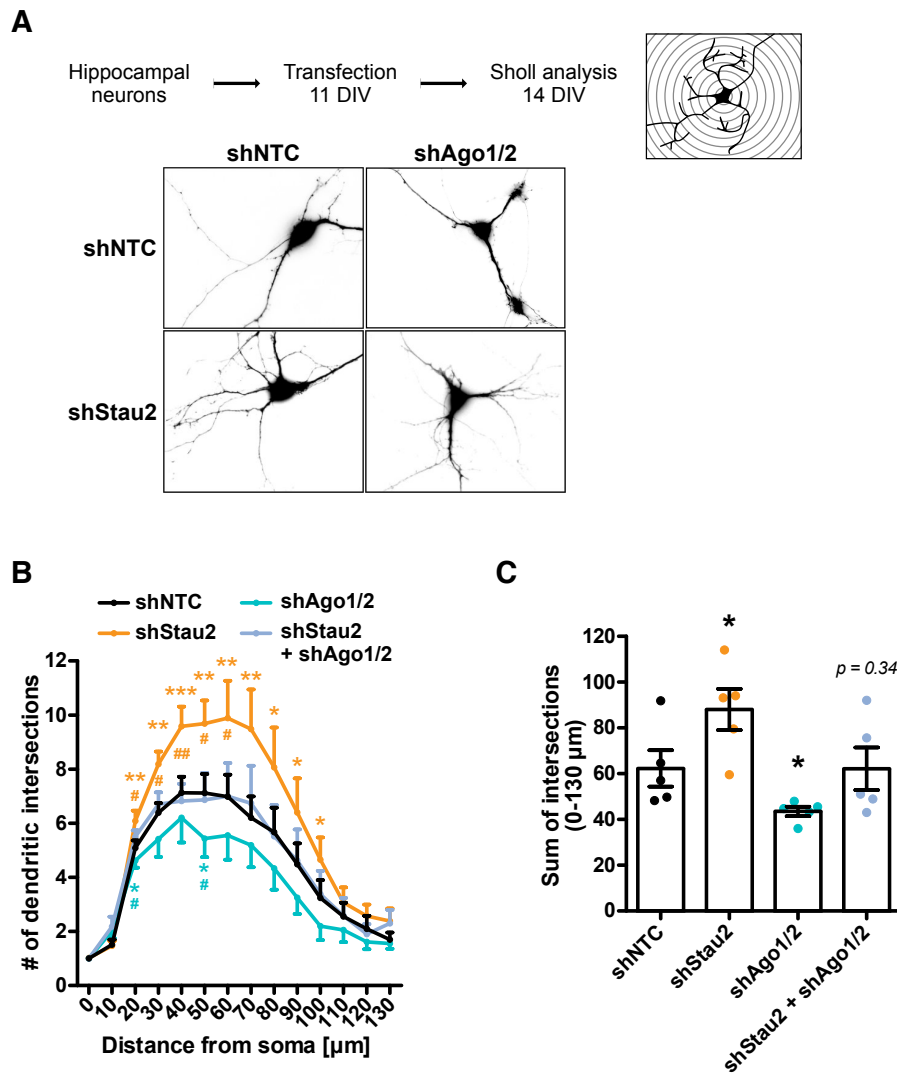
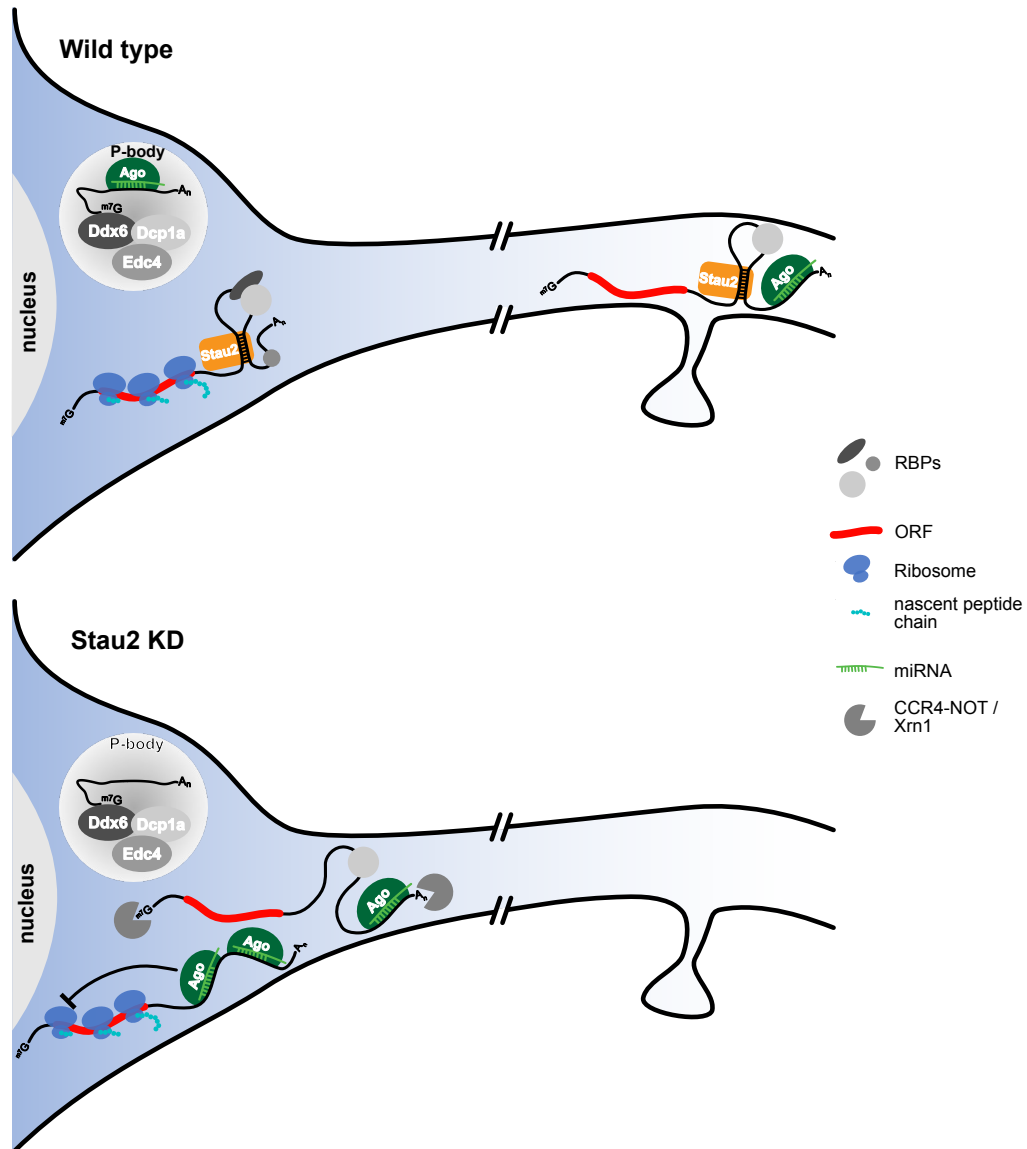
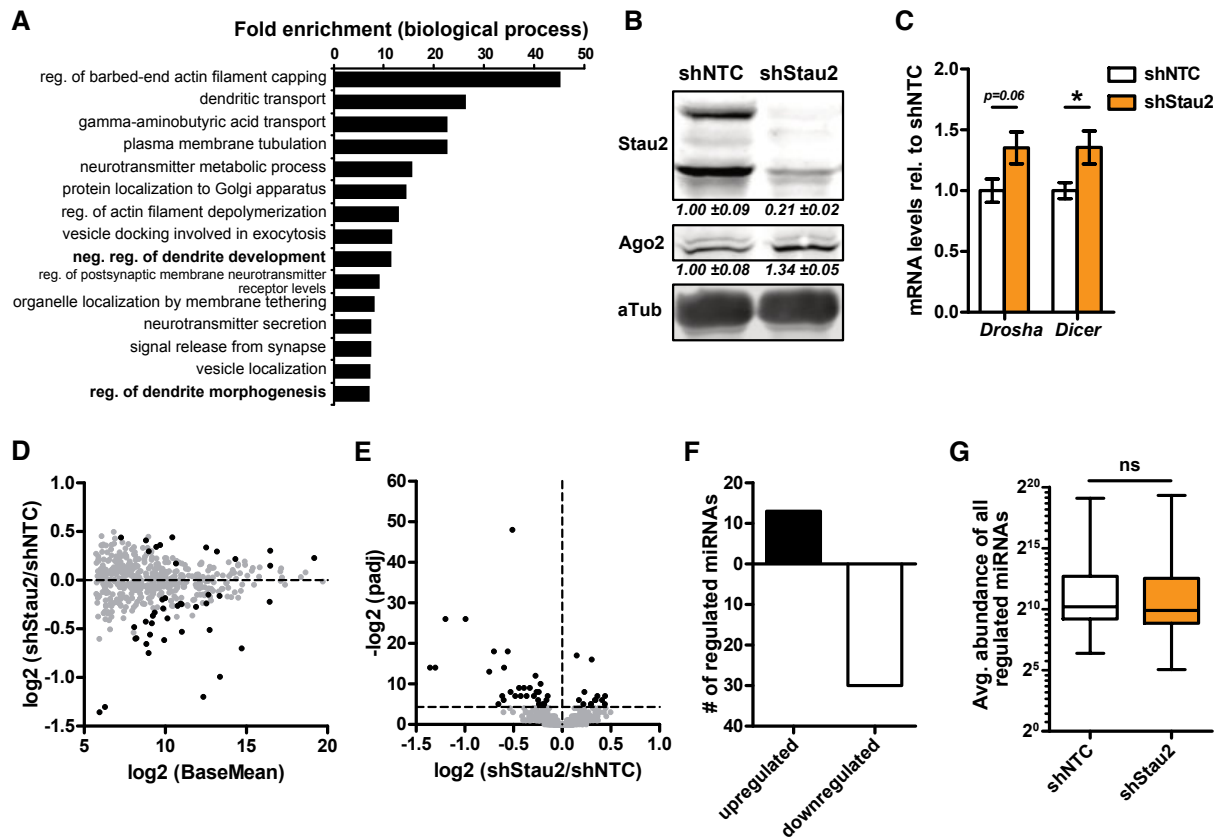


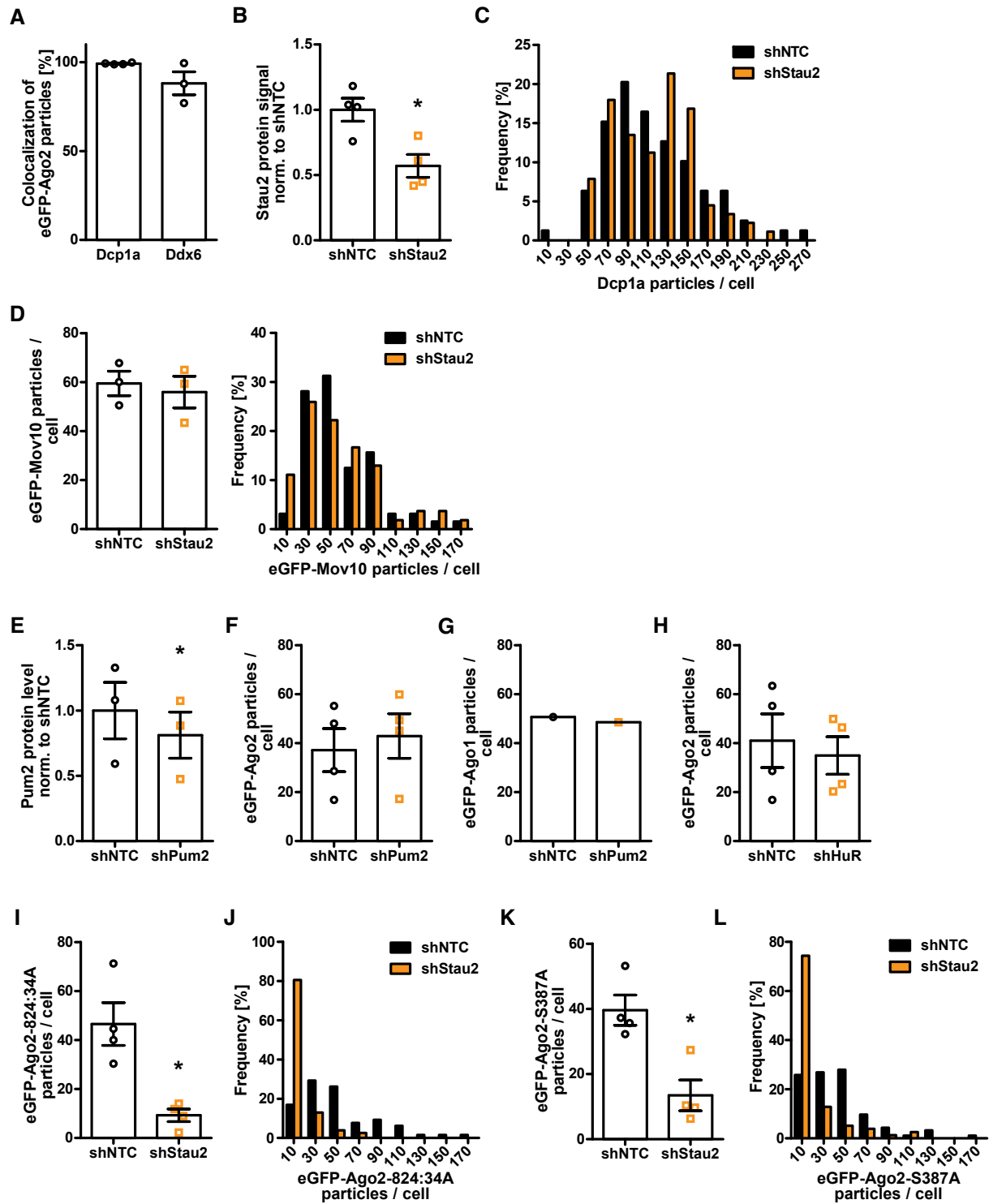
Figure 6: Proposed model of Stau2 governed Ago1/2 RNP assembly



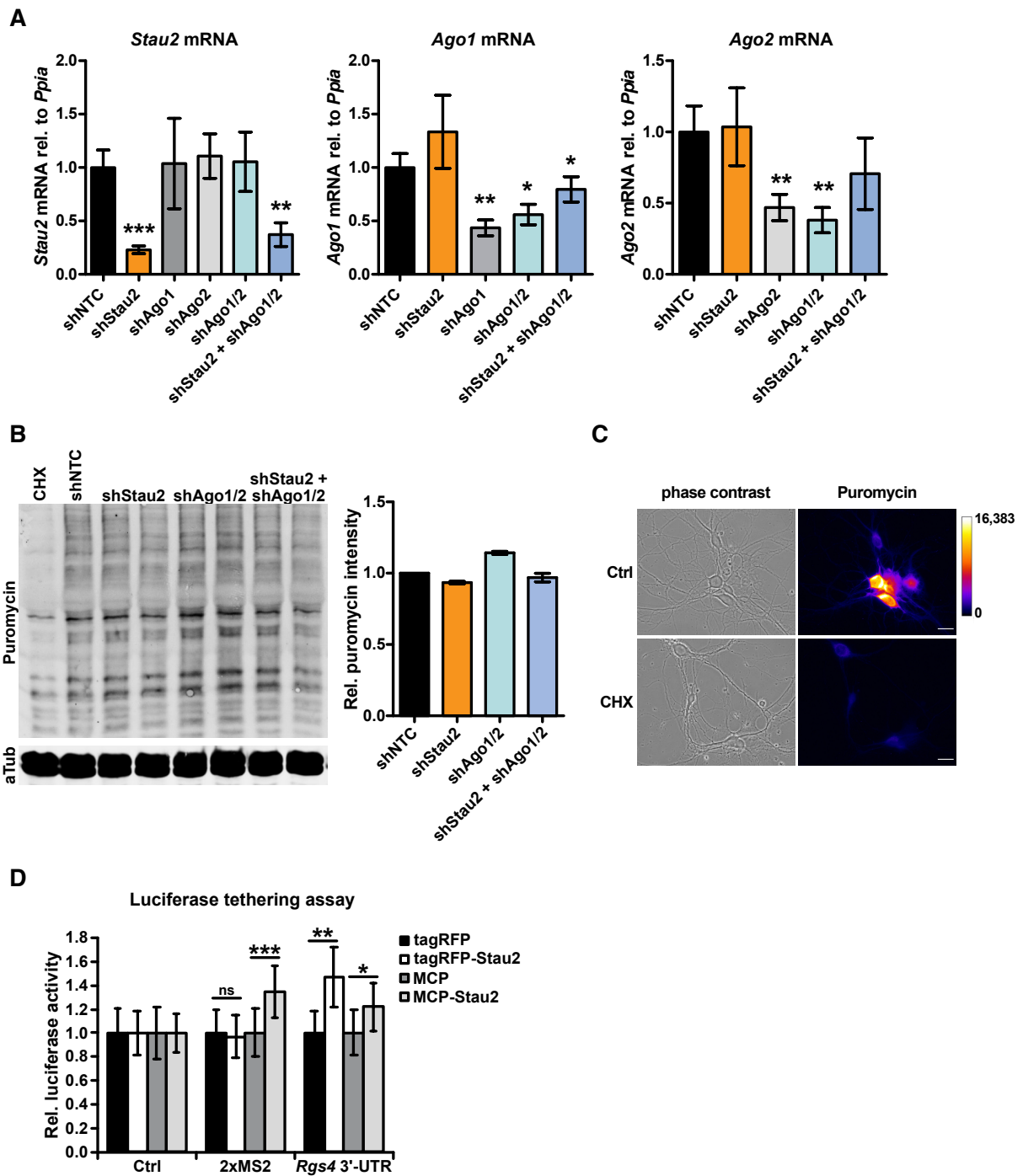
EV Figure 1: Stau2 KD does not affect global miRNA abundance



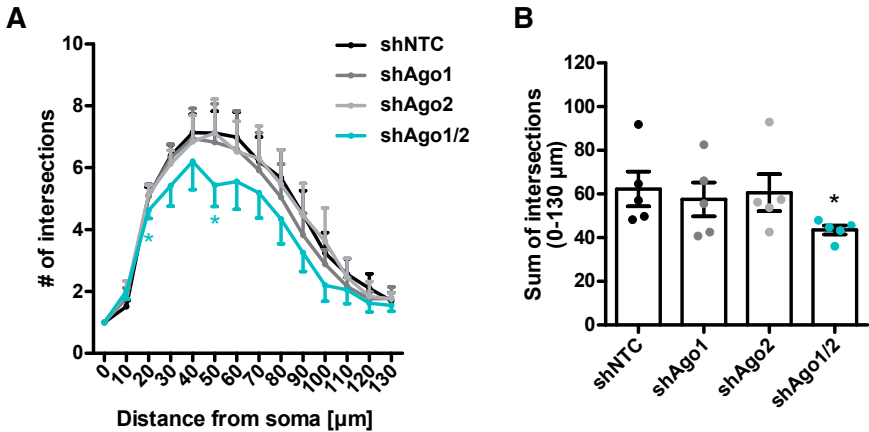
EV Figure 2: Ago1/2 localization is Stau2 specific



EV Figure 4: Stau2 tethering to mRNA promotes gene expression



EV Figure 5: Depletion of Ago1 or Ago2 alone is not sufficient to reduce dendritic complexity



5 Chapter C

The experiments and analyses presented in this chapter were performed by myself and contribute to a manuscript in preparation by Sandra M. Fernández-Moya. The running title of the manuscript is

RNA structure drives Stau2-dependent RNP assembly and localization in neurons

by

Sandra M. Fernández-Moya, **Janina Ehses**, Anob Chakrabarti, Karl E. Bauer, Rico Schieweck, Flora Lee, Jernej Ule and Michael A. Kiebler *

* corresponding author

5.1 Introduction

The assembly of RNPs is an essential cellular process that influences posttranscriptional gene regulation of the sequestered RNA. Recent evidence shows how the RNA component is one driving force for this process (Garcia-Jove Navarro et al., 2019; Tauber et al., 2020). It is therefore crucial to understand the processes underlying the recruitment of RBPs through cis regulatory RNA elements. Several different types of RNA elements regulating RBP binding have been described by now, from single-stranded sequence motifs to G-quadruplex helices (Kenny et al., 2014). Here, the invention of techniques based on high-throughput sequencing, such as individual-nucleotide resolution UV crosslinking and immunoprecipitation (iCLIP), revolutionized the detection and subsequent prediction of RNA binding sites for RBPs (Lee and Ule, 2018). The iCLIP technique uses UV light to crosslink RBP and RNA in intact cells or tissues. The unprotected RNA is then digested by RNase, followed by immunoprecipitation of the desired RBP, RNA extraction and high-throughput sequencing. This technique revolutionized the definition of RNA recognition sites for RBPs binding to single-stranded RNA elements. Such elements are defined through a specific binding sequence or base composition. iCLIP represents a major improvement compared to classical immunoprecipitation experiments, as the RBP-RNA interaction is trapped in physiological conditions, by crosslinking *in vivo*. In addition, more stringent washing and purification conditions can be applied to eliminate non-specific RNA binding.

In collaboration with Jernej Ule and colleagues, we were able to define RNA binding regions of the dsRBP Stau2 in embryonic mouse cortex exploiting the iCLIP technique (Sharangdhar et al., 2017). While we could show that Stau2 binding to an intron in the 3'-UTR of *Caln3* mRNA was important for activity driven dendritic localization of the RNA, we could not define the exact RNA structure Stau2 bound to. Deletion- and mutation-studies of areas defined by the Stau2 iCLIP dataset (Sharangdhar et al., 2017) and computational prediction of Stau2 recognition sites (Heraud-Farlow et al., 2013) did not result in detailed molecular insight into Stau2 RNA recognition (data not shown). Stau2 as an dsRBP binds to RNA secondary structures that are defined through two hybrid arms that can originate from different RNAs (intermolecular) or the same RNA (intramolecular). Further, the two hybrid arms from intramolecular RNA structures can be close or distal, resulting in short-range to long-range RNA hybrids. During the RNA preparation for downstream analysis in the iCLIP protocol this information on RNA structure gets lost. Now, the development of the RNA-hybrid and

individual-nucleotide resolution (hi)CLIP technique enables the detection of both strands bound by dsRBPs, as shown for Stau1 (Sugimoto et al., 2015). The introduction of sequential ligation of specific adaptors and adaptor-linkage of both hybrid strands, made the detection and assignment of both RBP bound RNA-hybrid strands possible (Fig. 5.1 A). However, sensitivity remained low due to inefficient adapter ligation and linkage. With recent improvements of the hiCLIP technology by the lab from Jernej Ule, they are now able to detect Stau2-bound RNA structures in depth (Chakrabarti A *et al.*, manuscript in preparation). These hiCLIP and additional iCLIP experiments were performed with cortices from rat brains at different developmental stages. Collaborative analysis of these data led to detection of a functionally relevant and Stau2-responsive long-range RNA structure in *Rgs4* RNA (Fig. 5.1 A-C). Deletion of one arm of the RNA hybrid in the first fragment of *Rgs4* 3'-UTR (*Rgs4* F1) resulted in the identification of a specific RNA structure important for Stau2-dependent RNP assembly and necessary for dendritic localization of *Rgs4* mRNA (Fernández-Moya SM, Ehses J, *et al.*, manuscript in preparation).

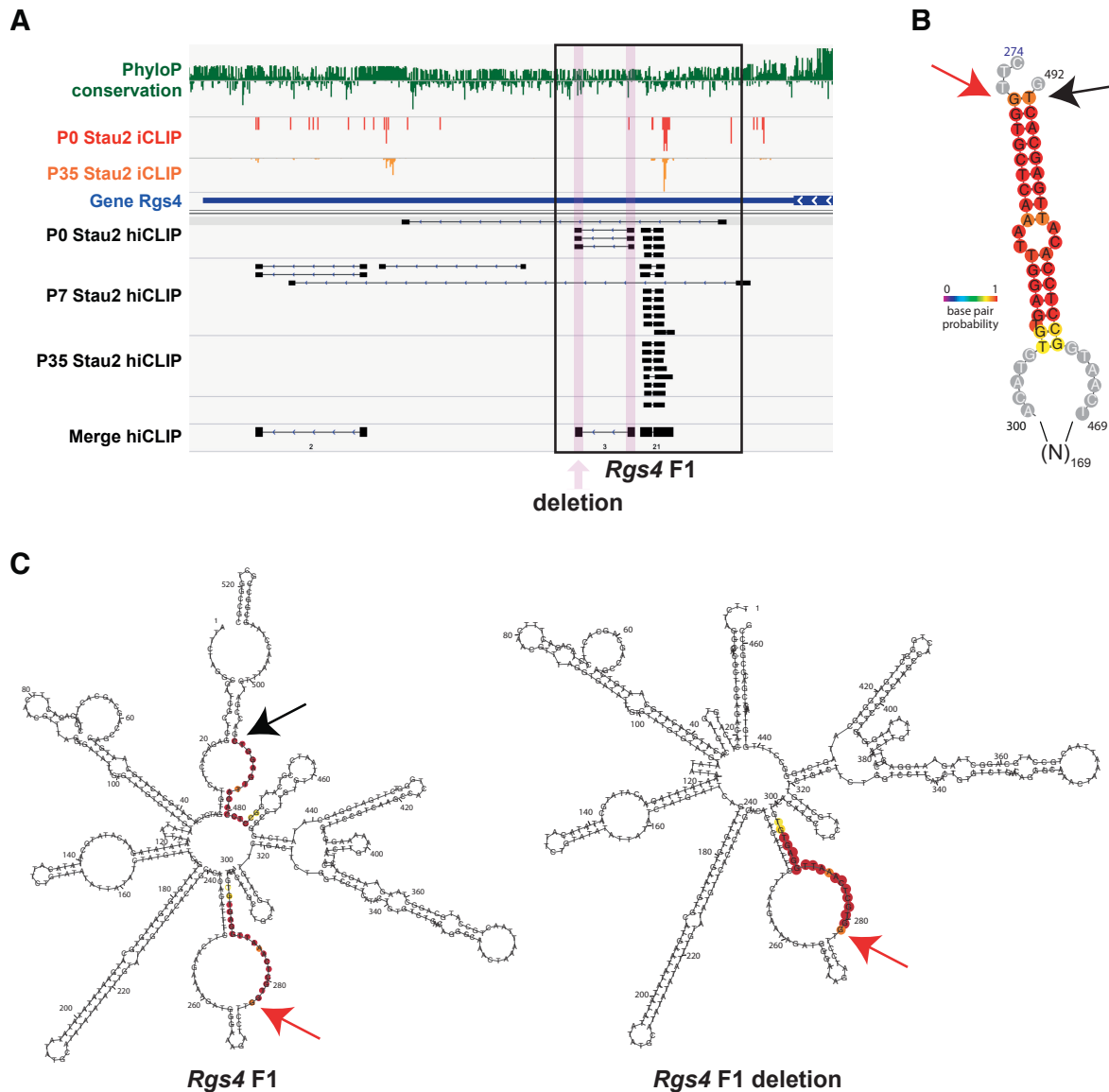


Figure 5.1: RNA structure detected by Stau2 hiCLIP. (A) Image from IGV genome browser depicting sequence conservation and Stau2 iCLIP and hiCLIP reads (black boxes) of *Rgs4* 3'-UTR from rat cortex at different postnatal (P) days. Cumulative hiCLIP reads over all timepoints are depicted in merge. Specific hiCLIP reads defining the Stau2-dependent functional RNA structure within the *Rgs4* fragment 1 (*Rgs4* F1) are highlighted in magenta. (B) Predicted folding (RNAfold web server) of the hiCLIP read highlighted in A. The loop region is depicted as (N)_{nucleotides}, numbers refer to nucleotide position in *Rgs4* 3'-UTR. (C) Predicted folding (RNAfold web server) of wildtype *Rgs4* F1 and with deletion of the second arm from the hiCLIP defined RNA structure (black arrow). Figure adapted from (Fernández-Moya SM, Ehses J, *et al.*, manuscript in preparation).

In this chapter, I present colocalization studies performed on Stau2 protein and MS2-RNA reporters fused to *Rgs4* RNA. These experiments revealed that the Stau2-dependent effects are indeed mediated by direct interaction of Stau2 and the RNA hybrid structure in fragment 1 of *Rgs4* mRNA. Further, this is the first time that deletion of an RNA hybrid structure was sufficient to abolish Stau2-RNA association.

5.2 Results and discussion

I decided to use colocalization-analysis between *Rgs4* RNA and Stau2 protein in neurons as a readout to measure Stau2-RNA association under physiological conditions. Visualization of the RNA was achieved through the well-established MS2-RNA reporter system (Bauer et al., 2019). Here, the RNA of interest is fused to an array of 128x MS2 RNA stem loops in combination with a LacZ open reading frame. Coexpression of a tandem MS2 coat protein (tdMCP) that is fused to GFP enables the visualization of the MS2-RNA reporter through specific binding of the tdMCP-GFP protein to the MS2-RNA stem loops (Fig. 5.2 A). Subsequently, quantification of colocalization between MS2-RNA reporter particles with tagRFP-Stau2 was performed in distal dendrites (Fig. 5.2 B). A strong and significant increase of colocalization with Stau2 was observed for the full-length *Rgs4* 3'-UTR (*Rgs4* FL) MS2 reporter compared to control MS2, indicating that the system is suitable to assess Stau2-RNA association (Fig. 5.2 C, D). Further, the level of Stau2-colocalization for *Rgs4* FL and *Rgs4* F1 MS2 reporter were comparable, with a minor yet not significant decrease in colocalization for *Rgs4* F1. This suggests that fragment 1 is sufficient to mediate the association between *Rgs4* 3'-UTR and Stau2 protein. Finally, I tested if the RNA-hybrid structure detected by Stau2 hiCLIP (Fig. 5.1) in *Rgs4* F1 was responsible for the association with Stau2. Indeed, colocalization between Stau2 and the *Rgs4* F1 MS2-RNA reporter with deletion of one RNA-hybrid arm was reduced to levels detected for the control reporter. This finding is important since it is the first time that (i) the RNA-structures detected by hiCLIP technique could be validated and (ii) destruction of an RNA-hybrid structure in a complex environment of a Stau2 target RNA is sufficient to eliminate Stau2 association. This is crucial as previous *in vitro* analysis of RNA characteristics important for Stau2-RNA association failed due to unspecific binding of Stau2 to control RNAs. While the hiCLIP data suggest that the investigated RNA-hybrid structure is indeed formed and bound by Stau2 *in vivo*, I cannot prove that this structure is also formed in our *Rgs4* F1 reporter RNA. In future, I will generate *Rgs4* F1 constructs containing single nucleotide insertions leading to RNA structure disruption followed by a construct with complementary insertions resulting in rescue of the RNA structure and test their capacity to regulate Stau2-dependent behavior.

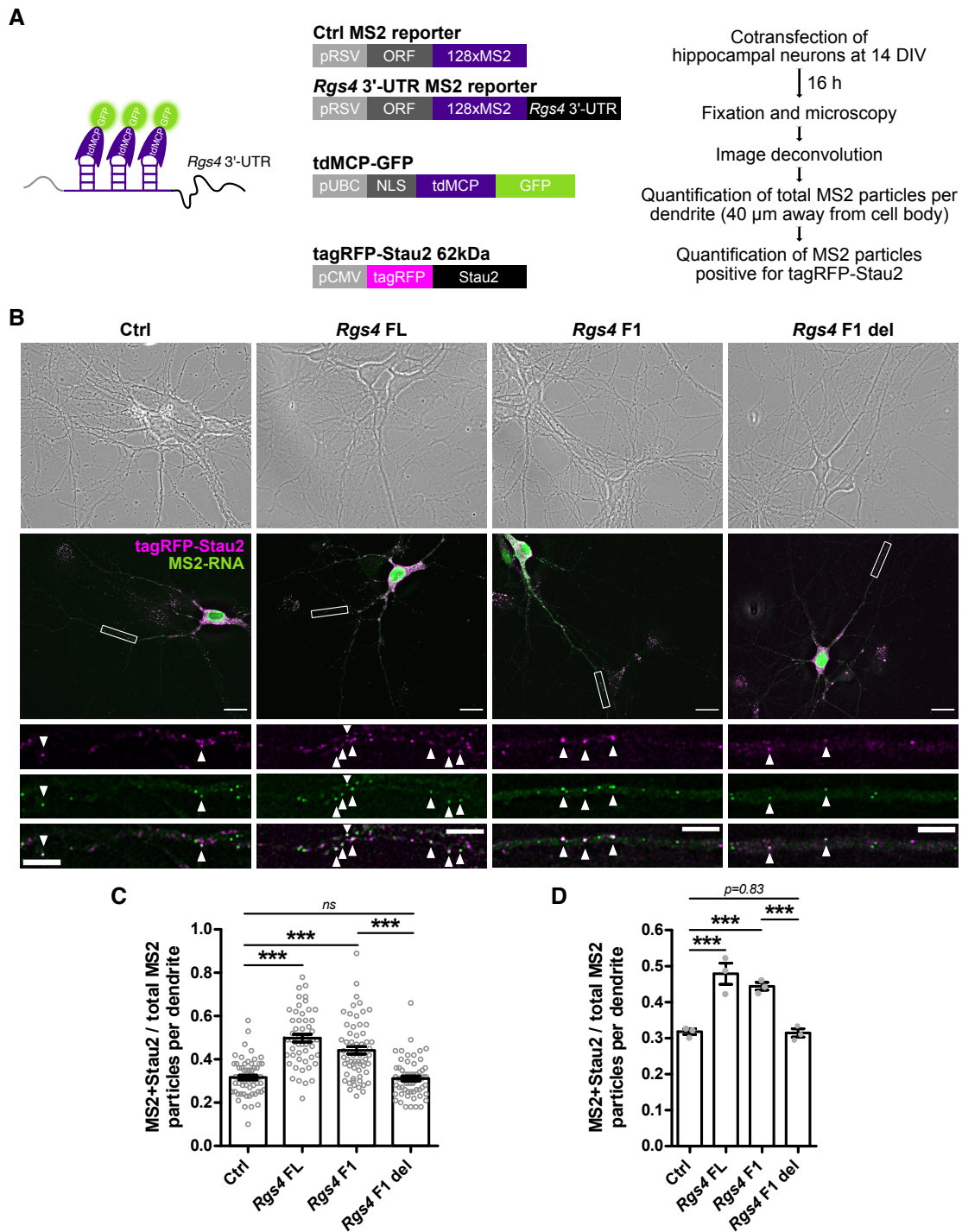


Figure 5.2: RNA structure in F1 of *Rgs4* 3'-UTR recruits Stau2. (A) Scheme of the MS2-RNA reporter system, plasmid design and experimental workflow of colocalization analysis. (B) Representative phase contrast and deconvolved fluorescent maximum z-projection images of hippocampal neurons transfected at 14 DIV with tagRFP-Stau2, tdMCP-eGFP and the indicated MS2-RNA reporters for 16 h. Scale bar, 20 μm . Magnified images of dendrites are single z-planes; scale bar, 5 μm . (C) Quantification of the colocalization between tagRFP-Stau2 and MS2 particles in entire dendrites, starting from 40 μm away from cell body. Mean \pm SEM over all dendrites (shown as individual dots) from three independent biological replicates. (D) Quantification as in C with mean \pm SEM from three independent biological replicates (shown as individual dots). One-way ANOVA and paired students t-test; *** $p < 0.001$. DIV days *in vitro*; tdMCP tandem MS2 coat protein.

In addition to the long-range RNA-hybrid structure, we investigated a second short-range RNA-hybrid detected in *Rgs4* F1 by Stau2 hiCLIP with a total of 21 merged reads (Fig. 5.1 A). Interestingly, deletion of this RNA structure, originally predicted and termed as Staufens recognition site 3 (SRS3) (Heraud-Farlow et al., 2013), was not sufficient to prevent Stau2-dependent regulation of the RNA. Possibly, Stau2 binding to *Rgs4* happens first through the RNA-hybrid structure in F1 and subsequently non-functional association with SRS3 by another Stau2 RBD might take place. Ultimately, the discovery of the Stau2 regulated RNA-hybrid structure will enable us to investigate the consequences of Stau2 binding for RNA structure and miRNA/RISC recruitment.

5.3 Materials and Methods

Plasmids

Plasmids expressing pUBC-NLS-ha-tdMCP-GFP and pRSV-LacZ-128xMS2 (control and rat *Rgs4* 3'-UTR (NM_017214.1)) have been described previously (Bauer et al., 2019). Generation of pRSV-LacZ-128xMS2 plasmids containing *Rgs4* 3'-UTR fragment 1 (*Rgs4* F1; bases 336 – 807 in *Rgs4* 3'-UTR) and *Rgs4* 3'-UTR fragment 1 hairpin deletion (*Rgs4* F1 deletion; bases 336 – 782 in *Rgs4* 3'-UTR) were performed by PCR amplification from pRSV-LacZ-128xMS2-*Rgs4* 3'-UTR plasmid and insertion into the pRSV-LacZ-128xMS2-Ctrl plasmid via Sall. Generation of plasmid overexpressing mouse Stau2 62kDa isoform was performed by blunt-end cloning of pCMV-tagRFP-Stau2 (Sharangdhar et al., 2017) into the FUW lentiviral expression vector (Heraud-Farlow et al., 2013) via EcoRV and NheI. It is important to note that the lentiviral pCMV-tagRFP-Stau2 plasmid does not contain a poly-A signal associated with the tagRFP-Stau2 ORF resulting in reduced overexpression levels.

Neuronal cell culture and transfection

Hippocampal neuronal cell cultures were generated from dissected hippocampal tissue of E17 embryos of timed pregnant rats (Sprague-Dawley, Charles River Laboratories) as published (Goetze et al., 2003). Briefly, cells were dissociated with 2.5% trypsin, plated on poly-L-lysine coated coverslips and cultured in NMEM+B27 medium (Invitrogen) at 37°C and 5% CO₂. Transient transfection of neurons was performed after 14 days *in vitro* (DIV) by calcium phosphate coprecipitation (Goetze et al., 2004). For each transfection condition the following DNA mixture was used: 2 µg of pUBC-NLS-ha-tdMCP-GFP, 3 µg of pRSV-LacZ-128xMS2 and 1 µg of pCMV-tagRFP-Stau2. After 16 h of expression, neurons were washed

with prewarmed HBSS (Invitrogen), fixed in 4% paraformaldehyde and coverslips were mounted using Prolong Gold antifade mounting medium (Invitrogen).

Microscopy and image analysis

Images were acquired on a Zeiss Z1 Axio Observer microscope including a 63x Plan-Apochromat oil immersion objective (1.40 NA), an HXP 120 C light source and the AxioCam 506 mono camera using Zeiss Zen software. Overview images, including phase contrast, were taken at the dendritic plane and a z-stack was acquired of the whole cell for fluorescent channels (30 planes with 0.26 μm step-size). The z-stack images were deconvolved using Zeiss Zen software deconvolution module with default settings of the constrained iterative method. Using ImageJ software, one dendrite per cell was selected for colocalization analysis. Regions of interest along the whole dendrite, 40 μm away from the cell body, were selected using the segmented line tool (40 pixel line-width). The total number of MS2 particles per dendrite was manually counted using the multipoint tool, followed by manual assessment of colocalization with tagRFP-Stau2 signal. The ratio of tagRFP-Stau2 positive MS2 particles over total number of MS2 particles per dendrite was calculated. For each condition and biological replicate 15 – 30 cells were analyzed and image analysis was performed blind. Data processing was performed in Excel (Microsoft) and statistical analysis was performed using Prism5 software (GraphPad). Figures represent mean \pm standard error of the mean (SEM) from three independent biological replicates. One-way ANOVA was performed followed by either paired or unpaired two-sided Student's t-test (***) $p < 0.001$, as indicated.

6 Discussion and outlook

The three individual projects of my PhD thesis presented here address the contribution of RNA characteristics and RBPs in neuronal granule assembly and gene regulation. The individual findings have been discussed separately in previous chapters (see **chapters A-C**). This discussion aims to provide a more general integration of my findings into the research field and to outline the novel findings and implications of my work. This enables me to propose a detailed new model of how Stau2 governs RNP assembly and RNAi function in neurons.

6.1 How is RNAi regulated by the neuronal RBP network?

The RNAi pathway depends on RBPs in multiple ways: (i) the biogenesis of miRNAs is dependent on the activity of a series of distinct RBPs, the canonical miRNA processing factors Drosha, DGCR8, TRBP, PACT and Dicer (Ha and Kim, 2014); (ii) Ago proteins as well as the downstream effectors of RISC, including the scaffolding protein TNRC6, the RNA helicase Ddx6, the CCR4/NOT complex, and the decapping enzymes Dcp1a and Dcp2, all of them are RBPs whose assembly and function being tightly controlled in cells (Nawalpuri et al., 2020); (iii) RNA binding of RISC and its function in gene expression, which is modulated by cooperative or competitive action of other RBPs (Loffreda et al., 2015). Here, I will discuss the influence of other RBPs on this RNAi protein network, with a specific focus on HuR and the neuronally enriched dsRBP Stau2.

6.1.1 miRNA biogenesis

The biogenesis of miRNAs can be influenced by several RBPs, as recently been shown in an unbiased biochemical approach (Treiber et al., 2017). For instance, DEAD-box helicases Ddx5 and Ddx17 are important for unwinding and processing of the pri-miRNA transcript, while other RBPs regulate recruitment of Dicer to the pre-miRNA (Connerty et al., 2015). Nuclear export of the largest Stau2 isoform of 62 kDa is coupled to the miRNA export factor Xpo5 (Lund et al., 2004; Macchi et al., 2004) and has been linked functionally to siRNA biogenesis (Yoon et al., 2018). Further, pre-miRNAs, specifically pre-miR-26a, co-immunoprecipitate with Stau2 from embryonic brain tissue (Fritzsche et al., 2013). This suggests, that Stau2 is potentially involved in regulating miRNA biogenesis in neurons. In the presented small RNA-Sequencing study (**Chapter B**) selected miRNAs were indeed differentially expressed upon depletion of Stau2, including miR-26a/b, while the overall abundance of miRNAs was

unchanged. The increased expression of miR-26 suggests a repressive effect of Stau2 on maturation of selected pre-miRNAs. Alternatively, elevated miR-26 levels could be explained by an increased processing by Dicer in a Stau2 dependent manner. Bose and Bhattacharyya proposed a mechanism, where miRNA biogenesis mediated by Dicer is enhanced by their target RNAs (Bose and Bhattacharyya, 2016). Opposite to the mechanisms described for HuR (Chapter A), Stau2 could compete with miR-26/Ago2 for target RNA binding. Increased accessibility of miRNA sites in Stau2-deficient neurons may therefore enhance miR-26 processing. The majority of differentially regulated miRNAs, however, was downregulated in Stau2 deficient neurons. Noteworthy, all members of the miR-29 family were downregulated. Since all members originate from the same gene locus, this effect could be caused by altered transcription. It will be interesting to see, in future, whether Stau2 indeed regulates biogenesis of specific miRNAs or whether the observed changes in miRNA expression are due to compensatory effects in the complex mRNA and RBP network of neurons.

In neurons, precursor miRNAs as well as some miRNA processing factors localize to distal dendrites, where synaptic stimulation leads to locally and spatially controlled miRNA maturation (Antonioni et al., 2018; Bicker et al., 2013; Sambandan et al., 2017). A prerequisite for local miRNA maturation is the regulated transport of specific pre-miRNAs, mediated by RBPs. The function of Stau2 in RNA transport is well-established (Bauer et al., 2019; Köhrmann et al., 1999; Sharangdhar et al., 2017). In addition, the long isoform of Stau2 (62 kDa, see above) indeed interacts with Exportin-5 (Macchi et al., 2004)(Stau2 proximity biotinylation assay; Fernández-Moya SM and Kiebler MA, unpublished data), the nuclear export factor for the majority of miRNAs (Bohnsack et al., 2004; Lund et al., 2004). Therefore, Stau2 could mediate nuclear export and/or dendritic transport of specific pre-miRNAs. This would also be supported by enrichment of specific pre-miRNAs in Stau2 RNA immunoprecipitation, *e.g.* of pre-miR-26a (Heraud-Farlow et al., 2013). Using microscopy approaches with labelled pre-miRNAs (Corradi et al., 2020), it will be interesting to see in future studies, if Stau2 indeed mediates pre-miRNA localization in neurons.

6.1.2 RISC assembly and localization

Aside from miRNA biogenesis itself, RNAi can be regulated at the level of the RISC proteins. Expression levels, posttranslational modification and localization of RISC associated proteins matter for RNAi function (Nawalpuri et al., 2020). I found a large proportion of RNAi associated proteins, *e.g.* Ago1, Ago2, Edc4, Dcp1a, Ddx6, to be upregulated in Stau2 deficient

primary neurons (**Chapter B**). Such increase suggests a gain of function for RNAi. This interpretation goes in line with previous data on Staufen in *C. elegans* (LeGendre et al., 2013; Ren et al., 2016), in which RNAi was enhanced by overexpression of Staufen mutants. The increase of RNAi protein expression is likely not being regulated by Stau2 directly but rather on the level of transcription, translation and/or protein stability. The expression levels itself, however, do not necessarily translate into increased RISC activity. Protein localization and posttranslational modifications influence RNAi activity. For instance, decapping activity is reduced upon assembly of Dcp1:Dcp2 and Edc3 into P-bodies or larger protein condensates (Schutz et al., 2017). This supports the idea of P-bodies as sites for RNA storage, than RNA degradation (Horvathova et al., 2017; Standart and Weil, 2018). It is imaginable that localization of RNAi components in P-bodies rather contributes to translational silencing. Stau2 has been proposed to be part of such P-bodies (Barbee et al., 2006; Hubstenberger et al., 2017), but I did not detect strong colocalization between Stau2 and P-body marker Ddx6 in neurons. Together with previous live imaging data from our lab, I rather propose a model in which Stau2 – as part of transport RNPs – delivers RNA to P-bodies, thereby shaping P-body composition (Zeitelhofer et al., 2008). This model agrees with our data showing increased colocalization of Ago2 and Stau2 in distal dendrites, where active transport takes place. During dendritic RNA transport, transcripts are thought to be translationally repressed until cue-dependent local translation at the synapse takes place (Doyle and Kiebler, 2011). Here, co-assembly of miRNA/Ago in Stau2-containing transport RNPs could mediate temporary and reversible translational repression (Kiebler and Bassell, 2006). The ultimate proof for this transport-dependent interaction would be two-color live imaging experiments of Ago2-Stau2 co-transport together with the mRNA, possibly by utilizing the MS2 system.

As discussed above, the interaction between Ago2 and Stau2 seems to be dependent on their dendritic localization in neurons. Interestingly, Stau2 and Ago2 both partially associate with actively translating polysomes (Höck et al., 2007) and the polysome-association of Ago2 is dependent on Stau2 (**Chapter B**). While the role of Stau2 in translation is largely unknown, several roles for miRNA/Ago2 polysome association have been proposed. These mechanisms range from translation-activation of *Tumor necrosis factor α* (*TNF α*) RNA (Vasudevan and Steitz, 2007) and enhancement of mitochondrial translation (Zhang et al., 2014) to protein production block by let-7a and Ago2, where the nascent chains are possibly destructed (Nottrott et al., 2006). In our hands, Stau2 depletion, and therefore Ago2 upregulation and association

with polysomes, coincides with a reduction in global translation, suggesting a rather repressive effect of Ago2 on translation in neurons. One alternative explanation for the association of Ago2 with translating polysomes would reside in the co-translational degradation of miRNA targeted mRNAs (Tat et al., 2016). Here, co-translational deadenylation is followed by decapping and 5'- to 3'-nucleolytic decay of the RNA. Detailed analysis of our RNA sequencing dataset for uridylation of the polyA tail and a 3'-read bias will yield first experimental indication whether this Ago-dependent mechanism is indeed enhanced in *Stau2* deficient neurons. In future, it will be crucial to better understand the function and underlying mechanisms of Ago2 polysome association.

The RNP/RISC assembly itself often depends on posttranslational modifications and especially phosphorylation (Nosella and Forman-Kay, 2021), as it has been shown for Ago2 phosphorylation at residues S387 and S824:34 and Ago2 to Ago3 switching upon *Limd1* knockdown (Bridge et al., 2017; Quévillon Huberdeau et al., 2017; Rajgor et al., 2018). In our hands, association of Ago2 with P-bodies was phospho-site dependent in neurons. Upon introduction of phosphomimic mutants at residues S824:34 of Ago2, localization to P-bodies was disrupted in neurons, but not in HEK-293T cells. Phosphorylation at residues S824:34 leads to reduced mRNA binding of miRNA-loaded Ago2 (Quévillon Huberdeau et al., 2017). This suggests that Ago2 association with P-bodies is in part mediated by RNA binding in neurons. However, mutation of Ago2 phosphorylation sites did not alter Ago2 localization behavior compared to wildtype Ago2 in *Stau2*-deficient neurons. It is therefore unlikely that *Stau2* affects RNAi through regulation of Ago2 phosphorylation.

6.1.3 Combinatorial binding of RBPs and RISC to mRNAs

RNA binding of RISC and its function in gene expression are modulated by cooperative or competitive action of other RBPs. Specifically, RBPs can modulate RISC recruitment to RNA (Kim et al., 2009) or, alternatively, the accessibility of miRNA binding sites (Ehse et al., 2020; Kenny et al., 2014; Sternburg et al., 2018). I and others have shown that the AU-rich element binding protein HuR exerts such functions (Chapter A). HuR regulates RISC effectiveness with a contrary outcome for individual RNAs. HuR can promote miRNA-mediated gene silencing by recruiting the a *let-7*/Ago2 complex to *c-Myc* RNA (Kim et al., 2009) or, as I have shown, by enabling binding of miR-26 to a previously hidden miRNA-binding site (Ehse et al., 2020). HuR, however, can also prevent RISC assembly to RNAs by competition for binding, if binding sites for HuR and the miRNA overlap (Li et al., 2018). This bidirectional

interaction between an RBP, here HuR, and RISC highlights the diversity of RBP function in the context of individual RNAs. Finally, the unique arrangement of RBP and miRNA binding sites on an RNA defines the RNA fate. This network depends on the local concentrations of miRNA/RISC and RBP components, resulting eventually in the dynamic rearrangement of the bound RBP. Together with transcription, these dynamics enable the regulation of gene expression levels in development, such as neurogenesis and neuronal maturation. Whereas miR-26 expression is high in mature neurons, HuR levels decrease with maturation, resulting in relief of *Rgs4* mRNA repression with neuronal development.

This two-dimensional interaction of miRNA/RISC and the RBP on the target mRNA fate can be further complexed by integration into the existing cellular RBP/RNA network (Schieweck et al., 2020). Such a mechanism has been beautifully shown by Sosanya *et al.* for the neuron-specific AU-rich element binding protein HuD (Sosanya et al., 2013). In this case, HuD competes with miR-129 for binding to *voltage-gated potassium channel subunit Kv1.1* (*Kv1.1*) mRNA, thereby promoting *Kv1.1* translation. Interestingly, this competition depends on the concentration of other high-affinity HuD target RNAs. Upon reduction of local dendritic mammalian target of rapamycin complex 1 (mTORC1) signaling, high-affinity HuD target RNAs are degraded and the freed HuD can subsequently bind to *Kv1.1* mRNA. It is therefore crucial to understand how RBPs integrate into the RBP-RNA network present in neurons.

The identification of such interdependencies in between Stau2 and other RBPs by an unbiased genome-wide approach was the aim of the second project (**Chapter B**). As discussed in 6.1.1 and 6.1.2, I detected increased expression of RNAi pathway components upon Stau2 downregulation in neurons and especially a relocation of Ago2 from P-bodies to polysomes. I excluded changes in global miRNA abundance or altered phosphorylation of Ago2 S387 or S824:34 as the molecular mechanism behind the Stau2-dependent Ago2 localization behavior in neurons. This led us to hypothesize that altered miRNA binding site availability in Stau2 target RNAs might be the underlying cause. In this case, Stau2 would prevent interaction of miRNA/Ago2 with actively translated mRNA targets thereby promoting translation, similar to the mechanism observed for HuD and miR-129 (Nawalpuri et al., 2020; Sosanya et al., 2013). Such an mechanism has been previously proposed for Stauf protein in *C. elegans* (LeGendre et al., 2013; Ren et al., 2016). Further, this mechanism would go in line with the observation that Stau2 target RNAs have longer 3'-UTRs (Heraud-Farlow et al., 2013) with potentially

more miRNA binding sites (Wehrspaun et al., 2014). Deep analysis of our RNA sequencing data from *Stau2* deficient neurons for differential expression in combination with enrichment of miRNA binding sites will enable us to test our hypothesis. These analyses could be complemented by Ago2 proximity RNA biotinylation experiments (APEX2 (Fazal et al., 2019)) in order to identify Ago2-bound transcripts in the presence and absence of *Stau2* *in vivo* in primary neurons. Here, a fusion protein of the engineered ascorbate peroxidase APEX2 and the protein of interest is overexpressed and the cells are incubated with biotinphenol. Subsequently, the biotinylation of RNAs or proteins in close proximity of the fusion protein occurs upon addition of hydrogen peroxide followed by enrichment and detection of the biotinylated molecules. I recently established RNA biotinylation using APEX2 in primary neurons in our lab. Ultimately, identification of polysome associated mRNAs and miRNAs upon *Stau2* depletion will complete our understanding of the role of *Stau2* in Ago association with polysomes.

6.2 How does the RNA structure contribute to RNP assembly?

Until recently the driving force of RNA granule assembly was thought to mainly originate from the condensation of RBPs. An increasing number of studies now corrects this picture by highlighting the importance of the RNA on granule formation (Langdon et al., 2018; Sanchez de Groot et al., 2019; Tauber et al., 2020). The concentration as well as intrinsic RNA characteristics, such as AU-richness (Courel et al., 2019), together with the accessibility of binding sites for RBPs all crucially contribute to RNP assembly (Tauber et al., 2020). One key finding of this thesis is that HuR and miR26/Ago2 can cooperatively bind to and act on *Rgs4* mRNA, possibly through remodeling of a specific local RNA structure found in the 3'-UTR of *Rgs4*. Cooperative and competitive action of RBPs on single mRNAs have been shown before (Iadevaia and Gerber, 2015). In our case, however, the RNA structure seems to serve as a regulatory element to control accessibility to the respective binding sites. This interpretation is based on binding site mutation studies in neurons, limiting the evidence for actual RNA structure changes. In future, *in vivo* RNA structure probing experiments, such as *in vivo* SHAPE (Spitale et al., 2013) or PARIS (Lu et al., 2016), should shed more light into the underlying mechanism. Such experiments would also be helpful to understand the contribution of dsRBPs to the transcriptome wide RNA architecture, by analyzing differentially folded RNAs or altered RNA-RNA interactions upon depletion of the dsRBP. In collaboration with

Jernej Ule (Crick Institute, London), we already determined Stau2-bound RNA duplexes in rat brain using the hiCLIP technology (Chapter C). These data show that a long-range RNA duplex (150 nt) in the 3'-UTR of *Rgs4* is necessary to drive Stau2 RNP assembly, thereby promoting *Rgs4* localization to distal dendrites. Interestingly, this RNA duplex is not merely necessary, but also sufficient to drive RNP formation (Fernández-Moya SM, Ehses J, *et al.*, manuscript in preparation). Previously, we have shown that Stau2 is important for directed *Rgs4* transport in dendrites (Bauer et al., 2019). Together, these data suggest a reciprocal relationship between RNA structure and RBP in RNP assembly. This link seems to be especially important in the brain, as neuron-enriched mRNAs harbor longer 3'-UTRs (Heraud-Farlow et al., 2013; Miura et al., 2013) that are more structured if the mRNA is bound by Stau2 (Fernández-Moya SM, Ehses J, *et al.*, manuscript in preparation). Using the above described genome-wide techniques, it should be possible in future to reveal the molecular contributions of Stau2 to RNP assembly. Does Stau2 mainly function in packaging mRNAs for transport, storage and protection from degradation by compacting the 3'-UTR or does Stau2 regulate RNA-RNA interactions to govern RNA granule assembly and size?

6.3 How does the RBP network contribute to neuronal physiology?

RBPs are the central effectors of posttranscriptional gene expression. Consequently, their malfunctioning has been connected to many central nervous system diseases (Gebauer et al., 2020; Schieweck et al., 2020). As discussed before (6.1 and 6.2), increasing evidence points towards an extensive interdependent regulatory network of RBPs that helps to maintain neuronal gene expression homeostasis (Schieweck et al., 2020). Stau2 is a known mediator of RNA localization in both stem cells (Kusek et al., 2012; Vessey et al., 2012) and neurons (Bauer et al., 2019; Sharangdhar et al., 2017). Its deficiency in neurons results in general reduction of RNA content in dendrites and RNA mislocalization (Goetze et al., 2006; Sharangdhar et al., 2017; Tang et al., 2001). This can possibly lead to abrogation of local translation in dendrites. Stau2 target mRNAs are enriched for synaptic proteins and converge in the GPCR signaling pathway, including the key signaling molecule *Rgs4*. On the one hand, we have shown that Stau2 regulates granule assembly, dendritic transport and RNA stability of *Rgs4* mRNA (Bauer et al., 2019; Heraud-Farlow et al., 2013). On the other hand, neuronal *Rgs4* expression is also negatively regulated through synergistic binding of HuR and miR-26/RISC (Chapter A). While it remains to be solved whether Stau2 and HuR/miR-26 can bind to *Rgs4* at the same

time, they functionally counteract each other in determining the fate of *Rgs4* mRNA. Interestingly, double knockout of *Rgs4* and *fragile X mental retardation 1* (FMR1) rescues several molecular and behavior phenotypes observed in FMR1 knockout mice (Pacey et al., 2011). FMRP localizes to synapses and contributes to RNA localization and translation control (Dictenberg et al., 2008; Pilaz et al., 2016; Wang et al., 2016). Furthermore, FMRP has been shown to be part of neuronal Stau2 particles (Fritzsche et al., 2013), in which it possibly contributes to translation repression of transport RNPs (Bolduc et al., 2008; Darnell et al., 2011). Both FMRP and Stau2, regulate the synaptic actin cytoskeleton and control dendritic spine maturation of neurons (Dictenberg et al., 2008; Goetze et al., 2006). Such changes in dendritic spine morphology upon knockdown of RBPs often come along with higher susceptibility for epileptic seizures, as it has been shown for FMRP (Contractor et al., 2015), Pum2 (Follwaczny et al., 2017) or Hu proteins (Ince-Dunn et al., 2012). Here, it is interesting to note that inhibition of *Rgs4* has been shown to promote the anti-seizure effect of endogenous adenosine (Chen et al., 2012) and *Rgs4* knockout rescued the epileptic and dendritic spine phenotypes observed in FMR1 knockout mice (Pacey et al., 2011). Together, these data place Stau2, FMRP, HuR, miR-26/Ago2 and *Rgs4* in one central pathway regulating dendritic spine maturation and, ultimately, seizure susceptibility. The molecular mechanisms, however, underlying these phenotypes are only beginning to be unraveled. FMRP-mediated translational control of *cofilin-1*, an F-actin stabilizer, (Feuge et al., 2019) and FMRP interaction with Cytoplasmic FMR1 Interacting Protein 1 (Cyfip1) (DeRubeis et al., 2013) have been proposed to mediate dendritic spine regulation in dependence of FMRP. In case of Stau2, no molecular mechanism underlying the dendritic spine phenotype could be determined until now. Previous data from our lab by Goetze *et al.* indicated that Stau2 dependent β -actin mRNA misregulation could be responsible (Goetze et al., 2006), but it cannot be excluded that the observation was rather a consequence of changes in actin cytoskeleton than mediated by direct Stau2 binding to β -actin mRNA. Here, also Stau2-dependent regulation of *Rhoa* or γ -actin expression, both direct Stau2 targets (Heraud-Farlow et al., 2013; Sharangdhar et al., 2017), or altered Cofilin-1/2 protein expression (Schieweck R *et al.*, Mol Cell, under revision) could explain the impact on dendritic spine maturity.

In addition to formation of dendritic spines and synapses, the overall dendritic or axonal outgrowth of neurons is regulated by RBPs (Antonacci et al., 2015; Nawalpur et al., 2020; Rehfeld et al., 2018; Vessey et al., 2010). Several proteins involved in the RNAi pathway have

been shown to promote dendritic outgrowth. Conditional loss of Dicer in excitatory neurons, and subsequent reduced miRNA levels, resulted in dendritic branching deficits in mice (Davis et al., 2008). Similar results were obtained from *C. elegans* deficient for *dcr-1* (Dicer) (Antonacci et al., 2015) suggesting that this mechanism is indeed conserved. Furthermore, knockdown of the RISC scaffolding protein GW182/Tnrc6 results in reduced dendritic arborization in developing neurons (Nawalpuri and Muddashetty, 2020). I have now shown that Stau2 depletion leads to increased dendritic arborization in mature neurons and downregulation of Ago1/2 was able to rescue this effect (**Chapter B**). Dicer, GW182/Tnrc6 and Ago1/2 are all part of the RNAi pathway (Bartel, 2018). Together these data suggest that miRNA mediated gene silencing promotes dendritic arborization through a mechanism that is yet largely unknown. Stau2, on the contrary represses dendritic branching, which fits with the opposing functions of Ago1/2 and Stau2 on global translation (**Chapter B**). Several mechanisms could possibly explain the arborization phenotype, starting from (i) uncontrolled branching induced by RNA mislocalization and general reduction of dendritic RNA content to (ii) specific changes of the actin cytoskeleton involved in neurite outgrowth as discussed in the previous paragraph for spine maturation, and finally (iii) reduction of functioning synapses due to dendritic spine deficits resulting in compensatory dendritic overgrowth. Further, the RNAi pathway is upregulated in Stau2 depleted neurons as shown by us (**Chapter B**) and LeGendre *et al.* for Staufen in *C. elegans* (LeGendre et al., 2013). This opens the possibility that the increased dendritic complexity in Stau2 deficient neurons is actually mediated by elevated RISC activity (LeGendre et al., 2013).

In conclusion, these examples of RBP function in dendritic spine morphogenesis and arborization support the idea that different RBPs converge on similar biological pathways or even on the same RNA target (here *Rgs4*). Further, those RBPs do not seem to act independently of each other, but rather in an interdependent network that shapes neuronal physiology and, ultimately, cognitive functions. The emerging association of nervous diseases to RBPs highlights the importance to understand the impact of balanced RBP expression for neuronal gene expression homeostasis. In addition, the rising field of RNA-based gene therapy, recently boosted by the development of RNA vaccinations against SARS-CoV-2, will be relying on our knowledge of RBP and RNAi function in gene expression homeostasis.

References

- Agarwal, V., Bell, G.W., Nam, J.W., and Bartel, D.P. (2015). Predicting effective microRNA target sites in mammalian mRNAs. *Elife* 4, 1–38.
- Allison, R., Czaplinski, K., Git, A., Adegbenro, E., Stennard, F., Houliston, E., and Standart, N. (2004). Two distinct Staufin isoforms in *Xenopus* are vegetally localized during oogenesis. *RNA* 10, 1751–1763.
- Andreassi, C., and Riccio, A. (2009). To localize or not to localize: mRNA fate is in 3'UTR ends. *Trends Cell Biol.* 19, 465–474.
- Antonacci, S., Forand, D., Wolf, M., Tyus, C., Barney, J., Kellogg, L., Simon, M.A., Kerr, G., Wells, K.L., Younes, S., et al. (2015). Conserved RNA-binding proteins required for dendrite morphogenesis in *Caenorhabditis elegans* sensory neurons. *G3 (Bethesda)*. 5, 639–653.
- Antoniou, A., Khudayberdiev, S., Idziak, A., Bicker, S., Jacob, R., and Schratt, G. (2018). The dynamic recruitment of TRBP to neuronal membranes mediates dendritogenesis during development. *EMBO Rep.* 19.
- Barbee, S.A., Estes, P.S., Cziko, A.-M., Hillebrand, J., Luedeman, R.A., Coller, J.M., Johnson, N., Howlett, I.C., Geng, C., Ueda, R., et al. (2006). Staufin- and FMRP-Containing Neuronal RNPs Are Structurally and Functionally Related to Somatic P Bodies. *Neuron* 52, 997–1009.
- Bartel, D.P. (2018). Metazoan MicroRNAs. *Cell* 173, 20–51.
- Bauer, K.E., Segura, I., Gaspar, I., Scheuss, V., Illig, C., Ammer, G., Hutten, S., Basyuk, E., Fernández-Moya, S.M., Ehse, J., et al. (2019). Live cell imaging reveals 3'-UTR dependent mRNA sorting to synapses. *Nat. Commun.* 10, 3178.
- Berger, S.M., Fernández-Lamo, I., Schönig, K., Fernández Moya, S.M., Ehse, J., Schieweck, R., Clementi, S., Enkel, T., Grothe, S., von Bohlen Und Halbach, O., et al. (2017). Forebrain-specific, conditional silencing of Staufin2 alters synaptic plasticity, learning, and memory in rats. *Genome Biol.* 18, 222.
- Berkovits, B.D., and Mayr, C. (2015). Alternative 3' UTRs act as scaffolds to regulate membrane protein localization. *Nature* 522, 363–367.
- Bicker, S., Khudayberdiev, S., Weiß, K., Zocher, K., Baumeister, S., and Schratt, G. (2013). The DEAH-box helicase DHX36 mediates dendritic localization of the neuronal precursor-microRNA-134. *Genes Dev.* 27, 991–996.
- Bohnsack, M.T., Czaplinski, K., and Gorlich, D. (2004). Exportin 5 is a RanGTP-dependent dsRNA-binding protein that mediates nuclear export of pre-miRNAs. *RNA* 10, 185–191.
- Bolduc, F. V, Bell, K., Cox, H., Broadie, K.S., and Tully, T. (2008). Excess protein synthesis in *Drosophila* Fragile X mutants impairs long-term memory. *Nat. Neurosci.* 11, 1143–1145.
- Bose, M., and Bhattacharyya, S.N. (2016). Target-dependent biogenesis of cognate microRNAs in human cells. *Nat. Commun.* 7, 12200.
- Brennan, C.M., and Steitz, J.A. (2001). HuR and mRNA stability. *Cell. Mol. Life Sci.* 58, 266–277.

- Bridge, K.S., Shah, K.M., Li, Y., Foxler, D.E., Wong, S.C.K., Miller, D.C., Davidson, K.M., Foster, J.G., Rose, R., Hodgkinson, M.R., et al. (2017). Argonaute Utilization for miRNA Silencing Is Determined by Phosphorylation-Dependent Recruitment of LIM-Domain-Containing Proteins. *Cell Rep.* *20*, 173–187.
- Bycroft, M., Grünert, S., Murzin, A.G., Proctor, M., and St Johnston, D. (1995). NMR solution structure of a dsRNA binding domain from *Drosophila* staufer protein reveals homology to the N-terminal domain of ribosomal protein S5. *EMBO J.* *14*, 3563–3571.
- Chang, N., Yi, J., Guo, G., Liu, X., Shang, Y., Tong, T., Cui, Q., Zhan, M., Gorospe, M., and Wang, W. (2010). HuR Uses AUF1 as a Cofactor To Promote p16INK4 mRNA Decay. *Mol. Cell. Biol.* *30*, 3875–3886.
- Chen, Y., Liu, Y., Cottingham, C., McMahan, L., Jiao, K., Greengard, P., and Wang, Q. (2012). Neurabin Scaffolding of Adenosine Receptor and RGS4 Regulates Anti-Seizure Effect of Endogenous Adenosine. *J. Neurosci.* *32*, 2683–2695.
- Chen, Y., Boland, A., Kuzuoğlu-Öztürk, D., Bawankar, P., Loh, B., Chang, C.-T., Weichenrieder, O., and Izaurralde, E. (2014). A DDX6-CNOT1 Complex and W-Binding Pockets in CNOT9 Reveal Direct Links between miRNA Target Recognition and Silencing. *Mol. Cell* *54*, 737–750.
- Connerty, P., Ahadi, A., and Hutvagner, G. (2015). RNA Binding Proteins in the miRNA Pathway. *Int. J. Mol. Sci.* *17*.
- Contractor, A., Klyachko, V.A., and Portera-Cailliau, C. (2015). Altered Neuronal and Circuit Excitability in Fragile X Syndrome. *Neuron* *87*, 699–715.
- Corradi, E., Dalla Costa, I., Gavoci, A., Iyer, A., Rocuzzo, M., Otto, T.A., Oliani, E., Bridi, S., Strohbuecker, S., Santos-Rodriguez, G., et al. (2020). Axonal precursor miRNAs hitchhike on endosomes and locally regulate the development of neural circuits. *EMBO J.* *39*, e102513.
- Cougot, N., Bhattacharyya, S.N., Tapia-Arancibia, L., Bordonné, R., Filipowicz, W., Bertrand, E., and Rage, F. (2008). Dendrites of mammalian neurons contain specialized P-body-like structures that respond to neuronal activation. *J. Neurosci.* *28*, 13793–13804.
- Courel, M., Clément, Y., Bossevain, C., Foretek, D., Vidal Cruchez, O., Yi, Z., Bénard, M., Benassy, M.-N., Kress, M., Vindry, C., et al. (2019). GC content shapes mRNA storage and decay in human cells. *Elife* *8*, 1–32.
- Darnell, J.C., Van Driesche, S.J., Zhang, C., Hung, K.Y.S., Mele, A., Fraser, C.E., Stone, E.F., Chen, C., Fak, J.J., Chi, S.W., et al. (2011). FMRP stalls ribosomal translocation on mRNAs linked to synaptic function and autism. *Cell* *146*, 247–261.
- Dassi, E. (2017). Handshakes and Fights: The Regulatory Interplay of RNA-Binding Proteins. *Front. Mol. Biosci.* *4*, 1–8.
- Davis, T.H., Cuellar, T.L., Koch, S.M., Barker, A.J., Harfe, B.D., McManus, M.T., and Ullian, E.M. (2008). Conditional Loss of Dicer Disrupts Cellular and Tissue Morphogenesis in the Cortex and Hippocampus. *J. Neurosci.* *28*, 4322–4330.
- DeRubeis, S., Pasciuto, E., Li, K.W., Fernández, E., DiMarino, D., Buzzi, A., Ostroff, L.E., Klann, E., Zwartkruis, F.J.T., Komiyama, N.H., et al. (2013). CYFIP1 coordinates mRNA translation and cytoskeleton remodeling to ensure proper dendritic Spine formation. *Neuron* *79*, 1169–1182.

- Dictenberg, J.B., Swanger, S.A., Antar, L.N., Singer, R.H., and Bassell, G.J. (2008). A Direct Role for FMRP in Activity-Dependent Dendritic mRNA Transport Links Filopodial-Spine Morphogenesis to Fragile X Syndrome. *Dev. Cell* *14*, 926–939.
- Djuranovic, S., Nahvi, A., and Green, R. (2011). A parsimonious model for gene regulation by miRNAs. *Science* *331*, 550–553.
- Doyle, M., and Kiebler, M.A. (2011). Mechanisms of dendritic mRNA transport and its role in synaptic tagging. *EMBO J.* *30*, 3540–3552.
- Duchaîne, T.F., Hemraj, I., Furic, L., Deitinghoff, A., Kiebler, M. a, and DesGroseillers, L. (2002). *Staufen2* isoforms localize to the somatodendritic domain of neurons and interact with different organelles. *J. Cell Sci.* *115*, 3285–3295.
- Duss, O., Stepanyuk, G.A., Puglisi, J.D., and Williamson, J.R. (2019). Transient Protein-RNA Interactions Guide Nascent Ribosomal RNA Folding. *Cell* *179*, 1357–1369.e16.
- Ehse, J., Fernández-Moya, S.M., Schröger, L., and Kiebler, M.A. (2020). Synergistic regulation of *Rgs4* mRNA by HuR and miR-26/RISC in neurons. *RNA Biol.* *00*, 1–11.
- Fareh, M., Yeom, K.-H., Haagsma, A.C., Chauhan, S., Heo, I., and Joo, C. (2016). TRBP ensures efficient Dicer processing of precursor microRNA in RNA-crowded environments. *Nat. Commun.* *7*, 13694.
- Fazal, F.M., Han, S., Parker, K.R., Kaewsapsak, P., Xu, J., Boettiger, A.N., Chang, H.Y., and Ting, A.Y. (2019). Atlas of Subcellular RNA Localization Revealed by APEX-Seq. *Cell* *178*, 473–490.e26.
- Fernández-Moya, S.M., Ehse, J., and Kiebler, M.A. (2017). The alternative life of RNA-sequencing meets single molecule approaches. *FEBS Lett.* *591*, 1455–1470.
- Feuge, J., Scharkowski, F., Michaelsen-Preusse, K., and Korte, M. (2019). FMRP Modulates Activity-Dependent Spine Plasticity by Binding Cofilin1 mRNA and Regulating Localization and Local Translation. *Cereb. Cortex* *29*, 5204–5216.
- Fire, A., Xu, S., Montgomery, M.K., Kostas, S.A., Driver, S.E., and Mello, C.C. (1998). Potent and specific genetic interference by double-stranded RNA in *Caenorhabditis elegans*. *Nature* *391*, 806–811.
- Follwaczny, P., Schieweck, R., Riedemann, T., Demleitner, A., Straub, T., Klemm, A.H., Bilban, M., Sutor, B., Popper, B., and Kiebler, M.A. (2017). *Pumilio2*-deficient mice show a predisposition for epilepsy. *Dis. Model. Mech.* *10*, 1333–1342.
- Freimer, J.W., Hu, T.J., and Belloch, R. (2018). Decoupling the impact of MicroRNAs on translational repression versus RNA degradation in embryonic stem cells. *Elife* *7*, 1–23.
- Friedman, R.C., Farh, K.K.H., Burge, C.B., and Bartel, D.P. (2009). Most mammalian mRNAs are conserved targets of microRNAs. *Genome Res.* *19*, 92–105.
- Fritzsche, R., Karra, D., Bennett, K.L., Ang, F. yee, Heraud-Farlow, J.E., Tolino, M., Doyle, M., Bauer, K.E., Thomas, S., Planyavsky, M., et al. (2013). Interactome of Two Diverse RNA Granules Links mRNA Localization to Translational Repression in Neurons. *Cell Rep.* *5*, 1749–1762.
- Furic, L., Maher-Laporte, M., and DesGroseillers, L. (2007). A genome-wide approach identifies distinct but overlapping subsets of cellular mRNAs associated with *Staufen1*- and *Staufen2*-containing ribonucleoprotein complexes. *RNA* *14*, 324–335.

- García-Jove Navarro, M., Kashida, S., Chouaib, R., Souquere, S., Pierron, G., Weil, D., and Gueroui, Z. (2019). RNA is a critical element for the sizing and the composition of phase-separated RNA–protein condensates. *Nat. Commun.* *10*, 1–13.
- Gebauer, F., Schwarzl, T., Valcárcel, J., and Hentze, M.W. (2020). RNA-binding proteins in human genetic disease. *Nat. Rev. Genet.*
- Gerber, K.J., Squires, K.E., and Hepler, J.R. (2016). Roles for Regulator of G Protein Signaling Proteins in Synaptic Signaling and Plasticity. *Mol. Pharmacol.* *89*, 273–286.
- Ghosh, M., Aguila, H.L., Michaud, J., Ai, Y., Wu, M.-T., Hemmes, A., Ristimäki, A., Guo, C., Furneaux, H., and Hla, T. (2009). Essential role of the RNA-binding protein HuR in progenitor cell survival in mice. *J. Clin. Invest.* *119*, 3530–3543.
- Di Giammartino, D.C., Nishida, K., and Manley, J.L. (2011). Mechanisms and consequences of alternative polyadenylation. *Mol Cell* *43*, 853–866.
- Giorgi, C., and Moore, M.J. (2007). The nuclear nurture and cytoplasmic nature of localized mRNPs. *Semin. Cell Dev. Biol.* *18*, 186–193.
- Goetze, B., Grunewald, B., Kiebler, M.A., and Macchi, P. (2003). Coupling the Iron-Responsive Element to GFP--An Inducible System to Study Translation in a Single Living Cell. *Sci. Signal.* *2003*, p112–p112.
- Goetze, B., Grunewald, B., Baldassa, S., and Kiebler, M. (2004). Chemically controlled formation of a DNA/calcium phosphate coprecipitate: Application for transfection of mature hippocampal neurons. *J. Neurobiol.* *60*, 517–525.
- Goetze, B., Tuebing, F., Xie, Y., Dorostkar, M.M., Thomas, S., Pehl, U., Boehm, S., Macchi, P., and Kiebler, M.A. (2006). The brain-specific double-stranded RNA-binding protein Staufen2 is required for dendritic spine morphogenesis. *J. Cell Biol.* *172*, 221–231.
- Gong, C., and Maquat, L.E. (2011). lncRNAs transactivate STAU1-mediated mRNA decay by duplexing with 3' UTRs via Alu elements. *Nature* *470*, 284–288.
- Graber, T.E., Freemantle, E., Anadolu, M.N., Hébert-Seropian, S., MacAdam, R.L., Shin, U., Hoang, H.-D., Alain, T., Lacaille, J.-C., and Sossin, W.S. (2017). UPF1 Governs Synaptic Plasticity through Association with a STAU2 RNA Granule. *J. Neurosci.* *37*, 9116–9131.
- Gu, Q.-H., Yu, D., Hu, Z., Liu, X., Yang, Y., Luo, Y., Zhu, J., and Li, Z. (2015). miR-26a and miR-384-5p are required for LTP maintenance and spine enlargement. *Nat. Commun.* *6*, 6789.
- Ha, M., and Kim, V.N. (2014). Regulation of microRNA biogenesis. *Nat. Rev. Mol. Cell Biol.* *15*, 509–524.
- Heber, S., Gáspár, I., Tants, J.-N., Günther, J., Moya, S.M.F., Janowski, R., Ephrussi, A., Sattler, M., and Niessing, D. (2019). Staufen2-mediated RNA recognition and localization requires combinatorial action of multiple domains. *Nat. Commun.* *10*, 1659.
- Hentze, M.W., Castello, A., Schwarzl, T., and Preiss, T. (2018). A brave new world of RNA-binding proteins. *Nat. Rev. Mol. Cell Biol.* *19*, 327–341.
- Heraud-Farlow, J.E., and Kiebler, M.A. (2014). The multifunctional Staufen proteins: conserved roles from neurogenesis to synaptic plasticity. *Trends Neurosci.* *37*, 470–479.

- Heraud-Farlow, J.E., Sharangdhar, T., Li, X., Pfeifer, P., Tauber, S., Orozco, D., Hörmann, A., Thomas, S., Bakosova, A., Farlow, A.R., et al. (2013). Staufen2 regulates neuronal target RNAs. *Cell Rep.* 5, 1511–1518.
- Höck, J., Weinmann, L., Ender, C., Rüdell, S., Kremmer, E., Raabe, M., Urlaub, H., and Meister, G. (2007). Proteomic and functional analysis of Argonaute-containing mRNA–protein complexes in human cells. *EMBO Rep.* 8, 1052–1060.
- Holt, C.E., Martin, K.C., and Schuman, E.M. (2019). Local translation in neurons: visualization and function. *Nat. Struct. Mol. Biol.* 26, 557–566.
- Horvathova, I., Voigt, F., Kotrys, A. V., Zhan, Y., Artus-Revel, C.G., Eglinger, J., Stadler, M.B., Giorgetti, L., and Chao, J.A. (2017). The Dynamics of mRNA Turnover Revealed by Single-Molecule Imaging in Single Cells. *Mol. Cell* 68, 615–625.e9.
- Hubstenberger, A., Courel, M., Bénard, M., Souquere, S., Ernoult-Lange, M., Chouaib, R., Yi, Z., Morlot, J.B., Munier, A., Fradet, M., et al. (2017). P-Body Purification Reveals the Condensation of Repressed mRNA Regulons. *Mol. Cell* 68, 144–157.e5.
- Iadevaia, V., and Gerber, A.P. (2015). Combinatorial Control of mRNA Fates by RNA-Binding Proteins and Non-Coding RNAs. *Biomolecules* 5, 2207–2222.
- Ince-Dunn, G., Okano, H.J., Jensen, K.B., Park, W.-Y., Zhong, R., Ule, J., Mele, A., Fak, J.J., Yang, C., Zhang, C., et al. (2012). Neuronal Elav-like (Hu) Proteins Regulate RNA Splicing and Abundance to Control Glutamate Levels and Neuronal Excitability. *Neuron* 75, 1067–1080.
- Irion, U., and St Johnston, D. (2007). bicoid RNA localization requires specific binding of an endosomal sorting complex. *Nature* 445, 554–558.
- Jia, M., Shan, Z., Yang, Y., Liu, C., Li, J., Luo, Z.-G., Zhang, M., Cai, Y., Wen, W., and Wang, W. (2015). The structural basis of Miranda-mediated Staufen localization during *Drosophila* neuroblast asymmetric division. *Nat. Commun.* 6, 8381.
- Jonas, S., and Izaurralde, E. (2015). Towards a molecular understanding of microRNA-mediated gene silencing. *Nat. Rev. Genet.* 16, 421–433.
- Katsanou, V., Milatos, S., Yiakouvaki, A., Sgantzis, N., Kotsoni, A., Alexiou, M., Harokopos, V., Aidinis, V., Hemberger, M., and Kontoyiannis, D.L. (2009). The RNA-binding protein Elavl1/HuR is essential for placental branching morphogenesis and embryonic development. *Mol. Cell. Biol.* 29, 2762–2776.
- Kenny, P.J., Zhou, H., Kim, M., Skariah, G., Khetani, R.S., Drnevich, J., Arcila, M.L., Kosik, K.S., and Ceman, S. (2014). MOV10 and FMRP regulate AGO2 association with microRNA recognition elements. *Cell Rep.* 9, 1729–1741.
- Kiebler, M.A., and Bassell, G.J. (2006). Neuronal RNA Granules: Movers and Makers. *Neuron* 51, 685–690.
- Kiebler, M.A., Jansen, R.-P., Dahm, R., and Macchi, P. (2005). A putative nuclear function for mammalian Staufen. *Trends Biochem. Sci.* 30, 228–231.
- Kim, H.H., Kuwano, Y., Srikantan, S., Lee, E.K., Martindale, J.L., and Gorospe, M. (2009). HuR recruits let-7/RISC to repress c-Myc expression. *Genes Dev.* 23, 1743–1748.

- Köhrmann, M., Luo, M., Kaether, C., Desgroseillers, L., Dotti, C.G., and Kiebler, M.A. (1999). Microtubule-dependent Recruitment of Staufén-Green Fluorescent Protein into Large RNA-containing Granules and Subsequent Dendritic Transport in Living Hippocampal Neurons. *Mol. Biol. Cell* *10*, 2945–2953.
- Kosik, K.S. (2006). The neuronal microRNA system. *Nat. Rev. Neurosci.* *7*, 911–920.
- Kress, T.L., Yoon, Y.J., and Mowry, K.L. (2004). Nuclear RNP complex assembly initiates cytoplasmic RNA localization. *J. Cell Biol.* *165*, 203–211.
- Kusek, G., Campbell, M., Doyle, F., Tenenbaum, S.A., Kiebler, M., and Temple, S. (2012). Asymmetric Segregation of the Double-Stranded RNA Binding Protein Staufén2 during Mammalian Neural Stem Cell Divisions Promotes Lineage Progression. *Cell Stem Cell* *11*, 505–516.
- Lal, A., Mazan-Mamczarz, K., Kawai, T., Yang, X., Martindale, J.L., and Gorospe, M. (2004). Concurrent versus individual binding of HuR and AUF1 to common labile target mRNAs. *EMBO J.* *23*, 3092–3102.
- Langdon, E.M., Qiu, Y., Ghanbari Niaki, A., McLaughlin, G.A., Weidmann, C.A., Gerbich, T.M., Smith, J.A., Crutchley, J.M., Termini, C.M., Weeks, K.M., et al. (2018). mRNA structure determines specificity of a polyQ-driven phase separation. *Science* (80-). *360*, 922–927.
- Laver, J.D., Li, X., Ancevicus, K., Westwood, J.T., Smibert, C.A., Morris, Q.D., and Lipshitz, H.D. (2013). Genome-wide analysis of Staufén-associated mRNAs identifies secondary structures that confer target specificity. *Nucleic Acids Res.* *41*, 9438–9460.
- Lazzaretti, D., Bandholz-Cajamarca, L., Emmerich, C., Schaaf, K., Basquin, C., Irion, U., and Bono, F. (2018). The crystal structure of Staufén1 in complex with a physiological RNA sheds light on substrate selectivity. *Life Sci. Alliance* *1*, e201800187.
- Lebeau, G., Miller, L.C., Tartas, M., McAdam, R., Laplante, I., Badeaux, F., DesGroseillers, L., Sossin, W.S., and Lacaille, J.-C. (2011). Staufén 2 regulates mGluR long-term depression and Map1b mRNA distribution in hippocampal neurons. *Learn. Mem.* *18*, 314–326.
- Lee, F.C.Y., and Ule, J. (2018). Advances in CLIP Technologies for Studies of Protein-RNA Interactions. *Mol. Cell* *69*, 354–369.
- Lee, H.Y., Zhou, K., Smith, A.M., Noland, C.L., and Doudna, J.A. (2013). Differential roles of human Dicer-binding proteins TRBP and PACT in small RNA processing. *Nucleic Acids Res.* *41*, 6568–6576.
- Lee, Y., Jeon, K., Lee, J.-T., Kim, S., and Kim, V.N. (2002). MicroRNA maturation: stepwise processing and subcellular localization. *EMBO J.* *21*, 4663–4670.
- Lee, Y., Ahn, C., Han, J., Choi, H., Kim, J., Yim, J., Lee, J., Provost, P., Rådmark, O., Kim, S., et al. (2003). The nuclear RNase III Drosha initiates microRNA processing. *Nature* *425*, 415–419.
- Lee, Y., Hur, I., Park, S.-Y., Kim, Y.-K., Suh, M.R., and Kim, V.N. (2006). The role of PACT in the RNA silencing pathway. *EMBO J.* *25*, 522–532.
- LeGendre, J.B., Campbell, Z.T., Kroll-Conner, P., Anderson, P., Kimble, J., and Wickens, M. (2013). RNA targets and specificity of Staufén, a double-stranded RNA-binding protein in *Caenorhabditis elegans*. *J. Biol. Chem.* *288*, 2532–2545.

- Li, Y., Estep, J.A., and Karginov, F. V. (2018). Transcriptome-wide Identification and Validation of Interactions between the miRNA Machinery and HuR on mRNA Targets. *J. Mol. Biol.* *430*, 285–296.
- Liu, J. (2006). Two mRNA-Binding Proteins Regulate the Distribution of Syntaxin mRNA in Aplysia Sensory Neurons. *J. Neurosci.* *26*, 5204–5214.
- Loffreda, A., Rigamonti, A., Barabino, S.M.L., and Lenzken, S.C. (2015). RNA-binding proteins in the regulation of miRNA activity: A focus on neuronal functions. *Biomolecules* *5*, 2363–2387.
- Lu, Z., Zhang, Q.C., Lee, B., Flynn, R.A., Smith, M.A., Robinson, J.T., Davidovich, C., Gooding, A.R., Goodrich, K.J., Mattick, J.S., et al. (2016). RNA Duplex Map in Living Cells Reveals Higher-Order Transcriptome Structure. *Cell* *165*, 1267–1279.
- Lund, E., Güttinger, S., Calado, A., Dahlberg, J.E., and Kutay, U. (2004). Nuclear export of microRNA precursors. *Science* *303*, 95–98.
- Luo, M., Duchaine, T.F., and DesGroseillers, L. (2002). Molecular mapping of the determinants involved in human Staufen-ribosome association. *Biochem. J.* *365*, 817–824.
- Macchi, P., Brownawell, A.M., Grunewald, B., DesGroseillers, L., Macara, I.G., and Kiebler, M.A. (2004). The Brain-specific Double-stranded RNA-binding Protein Staufen2. *J. Biol. Chem.* *279*, 31440–31444.
- Mallardo, M., Deitinghoff, A., Müller, J., Goetze, B., Macchi, P., Peters, C., and Kiebler, M.A. (2003). Isolation and characterization of Staufen-containing ribonucleoprotein particles from rat brain. *Proc. Natl. Acad. Sci. U. S. A.* *100*, 2100–2105.
- Mansfield, K.D., and Keene, J.D. (2012). Neuron-specific ELAV/Hu proteins suppress HuR mRNA during neuronal differentiation by alternative polyadenylation. *Nucleic Acids Res.* *40*, 2734–2746.
- Martel, C., Macchi, P., Furic, L., Kiebler, M.A., and Desgroseillers, L. (2006). Staufen1 is imported into the nucleolus via a bipartite nuclear localization signal and several modulatory determinants. *Biochem. J.* *393*, 245–254.
- Masliah, G., Barraud, P., and Allain, F.H.-T. (2013). RNA recognition by double-stranded RNA binding domains: a matter of shape and sequence. *Cell. Mol. Life Sci.* *70*, 1875–1895.
- Mathys, H., Basquin, J., Ozgur, S., Czarnocki-Cieciura, M., Bonneau, F., Aartse, A., Dziembowski, A., Nowotny, M., Conti, E., and Filipowicz, W. (2014). Structural and Biochemical Insights to the Role of the CCR4-NOT Complex and DDX6 ATPase in MicroRNA Repression. *Mol. Cell* *54*, 751–765.
- McGeary, S.E., Lin, K.S., Shi, C.Y., Pham, T.M., Bisaria, N., Kelley, G.M., and Bartel, D.P. (2019). The biochemical basis of microRNA targeting efficacy. *Science* (80-). *366*, eaav1741.
- Meer, E.J., Wang, D.O., Kim, S., Barr, I., Guo, F., and Martin, K.C. (2012). Identification of a cis-acting element that localizes mRNA to synapses. *Proc. Natl. Acad. Sci. U. S. A.* *109*, 4639–4644.
- Meister, G., Landthaler, M., Patkaniowska, A., Dorsett, Y., Teng, G., and Tuschl, T. (2004). Human Argonaute2 mediates RNA cleavage targeted by miRNAs and siRNAs. *Mol. Cell* *15*, 185–197.
- Micklem, D.R., Adams, J., Grünert, S., and St Johnston, D. (2000). Distinct roles of two conserved Staufen domains in oskar mRNA localization and translation. *EMBO J.* *19*, 1366–1377.

- Miki, T., and Yoneda, Y. (2004). Alternative Splicing of *Staufen2* Creates the Nuclear Export Signal for CRM1 (Exportin 1). *J. Biol. Chem.* *279*, 47473–47479.
- Mikl, M., Vendra, G., and Kiebler, M.A. (2011). Independent localization of MAP2, CaMKII α and β -actin RNAs in low copy numbers. *EMBO Rep.* *12*, 1077–1084.
- Miura, P., Shenker, S., Andreu-Agullo, C., Westholm, J.O., and Lai, E.C. (2013). Widespread and extensive lengthening of 3'UTRs in the mammalian brain. *Genome Res.* *23*, 812–825.
- Napoli, C., Lemieux, C., and Jorgensen, R. (1990). Introduction of a Chimeric Chalcone Synthase Gene into *Petunia* Results in Reversible Co-Suppression of Homologous Genes in trans. *Plant Cell* *2*, 279–289.
- Nawalpuri, B., and Muddashetty, R. (2020). Distinct temporal expression of GW182 in neurons regulates dendritic arborization. *BioRxiv* 2020.12.05.412932.
- Nawalpuri, B., Ravindran, S., and Muddashetty, R.S. (2020). The Role of Dynamic miRISC During Neuronal Development. *Front. Mol. Biosci.* *7*.
- Nosella, M.L., and Forman-Kay, J.D. (2021). Phosphorylation-dependent regulation of messenger RNA transcription, processing and translation within biomolecular condensates. *Curr. Opin. Cell Biol.* *69*, 30–40.
- Nottrott, S., Simard, M.J., and Richter, J.D. (2006). Human let-7a miRNA blocks protein production on actively translating polyribosomes. *Nat. Struct. Mol. Biol.* *13*, 1108–1114.
- Pacey, L.K.K., Doss, L., Cifelli, C., der Kooy, D. van, Heximer, S.P., and Hampson, D.R. (2011). Genetic deletion of regulator of G-protein signaling 4 (RGS4) rescues a subset of fragile X related phenotypes in the FMR1 knockout mouse. *Mol. Cell. Neurosci.* *46*, 563–572.
- Peters, L., and Meister, G. (2007). Argonaute Proteins: Mediators of RNA Silencing. *Mol. Cell* *26*, 611–623.
- Pilaz, L.-J., Lennox, A.L., Rouanet, J.P., and Silver, D.L. (2016). Dynamic mRNA Transport and Local Translation in Radial Glial Progenitors of the Developing Brain. *Curr. Biol.* *26*, 3383–3392.
- Popper, B., Demleitner, A., Bolivar, V.J., Kusek, G., Snyder-Keller, A., Schieweck, R., Temple, S., and Kiebler, M.A. (2018). *Staufen2* deficiency leads to impaired response to novelty in mice. *Neurobiol. Learn. Mem.* *150*, 107–115.
- Pullagura, S.R.N., Buas, B., Gray, N., Krening, L.C., Srivastava, A., and Braun, R.E. (2018). Functional Redundancy of DICER Cofactors TARBP2 and PRKRA During Murine Embryogenesis Does Not Involve miRNA Biogenesis. *Genetics* *208*, 1513–1522.
- Quévillon Huberdeau, M., Zeitler, D.M., Hauptmann, J., Bruckmann, A., Fressigné, L., Danner, J., Piquet, S., Strieder, N., Engelmann, J.C., Jannot, G., et al. (2017). Phosphorylation of Argonaute proteins affects mRNA binding and is essential for microRNA-guided gene silencing in vivo. *EMBO J.* *36*, 2088–2106.
- Rajgor, D., Sanderson, T.M., Amici, M., Collingridge, G.L., and Hanley, J.G. (2018). NMDAR-dependent Argonaute 2 phosphorylation regulates miRNA activity and dendritic spine plasticity. *EMBO J.* *44*, 1–21.
- Ramasamy, S., Wang, H., Quach, H.N.B., and Sampath, K. (2006). Zebrafish *Staufen1* and *Staufen2* are required for the survival and migration of primordial germ cells. *Dev. Biol.* *292*, 393–406.

- Ramos, A., Grünert, S., Adams, J., Micklem, D.R., Proctor, M.R., Freund, S., Bycroft, M., St Johnston, D., and Varani, G. (2000). RNA recognition by a Staufen double-stranded RNA-binding domain. *EMBO J.* *19*, 997–1009.
- Ravanidis, S., Kattan, F.G., and Doxakis, E. (2018). Unraveling the pathways to neuronal homeostasis and disease: Mechanistic insights into the role of RNA-binding proteins and associated factors. *Int. J. Mol. Sci.* *19*, 1–49.
- Rehfeld, F., Maticzka, D., Grosser, S., Knauff, P., Eravci, M., Vida, I., Backofen, R., and Wulczyn, F.G. (2018). The RNA-binding protein ARPP21 controls dendritic branching by functionally opposing the miRNA it hosts. *Nat. Commun.* *9*.
- Ren, Z., Veksler-Lublinsky, I., Morrissey, D., and Ambros, V. (2016). Staufen Negatively Modulates MicroRNA Activity in *Caenorhabditis elegans*. *Genes|Genomes|Genetics* *6*, 1227–1237.
- Rodgers, M.L., and Woodson, S.A. (2019). Transcription Increases the Cooperativity of Ribonucleoprotein Assembly. *Cell* *179*, 1370–1381.e12.
- Rouya, C., Siddiqui, N., Morita, M., Duchaine, T.F., Fabian, M.R., and Sonenberg, N. (2014). Human DDX6 effects miRNA-mediated gene silencing via direct binding to CNOT1. *RNA* *20*, 1398–1409.
- Sambandan, S., Akbalik, G., Kochen, L., Rinne, J., Kahlstatt, J., Glock, C., Tushev, G., Alvarez-Castelao, B., Heckel, A., and Schuman, E.M. (2017). Activity-dependent spatially localized miRNA maturation in neuronal dendrites. *Science* (80-.). *355*, 634–637.
- Sanchez de Groot, N., Armaos, A., Graña-Montes, R., Alriquet, M., Calloni, G., Vabulas, R.M., and Tartaglia, G.G. (2019). RNA structure drives interaction with proteins. *Nat. Commun.* *10*, 3246.
- Schieweck, R., Ninkovic, J., and Kiebler, M.A. (2020). RNA-binding proteins balance brain function in health and disease.
- Schratt, G.M., Tuebing, F., Nigh, E.A., Kane, C.G., Sabatini, M.E., Kiebler, M., and Greenberg, M.E. (2006). A brain-specific microRNA regulates dendritic spine development. *Nature* *439*, 283–289.
- Schreiner, D., Nguyen, T.-M., Russo, G., Heber, S., Patrignani, A., Ahrné, E., and Scheiffele, P. (2014). Targeted Combinatorial Alternative Splicing Generates Brain Region-Specific Repertoires of Neurexins. *Neuron* *84*, 386–398.
- Schutz, S., Noldeke, E.R., and Sprangers, R. (2017). A synergistic network of interactions promotes the formation of in vitro processing bodies and protects mRNA against decapping. *Nucleic Acids Res.* *45*, 6911–6922.
- Sharangdhar, T., Sugimoto, Y., Heraud-Farlow, J., Fernández-Moya, S.M., Ehse, J., Ruiz de Los Mozos, I., Ule, J., and Kiebler, M.A. (2017). A retained intron in the 3'-UTR of *Calm3* mRNA mediates its Staufen2- and activity-dependent localization to neuronal dendrites. *EMBO Rep.* *18*, 1762–1774.
- Shigeoka, T., Jung, H., Jung, J., Turner-Bridger, B., Ohk, J., Lin, J.Q., Amieux, P.S., and Holt, C.E. (2016). Dynamic Axonal Translation in Developing and Mature Visual Circuits. *Cell* *166*, 181–192.
- Skliris, A., Papadaki, O., Kafasla, P., Karakasiliotis, I., Hazapis, O., Reczko, M., Grammenoudi, S., Bauer, J., and Kontoyiannis, D.L. (2015). Neuroprotection requires the functions of the RNA-binding protein HuR. *Cell Death Differ.* *22*, 703–718.

- Sosanya, N.M., Huang, P.P.C., Cacheaux, L.P., Chen, C.J., Nguyen, K., Perrone-Bizzozero, N.I., and Raab-Graham, K.F. (2013). Degradation of high affinity HuD targets releases Kv1.1 mRNA from miR-129 repression by mTORC1. *J. Cell Biol.* *202*, 53–69.
- Spitale, R.C., Crisalli, P., Flynn, R.A., Torre, E.A., Kool, E.T., and Chang, H.Y. (2013). RNA SHAPE analysis in living cells. *Nat. Chem. Biol.* *9*, 18–20.
- St Johnston, D., Beuchle, D., and Nüsslein-Volhard, C. (1991). *Staufen*, a gene required to localize maternal RNAs in the *Drosophila* egg. *Cell* *66*, 51–63.
- Standart, N., and Weil, D. (2018). P-Bodies: Cytosolic Droplets for Coordinated mRNA Storage. *Trends Genet.* *34*, 612–626.
- Di Stefano, B., Luo, E.-C., Haggerty, C., Aigner, S., Charlton, J., Brumbaugh, J., Ji, F., Rabano Jiménez, I., Clowers, K.J., Huebner, A.J., et al. (2019). The RNA Helicase DDX6 Controls Cellular Plasticity by Modulating P-Body Homeostasis. *Cell Stem Cell* *25*, 622–638.e13.
- Stefl, R., Oberstrass, F.C., Hood, J.L., Jourdan, M., Zimmermann, M., Skrisovska, L., Maris, C., Peng, L., Hofr, C., Emeson, R.B., et al. (2010). The Solution Structure of the ADAR2 dsRBM-RNA Complex Reveals a Sequence-Specific Readout of the Minor Groove. *Cell* *143*, 225–237.
- Sternburg, E.L., Estep, J.A., Nguyen, D.K., Li, Y., and Karginov, F. V. (2018). Antagonistic and cooperative AGO2-PUM interactions in regulating mRNAs. *Sci. Rep.* *8*, 15316.
- Sugimoto, Y., Vigilante, A., Darbo, E., Zirra, A., Militti, C., D'Ambrogio, A., Luscombe, N.M., and Ule, J. (2015). hiCLIP reveals the in vivo atlas of mRNA secondary structures recognized by *Staufen 1*. *Nature* *519*, 491–494.
- Sun, K., Li, X., Chen, X., Bai, Y., Zhou, G., Kokiko-Cochran, O.N., Lamb, B., Hamilton, T.A., Lin, C.-Y., Lee, Y.-S., et al. (2018). Neuron-Specific HuR-Deficient Mice Spontaneously Develop Motor Neuron Disease. *J. Immunol.* *201*, 157–166.
- Tang, S.J., Meulemans, D., Vazquez, L., Colaco, N., and Schuman, E. (2001). A Role for a Rat Homolog of *Staufen* in the Transport of RNA to Neuronal Dendrites. *Neuron* *32*, 463–475.
- Tat, T.T., Maroney, P.A., Chamnongpol, S., Collier, J., and Nilsen, T.W. (2016). Cotranslational microRNA mediated messenger RNA destabilization. *Elife* *5*, 1–18.
- Tauber, D., Tauber, G., and Parker, R. (2020). Mechanisms and Regulation of RNA Condensation in RNP Granule Formation. *Trends Biochem. Sci.* *45*, 764–778.
- Treiber, T., Treiber, N., Plessmann, U., Harlander, S., Daiß, J.-L., Eichner, N., Lehmann, G., Schall, K., Urlaub, H., and Meister, G. (2017). A Compendium of RNA-Binding Proteins that Regulate MicroRNA Biogenesis. *Mol. Cell* *66*, 270–284.e13.
- Tushev, G., Glock, C., Heumüller, M., Biever, A., Jovanovic, M., and Schuman, E.M. (2018). Alternative 3' UTRs Modify the Localization, Regulatory Potential, Stability, and Plasticity of mRNAs in Neuronal Compartments. *Neuron* *98*, 495–511.e6.
- Vasudevan, S., and Steitz, J.A. (2007). AU-Rich-Element-Mediated Upregulation of Translation by FXR1 and Argonaute 2. *1105–1118*.
- Vessey, J.P., Schoderboeck, L., Gingl, E., Luzi, E., Riefler, J., Di Leva, F., Karra, D., Thomas, S., Kiebler, M.A., and Macchi, P. (2010). Mammalian *Pumilio 2* regulates dendrite morphogenesis and synaptic function. *Proc. Natl. Acad. Sci.* *107*, 3222–3227.

- Vessey, J.P., Amadei, G., Burns, S.E., Kiebler, M.A., Kaplan, D.R., and Miller, F.D. (2012). An asymmetrically localized Stauf2-dependent RNA complex regulates maintenance of mammalian neural stem cells. *Cell Stem Cell* *11*, 517–528.
- Visentin, S., Cannone, G., Douch, J., Harris, G., Gleghorn, M.L., Clifton, L., Smith, B.O., and Spagnolo, L. (2020). A multipronged approach to understanding the form and function of hStaufen protein. *RNA* *26*, 265–277.
- Wang, L., and Yi, R. (2014). 3'UTRs take a long shot in the brain. *BioEssays* *36*, 39–45.
- Wang, E.T., Taliaferro, J.M., Lee, J.A., Sudhakaran, I.P., Rossoll, W., Gross, C., Moss, K.R., and Bassell, G.J. (2016). Dysregulation of mRNA localization and translation in genetic disease. *J. Neurosci.* *36*, 11418–11426.
- Wang, Y., Guo, Y., Tang, C., Han, X., Xu, M., Sun, J., Zhao, Y., Zhang, Y., Wang, M., Cao, X., et al. (2019). Developmental Cytoplasmic-to-Nuclear Translocation of RNA-Binding Protein HuR Is Required for Adult Neurogenesis. *Cell Rep.* *29*, 3101–3117.e7.
- Wehrspau, C.C., Ponting, C.P., and Marques, A.C. (2014). Brain-expressed 3'UTR extensions strengthen miRNA cross-talk between ion channel/transporter encoding mRNAs. *Front. Genet.* *5*.
- Wei, L., Lee, S., Majumdar, S., Zhang, B., Sanfilippo, P., Joseph, B., Miura, P., Soller, M., and Lai, E.C. (2020). Overlapping Activities of ELAV/Hu Family RNA Binding Proteins Specify the Extended Neuronal 3' UTR Landscape in *Drosophila*. *Mol. Cell* *80*, 140–155.e6.
- Weiss, K., Treiber, T., Meister, G., and Schratt, G. (2019). The nuclear matrix protein Matr3 regulates processing of the synaptic microRNA-138-5p. *Neurobiol. Learn. Mem.* *159*, 36–45.
- Wickham, L., Duchaine, T., Luo, M., Nabi, I.R., and DesGroseillers, L. (1999). Mammalian stau1 is a double-stranded-RNA- and tubulin-binding protein which localizes to the rough endoplasmic reticulum. *Mol. Cell. Biol.* *19*, 2220–2230.
- Wu, P.-H., Isaji, M., and Carthew, R.W. (2013). Functionally diverse microRNA effector complexes are regulated by extracellular signaling. *Mol. Cell* *52*, 113–123.
- Yadav, D.K., Zigačková, D., Zlobina, M., Klumpler, T., Beaumont, C., Kubíčková, M., Vaňáčková, Š., and Lukavský, P.J. (2020). Stauf1 reads out structure and sequence features in ARF1 dsRNA for target recognition. *Nucleic Acids Res.* *48*, 2091–2106.
- Yoon, J.-S., Mogilicherla, K., Gurusamy, D., Chen, X., Chereddy, S.C.R.R., and Palli, S.R. (2018). Double-stranded RNA binding protein, Stauf, is required for the initiation of RNAi in coleopteran insects. *Proc. Natl. Acad. Sci.* 201809381.
- Zampa, F., Bicker, S., and Schratt, G. (2018). Activity-Dependent Pre-miR-134 Dendritic Localization Is Required for Hippocampal Neuron Dendritogenesis. *Front. Mol. Neurosci.* *11*, 171.
- Zeitelhofer, M., Karra, D., Macchi, P., Tolino, M., Thomas, S., Schwarz, M., Kiebler, M., and Dahm, R. (2008). Dynamic Interaction between P-Bodies and Transport Ribonucleoprotein Particles in Dendrites of Mature Hippocampal Neurons. *J. Neurosci.* *28*, 7555–7562.
- Zhang, X., Zuo, X., Yang, B., Li, Z., Xue, Y., Zhou, Y., Huang, J., Zhao, X., Zhou, J., Yan, Y., et al. (2014). MicroRNA Directly Enhances Mitochondrial Translation during Muscle Differentiation. *Cell* *158*, 607–619.

Zhao, Y.-F., He, X.-X., Song, Z.-F., Guo, Y., Zhang, Y.-N., Yu, H.-L., He, Z.-X., Xiong, W.-C., Guo, W., and Zhu, X.-J. (2020). Human antigen R-regulated mRNA metabolism promotes the cell motility of migrating mouse neurons. *Development* 147.

Zheng, D., Cho, H., Wang, W., Rambout, X., Tian, B., and Maquat, L.E. (2020). 3'READS + RIP defines differential Staufen1 binding to alternative 3'UTR isoforms and reveals structures and sequence motifs influencing binding and polysome association. *RNA* 26, 1621–1636.

Appendices

List of Abbreviations

Ago	Argonaute
APA	alternative polyadenylation
APEX2	L-ascorbate peroxidase
ARF1	ADP-ribosylation factor 1
Calm3	Calmodulin 3
CLIP	crosslinking and immunoprecipitation
CMV	cytomegalovirus
Ctrl	control
Dcp	mRNA-decapping enzyme
Ddx	DEAD-box RNA helicase
DIV	days <i>in vitro</i>
dsRNA	double-stranded RNA
Edc	enhancer of decapping
ELAVL	embryonic lethal abnormal vision like
FMRP	Fragile X mental retardation protein
GFP	green fluorescent protein
GPCR	G-protein coupled receptor
GTP	guanosine triphosphate
h	hours
HEK-293T	Human embryonic kidney cells 293T
hiCLIP	RNA hybrid and individual-nucleotide resolution ultraviolet crosslinking and immunoprecipitation
Hu	Human antigen
kDa	kilodalton
Kv1.1	potassium voltage-gated channel subfamily A member 1
LTD	long-term depression
LTP	long-term potentiation
min	minutes
miRNA	microRNA

mRNA	messenger RNA
ncRNA	non-coding RNA
NES	nuclear export signal
NLS	nuclear localization signal
NTC	non-targeting control
ORF	open reading frame
P-body	Processing body
pre	precursor
pri	primary
Pum2	Pumilio 2
qRT-PCR	quantitative real-time polymerase chain reaction
RBD	RNA-binding domain
RBP	RNA-binding protein
Rgs4	Regulator of G-protein signaling 4
RISC	RNA induced silencing complex
RNA	ribonucleic acid
RNAi	RNA interference
RNP	ribonucleoprotein particle
RRM	RNA recognition motif
RSV	Rous Sarcoma Virus
sec	seconds
shRNA	short hairpin RNA
SRS	Staufen recognition structures
ssRNA	single-stranded RNA
Stau	Staufen
tagRFP	monomeric red fluorescent protein
TBD	tubulin-binding domain
tdMCP	tandem MS2 coat protein
Tnrc6	trinucleotide repeat-containing gene 6 protein
TRBP	Trans-activation-responsive RNA-binding protein
UBC	Ubiquitin C
UTR	untranslated region
Xrn1	5'-3' exoribonuclease 1

Acknowledgements

First and foremost, I would like to thank PROF. DR. KIEBLER for giving me the opportunity to prepare my thesis in his lab. Thank you for your excellent support over the last years and your ongoing encouragement. In addition, I would like to thank PROF. DR. FÖRSTEMANN for supervising my thesis and PROF. DR. MEISTER and my thesis committee for helpful input

A special thank goes to SANDRA for introducing me into the world of RNA and molecular biology. Without you, I would have been lost at day one and every day after. Your creative and excellent intellectual input made this thesis possible and helped me to be patient and cope with the impossible protein Stau2. In addition, I want to thank CHRISTIN for your outstanding experimental support and always keeping my spirits up, be it through adventurous times with our rats or your excellent cooking abilities. My gratitude also goes to two excellent students that I had the honor to work with, MELINA and LUISE. You made supervising a piece of cake, exciting and fun. It was a pleasure to introduce you to our world of neuronal RBPs and your excellent experimental work shaped the last part of my PhD.

Moreover, I want to thank all members, former and current, of the Kiebler Lab for their outstanding support in the lab, advice and intellectual input. I want to thank TEJASWINI for teaching me RNA FISHing and the magic behind working with healthy neurons, RICO for the most fruitful discussions and your excellent scientific input and KARL for your excellent help with data analysis and visualization.

One crucial cornerstone for the success of my PhD was the financial support and the yearly getaway of the SPP1738 with lots of snow, scientific discussions, technical advice and lasting friendships. Thank you, these weeks always fueled my confidence to go above and beyond in my projects.

I am thankful to my friends from the GIESING WG, BEACHVOLLEYBALL and SOCCER crews for fun times and when running around in a lab is not enough and HANNES for your support when the end was near. I want to thank my parents, OLAF and INGRID, for injecting me with curiosity in science and for always supporting me and giving me the freedom to do what I love. My best friend and husband DANIEL, thank you for patiently waiting each day, when I was late because it never takes just 10 minutes to finish an experiment. With your love and support everything is possible.